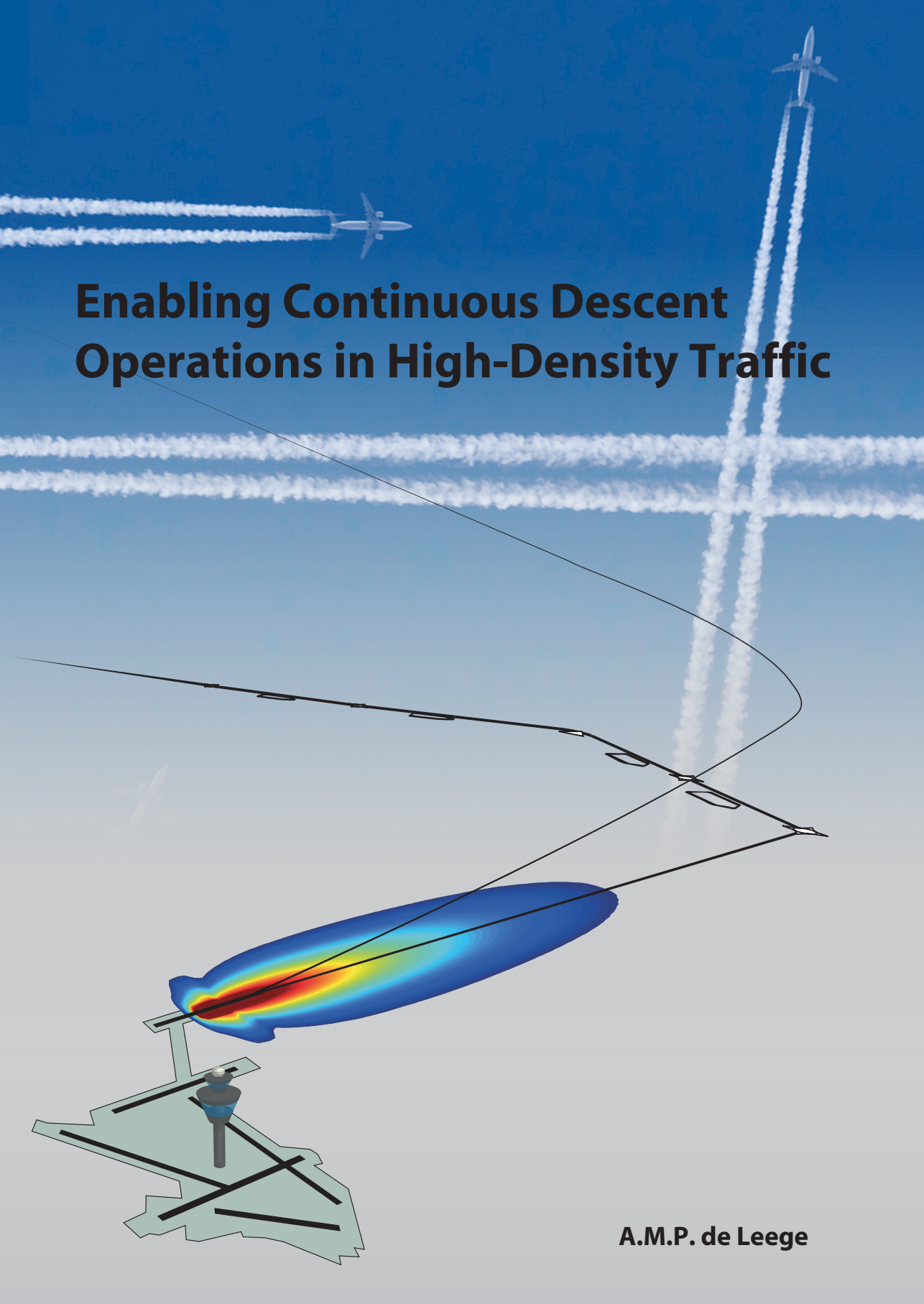# Enabling Continuous Descent Operations in High-Density Traffic

A.M.P. de Leege

Enabling Continuous Descent Operations in High-Density Traffic

A.M.P. de Leege

Enabling Continuous Descent Operations in High-Density Traffic

PROEFSCHRIFT

ter verkrijging van de graad van doctor
aan de Technische Universiteit Delft,
op gezag van de Rector Magnificus prof. ir. K.C.A.M. Luyben,
voorzitter van het College voor Promoties,
in het openbaar te verdedigen op 11 juli 2013 om 12.30 uur.

door

Arie Marinus Pieter DE LEEGE

ingenieur luchtvaart en ruimtevaart

geboren te Delft.

Dit proefschrift is goedgekeurd door de promotor:

Prof. dr. ir. M. Mulder

Copromotor:
Dr. ir. M.M. van Paassen

Samenstelling promotiecommissie:

Rector Magnificus	Technische Universiteit Delft, voorzitter
Prof. dr. ir. M. Mulder	Technische Universiteit Delft, promotor
Dr. ir. M.M. van Paassen	Technische Universiteit Delft, copromotor
Prof. dr. ir. J.M. Hoekstra	Technische Universiteit Delft
Prof. J.-P.B. Clarke, Sc.D.	Georgia Institute of Technology
Prof. dr. ing. H. Fricke	Dresden University of Technology
Prof. dr. P.J. Stappers	Technische Universiteit Delft
Ir. A.C. Hoekstra	To70 Holding B.V.
Prof. dr. D.G. Simons	Technische Universiteit Delft, reservelid

Summary

Enabling Continuous Descent Operations in High-Density Traffic

A.M.P. de Leege

The Air Traffic Management (ATM) community strives to reduce the environmental impact per flight. Continuous Descent Operation (CDO) has been identified by the ATM community as one of the operational improvements to reduce the environmental impact, both in terms of aircraft noise and gaseous emissions. When on a CDO, aircraft descend from an optimal position with minimum engine thrust. The noise at the source is less and the distance between the aircraft and the ground is larger compared to conventional approach procedures, yielding lower noise levels on the ground.

Tactical control interventions during the CDO are likely to reduce the aircraft's ability to fly the optimized descent with a detrimental effect on the environmental benefits and are therefore unwanted. The difficulty lies in accurately spacing the traffic for CDO. The spacing at the start of the CDO between two aircraft shall be sufficient to keep the aircraft safely separated during the approach but not lead to excess space between aircraft. The latter is required to provide the same capacity that is currently realized using conventional approach procedures. Currently the Air Traffic Controller (ATCO) applies arbitrarily large spacing buffers at the cost of capacity to avoid tactical interventions and ultimately to facilitate CDOs. The ATCO cannot determine the required spacing with sufficient accuracy because his or her ability to project the future aircraft behavior is insufficient. In an ATM system that enables CDO in high-density traffic, the dependency on the ATCO's projection capabilities must be reduced. Features of such an ATM system may include:

- Support tools that help ease the projection task for the ATCO;
- Delegation of the spacing task to the flight crew or an automation system;
- CDO procedures which are easier to predict by the ATCO.

The main objective of this thesis is the development of an ATM system that facilitates CDO in high-density traffic. This thesis focuses on two possible features of such an ATM system:

- Controller support for accurate arrival time control for CDO;
- Delegation of the spacing task during the CDO phase (self-spacing).

During the CDO phase, aircraft follow a fixed arrival route (closed-path). Minimal constraints are imposed on the vertical path to enable optimization of the CDO for the best environmental performance.

ATCO support tools for arrival time control and pilot support systems for self-spacing rely on accurate Trajectory Prediction (TP). The TP performance is a main driver of the overall system performance. Other research has shown that meteorological conditions are one of the main impacting factors on the aircraft trajectory. Accurate near real-time meteorological data is thus a prerequisite to enable CDO in high-density traffic.

In this thesis the use of Automatic Dependent Surveillance Broadcast (ADS-B) data to acquire meteorological data was explored. ADS-B is expected to be available on the ground and onboard the aircraft in the near future and provides real-time position and speed information. Methods to estimate wind, temperature, and pressure profiles were derived. These methods rely on existing systems and communication protocols. The ADS-B derived meteorological data was compared to forecasts to examine the performance of the developed methods. The ADS-B derived meteorological data can be used in TP on the ground as well as onboard aircraft.

Ground-based trajectory prediction accuracy may suffer from limited availability of aircraft state information, aircraft performance, and aircraft intent data. In this thesis TP was formulated as a supervised machine learning regression problem. Distinctive about this approach is the absence of explicit modeling of the aircraft performance, intent, procedures, and airspace. Historical trajectory and meteorological data are used to train a predictive model. Data that is readily available through surveillance and meteorological systems is used. During training, the model parameters are set to minimize the prediction error. The effectiveness of the method was examined by making arrival time predictions for CDO. The results showed that a machine learning approach to TP could be feasible. Subsequently, the TP was used to compute the required spacing between aircraft at the start of the CDO. When using the TP the number of conflicts during the CDO phase decreased and the landing rate increased.

Delegation of the spacing task to the flight crew during the CDO phase is referred to as self-spacing. In a self-spacing environment, the flight crew plan and execute, with the help of onboard systems, a CDO to remain safely separated. Delegation of the spacing task is proposed, because the maneuverability of the aircraft is limited and mainly driven by the aircraft performance. This data is readily available onboard the aircraft. Two promising concepts are relative distance-based and absolute time-based self-spacing. Main difference between these concepts is the interaction between aircraft during the descent. In the relative distance-based concept, the aircraft actively reacts to the

behavior of the preceding aircraft to stay separated. In the absolute time-spacing concept there is no interaction between aircraft. Instead thereof, a required time over the runway threshold is assigned to each aircraft at the start of the descent to ensure separation. Monte-Carlo simulations were conducted to examine the runway capacity that can be expected and the influence of operational aspects on the performance of the self-spacing concepts. The runway capacity achieved in the simulations was comparable to the throughput that is realized using conventional procedures. The highest throughput was achieved using the relative distance-based self-spacing concept. In the absolute time-spacing concept, buffer space was applied to account for deviations of the required time over the runway threshold. The simulation result also showed that accurate initial spacing is required, because CDO procedures provide limited maneuverability to take corrective actions.

As the last step in the work presented in this thesis, a decision support tool was developed and validated further to enable the ATCO to accurately space the aircraft for CDO. The starting point was earlier work done at Delft University of Technology on the Time-Space Diagram (TSD) support tool. The TSD provides the tools and information to the ATCO to accurately sequence, merge, and space traffic for CDO. The TSD is presented on secondary display next to the Plan View Display (PVD). Concepts applied in the design of the interface are ecological interface design, visual momentum, and direct manipulation interfaces. Work in this thesis focused on the latter two concepts. The integration of the information displayed on the PVD-TSD interface was improved using the concept of visual momentum. Also the solution guidance provided by the interface was redesigned. Static what-if tools showing the effect of computer selected actions were replaced by direct manipulation interfaces. These interfaces were developed for typical controller instructions (e.g., speed control).

In a human-in-the-loop experiment the TSD was tested against a more conventional stack list support solution. The experiment results clearly demonstrated the effects of the TSD on the ATCO's performance in comparison to the conventional solution. The TSD interface freed time to plan traffic ahead using direct manipulation interfaces, which according to all subjects worked intuitively. The number of instructions per aircraft was decreased by one third and instructions were given earlier. As a result CDOs started earlier at a higher altitude and greater distance from the runway. ATCO workload was significantly reduced and situation awareness increased.

Results of this thesis that support the development of an ATM system enabling CDO in high-density traffic are new methods to acquire meteorological data and to make trajectory predictions, the capacity and stability assessment of self-spacing scenarios, and the TSD controller support tool. The Monte-Carlo simulations showed that using

self-spacing during the CDO phase the runway throughput is comparable to the throughput realized today using conventional procedures. The simulation results also showed that accurate spacing of the aircraft at the start of the CDO is needed, which was addressed in the work TSD support tool. This work resulted in an interface that supports the ATCO in sequencing, merging, and spacing traffic for CDO. More in general, the TSD provides an example of applying the principles of ecological interface design, visual momentum, and direct manipulation interfaces to improve ATM system capabilities and performance, by leveraging automation and keeping the system human centered. The work on meteorological data acquisition and TP is also relevant to the development and implementation of other systems and procedures in new ATM systems. Methods to infer meteorological data from ADS-B may also be of interest outside the ATM domain.

An ATM system that facilitates CDO in high-density traffic encompasses more procedures, processes, and systems and other traffic than were addressed in this thesis. Research and development in other areas beyond the scope of this thesis is also needed to eventually enable CDO in high-density traffic. Examples of areas that were not covered are pilot support, controller support during self-spacing operations, CDO procedure design, and communication systems. It is recommended to investigate these areas.

Contents

List of Figures

List of Tables

xx |

1   Introduction

The Air Traffic Management (ATM) community strives to reduce the environmental impact per flight. This reduction is a precondition for sustainable growth of air transport. Air transport's main environmental impacts are aircraft noise and aircraft gaseous emissions. Noise has traditionally been given a higher priority due to the community reaction to aircraft noise.

An example of the focus on mitigating aircraft noise is the International Civil Aviation Organization's (ICAO) concept of a "Balanced Approach" to aircraft noise management that was endorsed in 2001 [1]. This approach consists of identifying the noise problem and analyzing the measures available to reduce noise in four areas:

- Noise reduction at the source;
- Land-use planning and management;
- Operating restrictions;
- Noise abatement procedures.

Several measures in each of the aforementioned areas have already been taken. In the past forty years the emphasis has mainly been on the reduction of noise at the source. Today's aircraft are 50% quieter than aircraft twenty years ago. Quieter aircraft also tend to be more fuel efficient; lowering emissions. But the gains are diminishing. On a much smaller scale, land-use planning and management is used to minimize the population exposed to aircraft noise. Operating restrictions have been imposed at noise-regulated airports. Noisy aircraft are being banned or their operation is highly restricted. The achieved noise reduction is significant but the phase-out of noisy aircraft is nearing completion in most developed countries.

In the field of noise abatement procedures significant improvements in noise reduction can still be made. Unlike measures in the other three areas, noise abatement procedures can have a detrimental effect on aircraft emissions. An example are noise preferential routes that have been agreed with communities surrounding the airport. These routes result in local noise reductions but often lead to an increase of the flying distance, hence increasing aircraft emissions.

Recently, the impact of aircraft gaseous emissions has gained more attention by the general public, policy makers, and the aviation industry. The reasons for this are high fuel prices, emission trading, and the concerns about human-induced climate change. A trade-off has to be made for operational changes with a possitive effect on noise and a negative effect on emission or vice versa. Operational changes that reduce both noise and emissions are preferred.

Continuous Descent Operation (CDO) has been identified by the ATM community as a promising operational improvement to reduce the aircraft's environmental impact during approach, both in terms of aircraft noise and aircraft emissions.

1.1 Benefits of Continuous Descent Operation

CDO is an aircraft operating technique to reduce aircraft noise, emissions, and fuel burn during approach [1-8]. Aircraft aim to descend continuously in a low drag configuration with minimum engine thrust. During a CDO, level flight segments that require high engine thrust settings are avoided. These segments are typical for the conventional step-down approach procedure, see Figure 1-1. As a result, aircraft remain higher for a longer period of time as compared to conventional approaches.
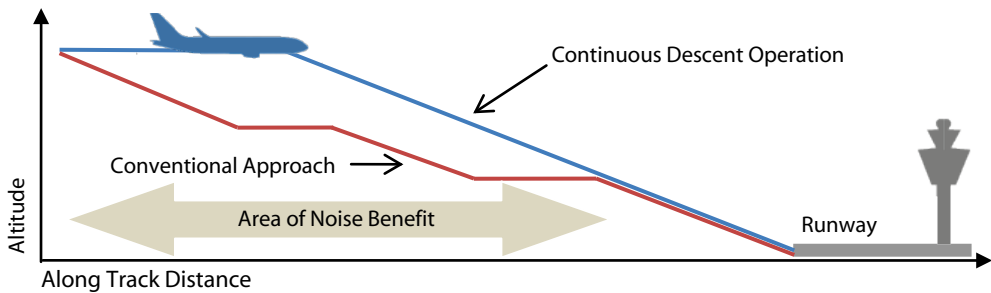
Figure 1-1 Vertical profiles of CDO and conventional step-down approach.

The noise benefit is the combined effect of reduced engine thrust, the low drag configuration, and the increased distance between the ground and the aircraft. Figure 1-2 shows the noise footprints of both a typical conventional approach and a CDO. The footprints show the maximum instantaneous noise level in A-weighing L_{Amax} dB(A). The footprint for the CDO is significantly smaller. CDO typically reduces aircraft noise in areas located at a minimum distance ranging from 6 NM to 9 NM from the airport. Locally, the L_{Amax} is reduced by 7 dB(A). In the example both aircraft intercept the instrument landing system's (ILS) glide slope at 9 NM from the runway. From this distance the aircraft follow the same vertical path. Also, the aircraft are in the same aerodynamic configuration with the same engine thrust settings. As a result, the maximum noise levels on the ground for the CDO and conventional approach are equal within approximately 9 NM from the runway.

The fuel burn reduction ranges between 50 kg and 400 kg per approach, depending on aircraft type and procedure [6-7]. This reduction corresponds with 150 kg to 1200 kg less CO_2 emission per approach.
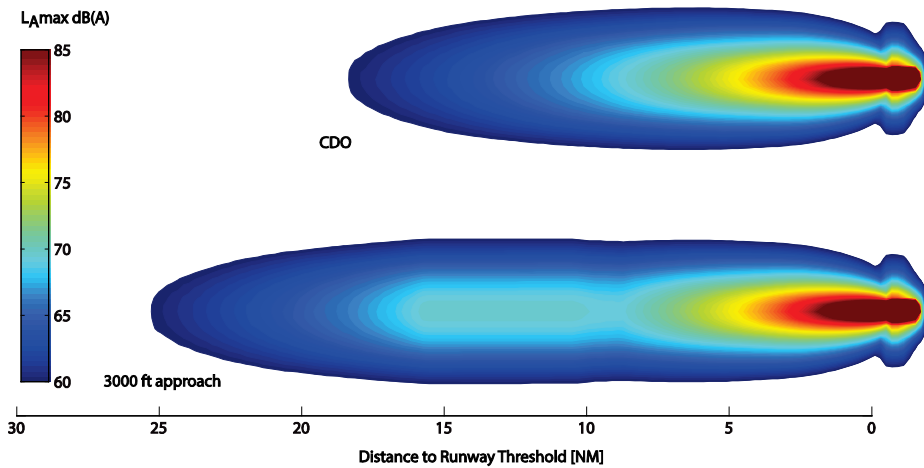
Figure 1-2 Comparison of the maximum instantaneous noise level on the ground between a CDO and a typical conventional approach.

1.2 Historic Background

The introduction of jet-powered aircraft in the late fifties marked the start of a period of rapid expansion of air transport. The jet-powered aircraft were much noisier than the propeller-driven aircraft they replaced. Aircraft noise became an increasing public problem. In response to this problem, research on noise abatement procedures started in the late sixties and early seventies. The development of noise abatement approach procedures was generally performed by research and government organizations, and by the aviation industry in Europe and the United States [8-14].

1.2.1 Steep Approaches

In this period NASA evaluated the operational feasibility of steep approach profiles in close collaboration with the Federal Aviation Administration, the aviation industry, and pilot associations [9, 10]. An example of a steeper approach is the two-segment approach depicted in Figure 1-3. The conventional ILS 3˚ glide slope was only used for the lower segment, while a steeper (i.e., 6˚) upper glide slope segment was established using an area navigation system. In this design, aircraft noise on the ground is reduced because a steeper approach segment requires less engine thrust and the aircraft is higher above the ground. Due to lack of pilot acceptance and the dependency of the procedure on new air- and ground systems the two-segment approach was unsuccessful, however.
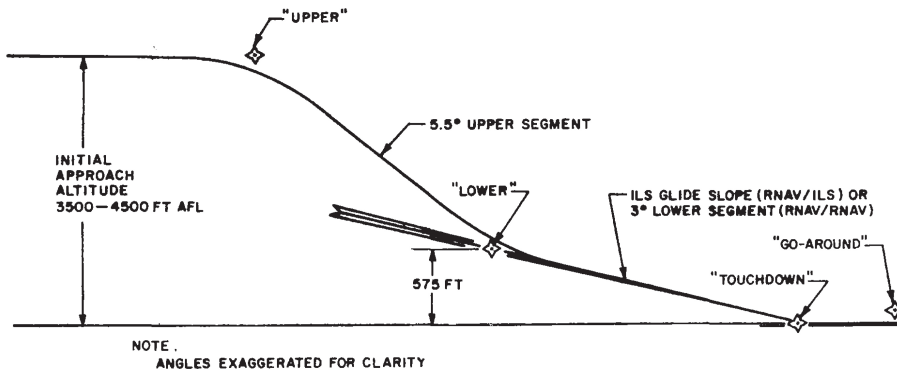
Figure 1-3 Example of a two-segment approach profile investigated by NASA, Source: NASA, Ref. [10].

1.2.2 Low-Power Low-Drag

In contrast, the low-power, low-drag (LPLD) noise abatement procedure developed primarily by Lufthansa in 1971 was more successful [11-13]. In this procedure the aircraft intercepts the ILS glide slope at approximately 3,000 ft with a partial flap and low thrust setting. Next, the aircraft slows down while flying down the glide slope. Landing flaps and gear are extended when the aircraft is near the airport and passes an altitude of 1,000 ft. There is no dependency on new air- or ground systems. The International Air Transport Association (IATA) recommended this procedure to its members in 1972.
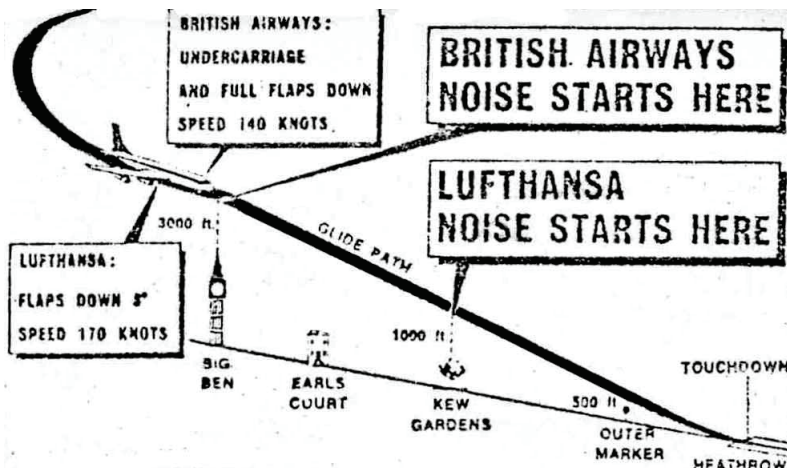
Figure 1-4 Lufthansa's low-power low-drag procedure used in the 1970's, Source: The Observer, Refs. [13, 15].

The 1973 oil crisis was another incentive for the development of CDOs. In addition to noise reduction, the reduction of fuel burn also became a driving factor. In 1974 Dibley, a Boeing 747 captain, proposed a procedure that allowed the flight crew to establish a continuous descent path at idle thrust [14]. The procedure required Distance Measurement Equipment (DME) to be installed near the runway's ILS to enable the crew to estimate the distance to touchdown and to compute the descent rate with a circular descent slide-rule shown in Figure 1-5. This procedure eventually resulted in the CDO procedure used today at London Heathrow [15].
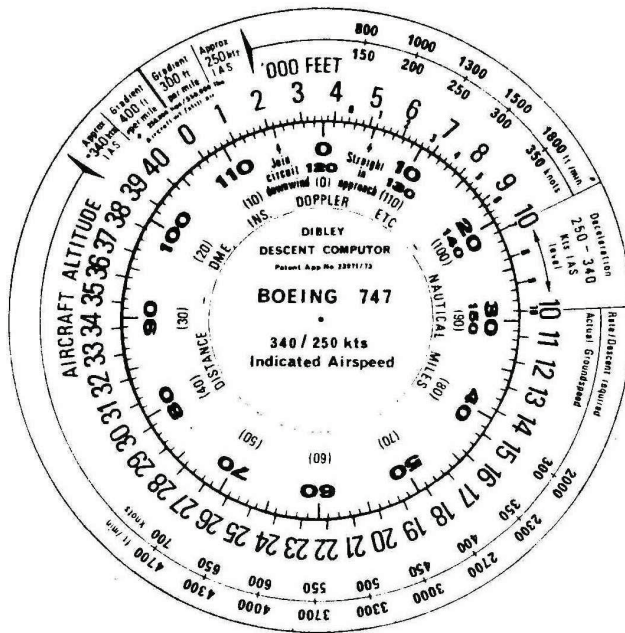
Figure 1-5 The Dibley slide-rule descent computer, Source: Dibley, Ref. [15].

1.2.3 New Technical Capabilities

The introduction of the Flight Management System (FMS) onboard modern aircraft in the early eighties provided new possibilities for the development of noise abatement procedures [16-19]. The lateral navigation (LNAV) and vertical navigation (VNAV) capabilities of the FMS enable aircraft to follow a predefined lateral path and vertical path. Typically, the lateral path is prescribed by ATC using an area navigation procedure. The vertical path (altitude and speed) can be optimized using the aircraft FMS for minimum fuel burn, emissions, and noise within the constraints set by ATC. Although the FMS has become one of the standard systems in cockpits of today's aircraft, the use of the FMS in CDO procedures is still limited.

1.3 Current CDO procedures

ICAO distinguishes two types of CDO procedures that are in use today. A CDO is characterized as an open-path procedure if the lateral path is not fixed during the CDO. If the lateral path is fixed, the procedure is referred to as a closed-path CDO procedure [2]. Only closed-path procedures enable the use of the FMS to optimize and fly the CDO such that it delivers the best environmental performance.

1.3.1 Open-path procedures

In open-path procedure designs, vectoring is used during the entire approach or a part of the approach. Vectoring in combination with speed control gives ATC the flexibility to separate and expedite traffic during the CDO. This procedure requires ATC to pass estimates of the remaining track distance to the flight crew. The Air Traffic Controller (ATCO) is the only actor with a plan for the remaining path. The flight crew uses the estimates to establish a continuous descent path to the glide slope intercept. Vertical profiles computed by the FMS cannot be used in this procedure.

The resulting approach is often sub-optimal in terms of the environmental benefits that are achieved. ATC and the flight crew play an important role in the achievement of the CDO and the associated benefits [20, 21]. Over-estimation or under-estimation of the remaining track distance might result in a rushed approach or level segments at low altitude, respectively. Out of caution, ATCOs tend to under-estimate the track distance [20]. Speed control by ATC might require early selection of a higher drag configuration and therefore more engine thrust. Finally, the procedure is also dependent on the ability of the flight crew to establish and maintain a continuous descent path, preferably in a LPLD configuration.

1.3.2 Closed-path procedures

Figure 1-6 gives a schematic overview of a typical closed-path CDO procedure. Aircraft fly a CDO from top of descent or an intermediate altitude. The ATCO de-conflicts, sequences, and spaces the aircraft before the CDO commences. Aircraft are accurately spaced on an intermediate metering fix. The spacing between aircraft should ensure separation throughout the CDO and efficient traffic handling.

In case traffic does not remain separated tactical controller interventions are needed. Closed-path CDO procedures have limited flexibility to accommodate tactical interventions and are therefore unwanted. Tactical interventions often take the aircraft off the closed-path and reduce the aircraft's ability to fly the optimized descent profile. In such situations the environmental and economic benefits are (partially) lost.
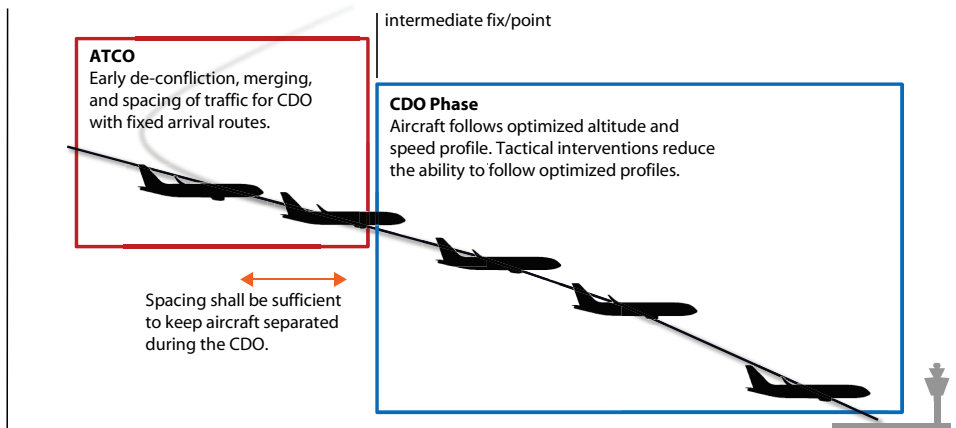
Figure 1-6 Schematic representation of a typical closed-path CDO procedure.

On the other hand, if the aircraft spacing at the start of the procedure is too large, traffic throughput is likely to drop below the demanded capacity. This could lead to delays and excessive airborne holding, with a detrimental effect on the overall (environmental) performance.

The required spacing at the intermediate fix varies per aircraft pair, because of differences in speed and altitude profiles between aircraft. Figure 1-7 shows the distribution of the required spacing for a 63 NM CDO procedure. The distribution was created using flight data of aircraft on nightly approach to Amsterdam Airport Schiphol, the Netherlands. All aircraft followed the mandatory CDO procedure from the same IAF. The 95% confidence interval of the required spacing ranged from 5 NM to 16 NM. Using a fixed spacing interval would result in a significant capacity penalty. For example, assuming an entry speed between 300 and 350 kts and 16 NM spacing yields a 19 – 22 aircraft per hour throughput. Tailoring of the aircraft spacing based on future trajectories is needed to provide the same capacity as conventional procedures.

The environmental performance of closed-path CDO procedures is better than that the performance of open-path procedures. Although most modern aircraft are able to fly closed-path CDO procedures, the use of these procedures is limited. Most aircraft still follow conventional approach procedures, while at some airports open-path CDO procedures are used. Closed-path CDOs in high-density traffic are an integral part of the SESAR and NextGen ATM concepts that are currently being developed and implemented [22, 23].
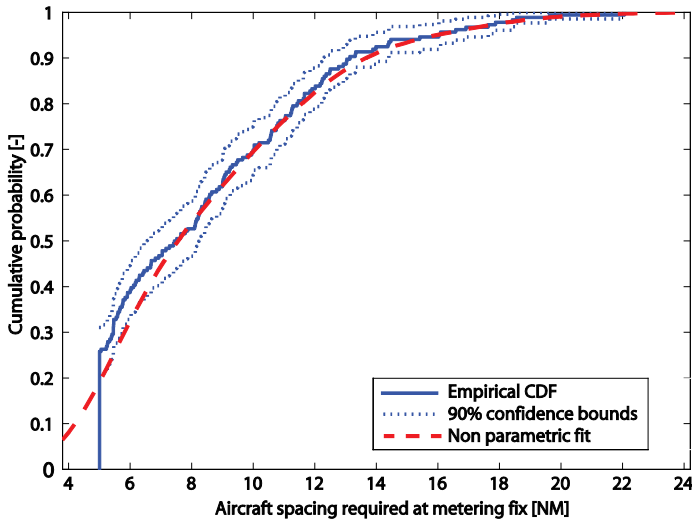
Figure 1-7 Variation of the required spacing at the start of a 63 NM CDO procedure at Amsterdam Airport Schiphol.

1.4 Problem Statement

Closed-path CDO procedures provide insufficient capacity in order to be used in high-density traffic, due to trajectory unpredictability from the ATCO's perspective. Large spacing buffers are used to account for the trajectory unpredictability and therefore avoid tactical interventions during the CDO.

In the current ATM system it is the task of the ATCO to determine the required spacing at the start of the CDO. The ATCO will base the spacing on mental projections of future aircraft behavior. However, Reynolds et al. showed in Ref. [24] that the ability of the ATCO to project future aircraft behavior is insufficient. The transitional nature of the CDO and the long prediction horizon result in low precision of the projections. The ATCO applies arbitrarily large spacing buffers to account for the trajectory unpredictability at the cost of capacity.

In an ATM system that enables CDO in high-density traffic, the dependency on the ATCO's projection capabilities must be reduced. Features of such an ATM system may include:

- Support tools that help ease the projection task for the ATCO;
- Delegation of the spacing task to the flight crew or an automation system;
- CDO procedures which are easier to predict by the ATCO.

Decision support and delegation of the spacing task both entail increased use of automation systems. In these systems extensive use is made of trajectory prediction (TP). The TP performance determines to great extent the operational performance. Accurate TP of the aircraft behavior during CDO is a prerequisite for CDO in high-density traffic. Important input parameters are the actual aircraft state and meteorological conditions.

1.5   Scope and Objectives of Thesis

The ultimate goal of this thesis is the development of an ATM system that facilitates CDO in high-density traffic. Within the scope of this thesis are two of the features of such a system:

- Delegation of the spacing task during the CDO phase (self-spacing);
- Controller support for accurate arrival time control for CDO.

Also two enabling technologies for the above features are addressed:

- Meteorological data acquisition;
- Ground-based trajectory prediction.

Figure 1-8 gives a schematic representation of the general scope and the four resulting objectives. The following sections address the objectives in more detail.
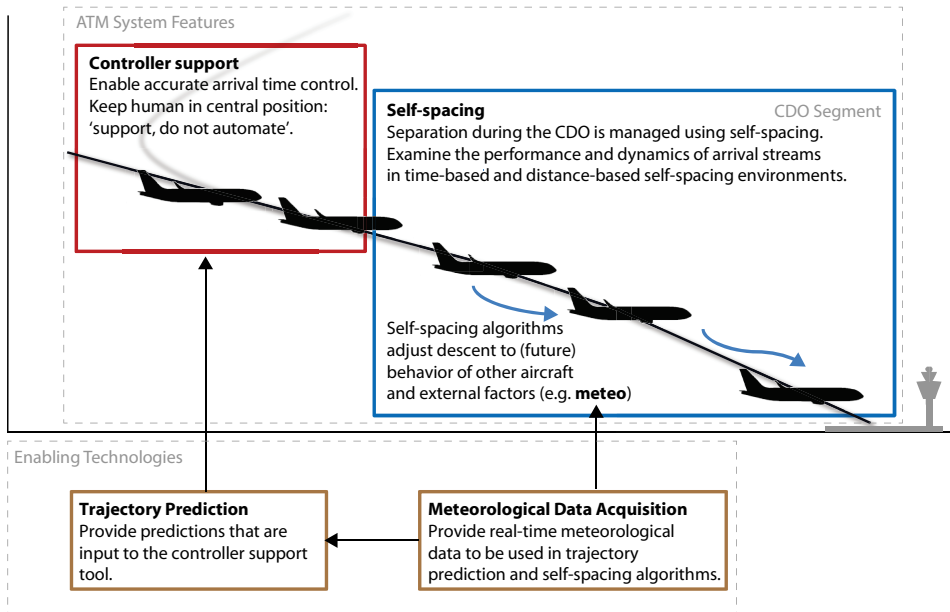
Figure 1-8 Schematic representation of scope and objectives.

1.5.1 Meteorological data acquisition

Sources of meteorological data are aircraft observations that are relayed or estimation from radar surveillance data [25-29]. The number of observations that is relayed to the ground is limited and communication costs are high. Using secondary surveillance radar a large number of observations can be made, but depending on the method additional bandwidth is used. Using both systems the meteorological data is only available on the ground. An uplink is required to make the data available onboard the aircraft. Examples of systems uplinking meteorological data are Boeing Wind Updates and the Avtech Aventus Nowcast system [30, 31]. The thesis objective is to develop and validate methods to infer meteorological data from ADS-B data both on the ground and onboard the aircraft. ADS-B is a surveillance system based on aircraft autonomously transmitting position and velocity information. ADS-B is expected to replace radar surveillance and to expand surveillance coverage. Advantages of using ADS-B to acquire meteorological data are the use of existing data-link and communication protocols, the (future) availability of the data on the ground and onboard the aircraft. There are no additional costs or bandwidth for the uplink or downlink of meteorological data. Most commercial aircraft are already equipped to broadcast ADS-B data and these data can be used by any ADS-B user to acquire meteorological data.

1.5.2 Ground-based Trajectory Prediction

Typically, kinematic or kinetic models are used for the TP. Such models required explicit modeling of aircraft performance, control strategy, airspace, and procedures. These models and input data are not always available on the ground or onboard the aircraft, as discussed in for example Refs. [32, 33]. Some data is commercially sensitive or a data link to exchange the data is not available. The objective here is to explore the use of machine learning techniques to generate predictions for arrival management. Using machine learning techniques, trajectory predictions can be made without explicit modeling. Instead, predictive models are trained to predict aircraft trajectories based on historical aircraft trajectory and meteorological data that is readily available. During the training, the model parameters are tuned to minimize prediction error.

1.5.3 Self-spacing to manage separation during the CDO

The objective is to give insights in the runway capacity that can be expected and the effect of operational aspects on the performance of two self-spacing concepts. These concepts are absolute time-based and relative distance-based self-spacing and were developed earlier at Delft University of Technology [34-38]. In the self-spacing concepts the flight crew plans and executes with the help of onboard systems a CDO to remain safely separated. Main difference between the two concepts is the interaction between aircraft during the descent. In the relative distance-based concept, the aircraft actively reacts to the behavior of the preceding aircraft to stay separated. In the absolute time-

spacing concept there is no interaction between aircraft. Instead thereof, a required time over the runway threshold is assigned to each aircraft at the start of the descent to ensure separation. The self-spacing algorithms and pilot support interfaces are described in Refs. [34-38]. In this research the behavior of individual aircraft or aircraft pairs was studied. In this thesis the step is made to simulate arrival streams. These simulations are used to compare the performance of the two self-spacing concepts in terms of safety, capacity, and environment in arrival streams. Also the dynamics of the arrival streams are examined for their stability.

1.5.4 Controller Support for CDO

Delft University of Technology developed the Time Space Diagram (TSD) which provides the ATCO with tools and information to manage CDO in high-density traffic [39-41]. In this thesis the latest iteration of the interface design is described.
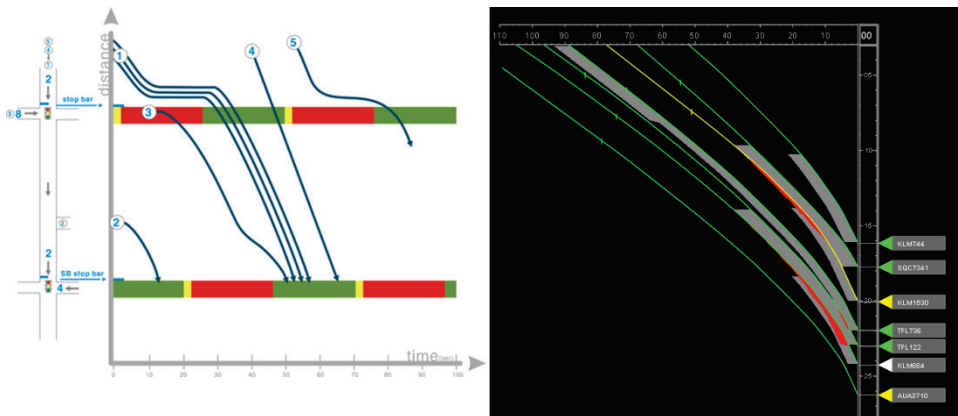
Figure 1-9 Left: Time-space diagram used for traffic signal timing,
Source: Ref. [43]. Right: Time Space Diagram controller support tool.

Time-space diagrams are commonly used to investigate transportation related problems, where traffic shares a common path [42]. The left part of Figure 1-9 gives an example of a time-space diagram used in traffic and highway engineering to analyze a coordination strategy and modify timing plans for traffic signals [43]. The Time-Space Diagram is a visual tool to estimate vehicle delay, stops, queuing, and progression opportunities. The right part of Figure 1-9 gives an impression of the TSD developed to support the ATCO to enable CDO. The TSD is presented on a second display next to the Plan View Display (PVD) and gives a graphical representation of the current and future traffic situation in the time-space reference frame. In PVD-TSD interface information is presented on two displays in different reference frames.

In evaluations of the interface, ATCOs reported difficulties integrating information displayed on the PVD and TSD in one mental picture [41]. The concept of visual momentum developed by Woods [44] provides a series of techniques to support the rapid comprehension of data following the transition to a new display. The concept of visual momentum is applied to the PVD-TSD interface design to make working with the PVD-TSD interface easier. Direct Manipulation Interfaces (DMIs) are developed that provide solution guidance [45]. The DMIs replace the static what-if tools, which proved cumbersome in the previous version [41].

The effects of the PVD-TSD interface on the benefits of the PVD-TSD interface on ATCO's workload, ATCO's situation awareness, safety, capacity, and efficiency are examined in a human-in-the-loop experiment. The PVD-TSD is tested against a more conventional support solution that provides the required spacing and time to loose or gain in tabular form.

1.6   Assumptions

An ATM system that facilitates CDO in high-density traffic encompasses more procedures, processes, and systems and other traffic than can be addressed in this thesis. Therefore, the following main assumptions are made:

Arrivals Only

Departing and crossing traffic are both omitted. Strategic de-confliction from other traffic is foreseen during the CDO phase. However, departing and crossing traffic is likely to be present in the same airspace where merging, sequencing, and spacing for CDO takes place. Departing and crossing traffic do not affect the arrival sequence or required spacing. The presence of other traffic might inhibit the realization of the optimal sequence and exact spacing of arriving traffic, and result in higher workload levels. These effects are not accounted for here.

Trajectory Uncertainty

TP uncertainty has not been addressed in the design of the TSD support tool. However, including TP uncertainty is considered to be an important next step in development.

In addition to the above the following is assumed:
- All aircraft are fully equipped and capable;
- One runway is used for arrivals only;
- No runway changes;
- All flights are longer than the maximum prediction horizon;
- Normal operations (e.g., no emergencies and adverse weather).

System Wide Information Management

For the work on the TSD tool and self-spacing it is assumed that System Wide Information Management (SWIM) is available to exchange data (e.g., 4D trajectories, aircraft intent). SWIM facilitates ground-ground, air-ground, and air-air communication and is a key element of the SESAR and NextGen concepts.

1.7   Thesis Outline

Figure 1-10 gives a graphical representation of the outline of this thesis. This thesis consists of six chapters. The research that was conducted is described in Chapters 2 to 5. A discussion of the results and conclusions are given in Chapter 6.

ATM System Features

Controller support (Chapter 5)
Enable accurate arrival time control.
Keep human in central position:
'support, do not automate'.

Self-spacing (Chapter 4)   CDO Segment
Separation during the CDO is managed using self-spacing.
Examine the performance and dynamics of arrival streams
in time-based and distance-based self-spacing environments.

Self-spacing algorithms
adjust descent to (future)
behavior of other aircraft
and external factors (e.g., **meteo**).

Enabling Technologies

Trajectory Prediction (Chapter 3)
Provide predictions that are
input to the controller support
tool.

Meteorological Data Acquisition (Chapter 2)
Provide real-time meteorological
data to be used in trajectory
prediction and self-spacing algorithms.

Figure 1-10 Thesis Outline.

In the first two chapters the work on the enabling technologies is presented. Chapter 2 describes the methods to derive meteorological conditions from ADS-B data. The machine learning approach to TP is presented in Chapter 3. Chapters 4 and 5 address the ATM system features that were investigated. Chapter 4 presents the results of an extensive Monte-Carlo simulation study of the self-spacing concepts. Finally, Chapter 5 discusses the PVD-TSD interface.

Chapters 2 to 5 consist of papers that have been (or are to be) published in peer reviewed scientific journals and conference proceedings. Minor changes have been

made to these publications for consistent use of terminology and symbols throughout the thesis. These chapters can be read independently from each other. The following sections give a short description of the publications in relation to the overall research presented in this thesis.

Chapter 2 – Using Surveillance Data for Meteorological Data Acquisition
Methods to estimate wind, pressure, and temperature from aircraft surveillance data are presented. Methods are developed for use with the ADS-B system. The methods are validated using 130 days of ADS-B data collected around Amsterdam Schiphol and GFS forecasts. It is demonstrated that ADS-B provides a data source to acquire meteorological data in real-time both on the ground and onboard the aircraft without the need for additional communication protocols.

Chapter 3 - A Machine Learning Approach to Trajectory Prediction
A machine learning approach to trajectory prediction is presented. The trajectory prediction problem is defined as a supervised learning regression problem. The developed approach is applied to a CDO procedure used at Amsterdam Airport Schiphol. The prediction performance is quantified using the along track error and time error. Finally, the effect of the prediction performance on the runway throughput for CDO is analyzed.

Chapter 4 – Self-Spacing to Increase Capacity for Continuous Descent Operations
The setup and results of a series of Monte-Carlo simulations are discussed. In the simulations arrival streams of eight aircraft are simulated in a relative distance-based or absolute time-based self-spacing environment. These self-spacing concepts are used in combination with the Three-Degree Decelerating Approach (TDDA) that gives control over the speed-profile of the descent to perform the spacing task [46]. Simulation results include the runway throughput, arrival delay, and the number of separation losses. For the relative distance-based spacing concept a sensitivity study is performed to assess the effects of operational aspects and arrival time uncertainty of the performance.

Chapter 5 – A Time-Space Diagram based Controller Support Tool
The PVD-TSD support tool is presented. As outlined earlier, one of the objectives of the work described in the thesis is to improve working with the multi-display PVD-TSD interface. An evaluation of the PVD-TSD interface according to the concept of visual momentum is given. Subsequently, changes made to the interface design improving visual momentum are discussed. Furthermore, five DMIs for typical controller actions are discussed. The PVD-TSD interface with the changes for enhanced visual momentum and DMIs is validated in a human-in-the-loop experiment. The experiment is also used to the PVD-TSD interface against a more conventional stack list support solution. The stack list

visualization provides the ATCO with the required initial spacing and requires minimal changes to the existing interface.

The research described in this thesis is the result of a four year research project "*Dag en Nacht Stiller Landen*". This project was funded in part by a "*Casimir*" grant by the Netherlands Organisation for Scientific Research (NWO). This grant was awarded to the author in 2008 (grant number 018.003.022).

1.8   References

1. ICAO, "Guidance on the Balanced Approach to Aircraft Noise Management," Doc. 9829-AN/451, Second Edition, 2008.
2. ICAO, "Continuous Descent Operation Manual," Doc. 9931 AN/479, advanced edition, 2010.
3. Wilson, I., and Hafner, F., "Benefit assessment of using continuous descent approaches at Atlanta," *The 24th Digital Avionics Systems Conference Proceedings*, Institute of Electrical and Electronics Engineers, Vol. 1, Washington, DC, 2005, pp. 2.B.2- 2.1-7.
    DOI: 10.1109/DASC.2005.1563318
4. Dinges, E., "Determining the Environmental Benefit of Implementing Continuous Descent Approach Procedures," USA/Europe Air Traffic Management Research and Development Seminars, Paper 17, July 2007.
5. Coppenbarger, R.A., Mead, R.W., and Sweet, D.N., "Field Evaluation of the Tailored Arrivals Concept for Datalink-Enabled Continuous Descent Approaches," AIAA Paper 2007-7778, 2007.
6. Wubben, F.J.M., and Bussink, J.J., "Environmental Benefits of Continuous Descent Approaches at Schiphol Airport Compared with Conventional Approach Procedures," National Aerospace Laboratory, TR NLR-TP-2000-275, Amsterdam, The Netherlands, May 2000.
7. Clarke, J.-P.B., Tan Ho, T., Ren, L., Brown, J.A., Elmer, K.R., Tong, K., and Wat, J.K., "Continuous Descent Approach: Design and Flight Test for Louisville International Airport.", *Journal of Aircraft*, Vol. 41, No. 5, 2004, pp. 1054-1066. DOI: 10.2514/1.5572
8. Elmer, K., Wat, J., Shivashankara, B., McGregor, D., and Lambert, D., "A Continuous Descent Approach Study using Ames B747-400 Flight Simulator," *AIAA Aircraft Technology Integrationand Operations ATIO*, 2002, pp. 1–9.
9. Zalovick, J.A., and Schaefer, W.T. Jr., "NASA Research on noise-abatement approach profiles for multiengine jet transport aircraft," Technical Note NASA TN-D-4044, Hampton (VA), USA, June 1967.
10. Schwind, G.K., Morrison, J.A., Nylen, W.E., and Anderson, E.B., "Flight Evaluation of the Two-Segment Approaches Using Area Navigation Guidance Equipment," NASA Contractor Report, NASA CR-2679, United Airlines, USA, April 1976.
11. Anon., "Low Drag, Low Noise," *Flight International*, September 25, 1975.
12. Anon., "The German way," *The Economist*, September 20, 1975.

13. Wilson, A., "'Gliding' Jets halve the noise," *The Observer*, September 21, 1975

14. Dibley, H., "How to Reduce Noise and Save Fuel - Now," *Journal of the Guild of Air Pilots and Air Navigators*, March 1974.

15. Dibley, H., "Aircraft Operational Fuel Savings & Noise Reductions Past and Future," Conference European Air and Space, October 27 2009.

16. Erkelens, L.J.J., Research into New Noise Abatement Procedures for the 21st Century. *AIAA Guidance, Navigation, and Control Conference & Exhibit*, AIAA 2000-4474, Denver (CO), USA, August, 2000.

17. Clarke, J.-P.B., "Systems Analysis of Noise Abatement Procedures Enabled by Advanced Flight Guidance Technology", *Journal of Aircraft*, Vol. 37, No. 2, 2000, pp. 266-273. DOI: 10.2514/2.2590

18. Koeslag, M.F., Advanced Continuous Approaches, an Algorithm Design for the Flight Management System, Technical Report NLR-TR-2001-359, National Aerospace Laboratory (NLR), Amsterdam, The Netherlands, March 1999.

19. Tan Ho, N., and Clarke, J.-P.B.,"Mitigating Operational Aircraft Noise Impact by Leveraging on Automation Capability", AIAA Paper 2001-5239, 2001.

20. Kershaw, D., Rhodes, D.P., and Smith, N.A., "The influence of ATC in approach noise abatement," *3rd USA-Europe Air Traffic Management RD Seminar*, Napoli, Italy, June 2000.

21. EUROCONTROL, *A guide to implementing Continuous Descent*, October 2011.

22. EUROCONTROL, "SESAR Master Plan D5: SESAR Definition Phase - Milestone Deliverable 5" DLM-0710-001-02-00, SESAR Consortium for the SESAR Definition Phase Project co-funded by the European Commission and EUROCONTROL, April 2008.

23. Joint Planning and Development Office (JPDO), "NextGen Integrated Work Plan: A Functional Outline," Tech. rep., Joint Planning and Development Office, 2008.

24. Reynolds, H.J.D., Reynolds, T.G., and Hansman, R.J., "Human Factors Implications of Continuous Descent Approach Procedures for Noise Abatement in Air Traffic Control," 2005.

25. Stickland, J., and Grooters, A.T.F., "The Global AMDAR Programme," *International Symposium on Remote Sensing of Environment, Saint Petersburg, Russia,* 2005. DOI: 10.1.1.141.2511

26. AMDAR Panel, "Aircraft Meteorological Data Relay (AMDAR) Reference Manual," Tech. rep., World Meteorological Organization, 2003.

27. de Haan, S., "High-Resolution Wind and Temperature Observations from Aircraft Tracked by Mode-S Air Traffic Control Radar," *Journal of Geophysical Research*, Vol. 116, No. D10, May 2011, pp. 1–13. DOI:10.1029/2010JD015264

28. Delahaye, D., and Puechmorel, S., "TAS and wind estimation from radar data," *Digital Avionics Systems Conference 2009,* IEEE, Orlando, FL, 2009, pp. 2.B.5-1 - 2.B.5-16. DOI: 10.1109/DASC.2009.5347547

29. Hollister, W.M., Bradford, E. R., and Welch, J.D., "Using Aircraft Radar Tracks to Estimate Wind Aloft," *The Lincoln Laboratory Journal*, Vol. 2, No. 3, 1989, pp. 555-565.

30. Durham, M., "InFlight Optimization Services Offers Airliners More Fuel-Efficient En-Route Operations", *AERO Quarterly*, Boeing Commercial Airplanes, Seattle, 2011.

31. AVTECH, *"Aventus Nowcast^{TM} Great fuel savings by accurate wind information,"* Product sheet, 2012.

32. Coppenbarger, R.A., "En Route Climb Trajectory Prediction Enhancement Using Airline Flight-Planning Information." *AIAA Guidance Navigation and Control Conference*, 1999.

33. Bronsvoort, J., McDonald, G., Paglione, M., Garcia-Avello, C., Bayraktutar, I., and Young, C. M., "Impact of missing longitudinal aircraft intent on descent trajectory prediction," *IEEE/AIAA 30th Digital Avionics Systems Conference*," Seattle (WA), USA, pp. 3E2-1 - 3E2-14, December, 2011. DOI: 10.1109/DASC.2011.6096062

34. in 't Veld, A.C., Self-Spacing Algorithms for Continuous Descent Approaches, Ph.D. Dissertation, Delft University of Technology, Delft, The Netherlands, June 2011. ISBN 978-90-8570-765-3.

35. de Gaay Fortman, W.F.M., van Paassen, M.M. ,Mulder, M., in 't Veld, A.C., and Clarke, J.-P.B., "Implementing Time-Based Spacing for Decelerating Approaches," *Journal of Aircraft*, Vol. 44, No. 1, January-February 2007, pp. 106-118. DOI: 10.2514/1.22253

36. de Prins, J.L., Schippers, K.F.M., Mulder, M., van Paassen, M.M., in 't Veld, A.C., and Clarke, J.-P.B., "Enhanced Self-Spacing Algorithm for Three-Degree Decelerating Approaches," Vol. 30, No. 5, Mar-Apr 2007, pp. 576-590. DOI: 10.2514/1.24542

37. in 't Veld, A.C., van Paassen, M.M., Mulder, M., and Clarke, J.-P.B, "Pilot Support for Self-Separation during Decelerating Approaches," AIAA Paper 2004-5102, 2004.

38. de Beer, B.A.F., Mulder, M., van Paassen, M.M., and in't Veld, A.C., "Development of an Ecological Interface for the Three-Degree Decelerating Approach," AIAA Paper 2008-7108, 2008.

39. Vicente, K.J., and Rasmussen, J. Ecological interface design: theoretical foundations. *IEEE*, 1992, pp. 589-606.

40. Tielrooij, M., in 't Veld, A.C., Mulder, M., and van Paassen, M.M., "Development of a Time-Space Diagram to Assist Air Traffic Controllers in Monitoring Continuous Descent Approaches," *Air Traffic Control*, edited by M. Mulder, Sciyo, Rijeka, Croatia, August 2010, pp. 135- 147.

41. van der Eijk, A., Borst, C., Mulder, M., van Paassen M.M., and in't Veld, A.C. "Assisting Air Traffic Control in Planning and Monitoring Continuous Descent Approach Procedures," *Journal of Aircraft*, Vol. 5, No. 5, 2012, pp. 1376-1390. DOI: 10.2514/1.C031686

42. Garber, N.J., and Hoel, L.A., *Traffic & Highway Engineering*, University of Virginia, Cengage Learning Engineering, 2010.

43. United States Department of Transport, *Traffic Signal Timing Manual*, Kittelson & Associates. Inc., Cengage Learning Engineering, June 2008.

44. Woods, D.D., "Visual Momentum: A concept to improve the cognitive coupling of person and computer," *International Journal of Man-Machine Studies*, Vol. 21, No. 3, September 1984, pp. 229-244.

45. Kaber, D.B., Riley, J.M., Tan, K., and Endsley, M.R., "On the design of adaptive automation for complex systems.," *International Journal of Cognitive Ergonomics*, Vol. 5, 2001, pp. 37-57.

46. Ren, L., Clarke, J.-P.B., and Tan Ho, N., "Achieving Low Approach Noise Without Sacrificing Capacity," Institute of Electrical and Electronics Engineers,Vol. 1, Piscataway, NJ, 2003, pp.1.E.3- 1.1-9. DOI: 10.1109/DASC.2003.1245810

2 Using Automatic Dependent Surveillance-Broadcast for Meteorological Data Acquisition

Methods to estimate wind, pressure, and temperature from aircraft surveillance data are presented. Methods are developed for use with the Automatic Dependent Surveillance Broadcast (ADS-B) system. The methods are validated using 130 days of ADS-B data collected around Amsterdam Airport Schiphol and Global Forecast System forecasts. It is demonstrated that ADS-B provides a data source to acquire meteorological data in real-time both on the ground and onboard the aircraft without the need for additional communication protocols.

Abstract

The use of Automatic Dependent Surveillance-Broadcast (ADS-B) for meteorological monitoring is explored. Although originally developed for surveillance, the data that the system provides can be used to estimate wind, pressure, and temperature profiles. Two methods for estimating wind speed and direction are presented. These make use of velocity vector information from a single aircraft or multiple aircraft, respectively. Air pressure is derived from the barometric altitude and height above the World Geodetic System 1984 ellipsoid. From this pressure estimate the temperature in the troposphere is estimated, using the hydrostatic equilibrium and the ideal gas law. To validate the methods, ADS-B data were collected over a 100 day period and the resulting estimates compared to Global Forecast System forecasts. Estimating wind using velocity information from one aircraft resulted in a low number of estimates for which relatively large track angle sweeps were needed. When using data from multiple aircraft, more accurate wind estimates could be produced, at fixed time intervals and at altitude intervals between 4000 ft and 40,000 ft. The mean absolute errors for wind speed and direction estimates were 9.2 kt and 29.0 deg, respectively. The mean error for pressure and temperature estimates made between 1000 ft and 36,000 ft ranged from -1.1 hPa to 1.0 hPa and from 0.2 K to 1.3 K, respectively. The maximum mean absolute errors for the pressure and temperature estimates were 1.5 hPa and 2.4 K, respectively.

2.1   Introduction

Automatic Dependent Surveillance-Broadcast (ADS-B) is a surveillance technique based on aircraft autonomously transmitting position and velocity information along with other data.[1, 2] The past years have seen more and more aircraft being ADS-B equipped. The wide availability of ADS-B receivers at relatively low cost makes ADS-B an interesting and accessible data source for various applications, including meteorological monitoring.

The availability of more accurate meteorological data has been identified as one of the enablers for improved navigation, planning, and trajectory prediction.[3-6] Aircraft in-situ measurements made using dedicated onboard equipment, e.g., the measurements made onboard aircraft that participate in the Aircraft Meteorological Data Relay (AMDAR) program, form one of the available sources of meteorological data.[7, 8] Broadcast of these meteorological data using ADS-B is being investigated.[9, 10] Alternatively, meteorological circumstances can be estimated from surveillance data, as was shown in Refs. [11-13]. Secondary Surveillance Radar (SSR) position and speed data, possibly supplemented with Downlink Airborne Parameters (DAP) are used to determine wind, temperature, and pressure.

In this paper we will describe methods to estimate meteorological data from standard ADS-B surveillance data. As these ADS-B data are already being broadcast, no additional bandwidth or new communication protocols are required. We will also compare our wind, pressure, and temperature estimates with Global Forecast System (GFS) forecasts.

Methods described by De Haan and Stoffelen in Ref. [11] for estimating wind, pressure, and temperature from Mode-S data cannot be readily applied to ADS-B data, because the Mach number, aircraft heading, and true airspeed (TAS) are not broadcast. Delahaye and Puechmorel, and Hollister et al. in Refs. [12, 13] describe methods to estimate wind from the ground velocity vector of a single aircraft that completes a turn. This method can also be used here, as ADS-B provides ground velocity vector information measured using a Global Navigation Satellite System (GNSS). In this paper we use a Modified Extended Kalman Filter to estimate the wind recursively from an aircraft in a turn. In addition, we use a new method to estimate wind using data from multiple aircraft. This method was first described by the authors in Ref. [14] and has been further developed and validated. It is assumed that aircraft at the same altitude travel – on average – at the same TAS in all directions. This enables estimating wind for a larger area at fixed time and altitude intervals.

To estimate pressure we make use of the barometric altitude and the difference between the barometric altitude and the GNSS height above the ellipsoid (HAE), both of which ADS-B provides. This method can be seen as the reverse approach of the height monitoring processes for Reduced Vertical Separation Minimum operations using ADS-B [15], and was also recently described in Ref. [16]. In case of height monitoring use is made of meteorological data to determine the actual height of the aircraft. The method to estimate temperature is an extension of the method to estimate pressure. Assuming air is an ideal gas, the temperature can be derived from the pressure profile, using the hydrostatic equilibrium and the ideal gas law.[17]

This paper is organized as follows: In Section 2.2 the elements of the ADS-B system relevant for meteorological monitoring are described. Two methods for estimating the wind speed and direction from ADS-B messages are presented in Section III. Methods to estimate pressure and temperature are presented in Section 2.4. The setup and results of the comparative analyses are given in Sections V and 5.6. Sections 5.7 and 2.8 contain the discussion of the results and conclusions.

2.2   Automatic Dependent Surveillance-Broadcast

Our discussion of the ADS-B system is limited to a short introduction and a list of data parameters that are relevant for meteorological monitoring. For more information on the ADS-B system, see Refs. [1, 2].

2.2.1 Equipage and Coverage

ADS-B is anticipated to replace radar surveillance and expand surveillance into areas currently lacking radar surveillance for the provision of Air Traffic Services.[18] Current deployment areas include Australia, the Hudson Bay, and the Gulf of Mexico. Also, the reception of ADS-B by aircraft (referred to as ADS-B In) is foreseen. Although broadcast of ADS-B data is not yet mandated, the equipage level is relatively high. Based on the aircraft transponder identifications in Mode-S interrogation replies and ADS-B messages in Western Europe, the current equipage level is estimated at 75% to 80% for commercial aircraft. The equipage level for aircraft used in general aviation is still very low.

The ability to receive ADS-B data from an aircraft depends on the aircraft altitude, distance from the receiver, obstructing terrain and buildings, and weather conditions. The maximum range for the reception of data from high altitude traffic is approximately 250 NM.

2.2.2 Relevant Parameters

In this paper we use ADS-B data output by the Mode-S transponder with extended squitter interpreted following the version 0 format.[1] The data includes the aircraft state and other information. Table 2-1 gives an overview of the parameters relevant for meteorological monitoring.

Table 2-1 does not include the TAS and magnetic heading that would enable direct derivation of the wind from the aircraft state information. ADS-B messages can contain the TAS and magnetic heading.[1] However, analysis of recorded data showed that only a very limited number of aircraft broadcast these, and never in combination with the ground speed components.

The Navigational Uncertainty Category (NUC) for position and rate information provides an indication of either accuracy or integrity. The NUC_p ranges from 0 to 9. The accuracy or integrity level increases with the NUC value. Data with a $NUC_p < 5$ is considered low integrity data. Data analysis showed typical NUC_p values are 5 (14%), 6 (26%), and 7 (33%). Position data from aircraft broadcasting a NUC_p of 0 (25%) is in most cases very inaccurate and determined using a different sensor than GNSS.

Table 2-1 Parameters broadcast over ADS-B relevant for meteorological monitoring.

Parameter	Unit	Resolution
Position (WGS 84)	deg	85 ft
Barometric pressure altitude	ft	25 ft or 100 ft
Difference between barometric altitude and GNSS height above the WGS 84 ellipsoid	ft	25 ft

Parameter	Unit	Resolution
North – South ground speed	kts	1 kts
East – West ground speed	kts	1 kts
Navigational Uncertainty Category – position (NUCp)	figure of merit	
Navigational Uncertainty Category – rate (NUCr)	figure of merit	

2.3 Wind Estimation

Figure 2-1 shows the relation between airspeed, ground speed, and wind in the horizontal plane. The ground speed vector is the sum of the airspeed and wind vectors:

$$\overline{V}_g = \overline{V}_a + \overline{V}_w ,$$

(2-1)

where $\overline{V}_g$ is the aircraft speed relative to the ground, $\overline{V}_a$ the aircraft speed relative to the air and $\overline{V}_w$ the speed of the wind relative to the ground. Wind can be estimated from a series of observations of the aircraft ground speed vector at different track angles.[12,13]
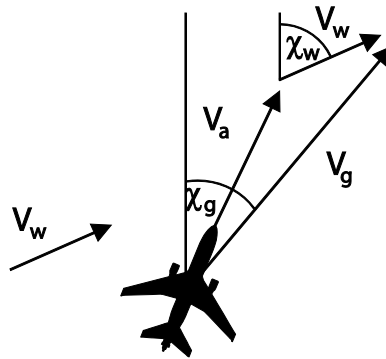
Figure 2-1 Relation between airspeed, ground speed, and wind vector.

2.3.1 Wind estimate using one aircraft

To estimate the wind from the ADS-B data from one aircraft, the east and north components of the aircraft true airspeed are written as:

$$V_{a_x} = \left\| V_g \right\| \sin \chi_g - \left\| V_w \right\| \sin \chi_w ,$$

(2-2)

and:

$$V_{a_y} = \left\| V_g \right\| \cos \chi_g - \left\| V_w \right\| \cos \chi_w ,$$

(2-3)

where χ_g and χ_w are the angles of the ground speed and wind vector with respect to the north. It follows that during a turn at constant airspeed and wind vector:

$$\left\| V_a \right\|^2 - \left(\left\| V_g \right\| \cos \chi_g - \left\| V_w \right\| \cos \chi_w \right)^2 - \left(\left\| V_g \right\| \sin \chi_g - \left\| V_w \right\| \sin \chi_w \right)^2 = 0 \qquad (2\text{-}4)$$

Eq. (2-4) is treated as a nonlinear least-squares problem with measurement vector:

$$\overline{x} = \left[\left\| V_g \right\|, \chi_g \right], \qquad (2\text{-}5)$$

and solution vector:

$$\overline{w} = \left[\left\| V_a \right\|, \left\| V_w \right\|, \chi_w \right], \qquad (2\text{-}6)$$

that minimizes:

$$\sum_{i=0}^{t} \left\| y_i - \gamma(\overline{w}, \overline{x}_i) \right\|^2, \qquad (2\text{-}7)$$

where y_i and $\gamma(\overline{w}, \overline{x})$ are equal to the right (0) and left parts of Eq. (2-4), respectively.

To solve this nonlinear least-squares problem recursively, a Modified Extended Kalman Filter (MEKF) algorithm is used [19]: For $t = 0, 1, 2,..n$ the solution is:

$$\overline{w}_{t+1} = \overline{w}_t + K_t \left[y_t - \gamma(\overline{w}_t, \overline{x}_t) \right], \qquad (2\text{-}8)$$

where:

$$H_t = \left. \frac{\partial \overline{\gamma}(\overline{w}, \overline{x})}{\partial \overline{w}} \right|_{\overline{w}=\hat{w}_t, \overline{x}=\overline{x}_t}, \qquad (2\text{-}9)$$

$$K_t = P_t H_t^T \left(H_t P_t H_t^T + R_t \right)^{-1},$$
$$P_{t+1} = (\alpha + 1)\left(P_t - K_t H_t P_t + \varepsilon I \right), \qquad (2\text{-}10)$$

and $\alpha > 0$, $\varepsilon > 0$, and P_0 and R_t are symmetric positive definite covariance matrices.

Figure 2-2a shows an example of the MEKF applied to actual ground speed and track angle data of a single aircraft flying a holding pattern. During approximately one full holding pattern of approximately 400 s, 718 airborne position reports and 291 airborne velocity reports were received, respectively. The altitude was constant, and it is assumed that the TAS was also constant. Figures 2b, c, and d show the solutions determined using the MEKF. Convergence is reached after approximately 100 s and 180˚ change of track angle. In the second half turn, the estimate remains unchanged.
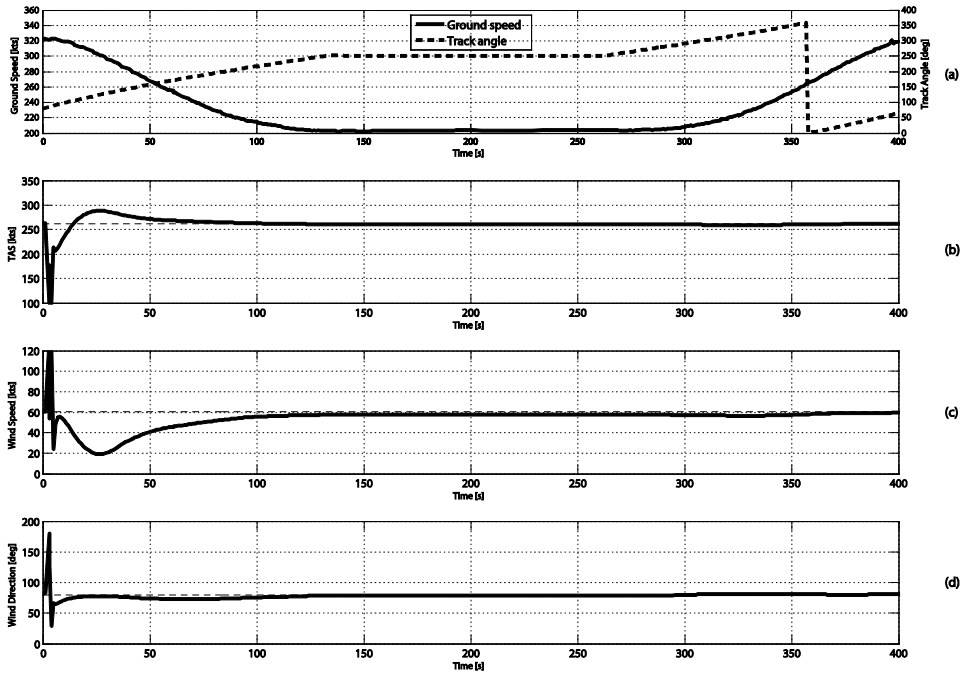
Figure 2-2 Wind estimate based on single aircraft in hold using MEKF.

2.3.2 Wind estimate for a larger area using multiple aircraft

The method outlined in Section 2.3.1 requires multiple measurements of a single aircraft at different track angles. In practice, this limits the number of estimates to the number of aircraft that complete a turn at a constant altitude and TAS. This limitation can be circumvented by assuming that aircraft in the same flight phase at the same altitude travel – on average – at the same TAS in all directions. Using multiple aircraft, a wind estimate for a larger area can be made at any moment at different altitudes, given sufficient aircraft.

Figure 2-3 shows a plot of the north and east component of the ground speed for aircraft travelling at FL300 in different directions. The plot is based on actual ADS-B data. The data points approximate a circle. The circle center is offset from the origin by the wind vector.

The circle equation is given by:

$$\left(V_{g_x} - V_{w_x} \right)^2 + \left(V_{g_y} - V_{w_y} \right)^2 = \left\| \bar{V}_a \right\| \tag{2-11}$$

For *n* observations, the wind can be estimated by minimizing the sum of squares:

$$S = \sum_{i=1}^{n} \left(\left(V_{g_{x_i}} - V_{w_x} \right)^2 + \left(V_{g_{y_i}} - V_{w_y} \right)^2 - \left\| \bar{V}_a \right\|^2 \right) \tag{2-12}$$

This weighted non-linear least-squares problem is solved for $\left\| \bar{V}_a \right\|$ and $\bar{V}_w$.

Data Selection

Aircraft in different flight phases are likely to operate at different airspeeds, as observed in Ref. [14]. Therefore, a wind estimate must be based on data from aircraft that are in the same flight phase. To determine which flight phase to use, the concept of Dilution of Precision (DOP) is used, described in more detail in Ref. [14]. The data set with the lowest DOP-value is selected as the primary data set, in other words the estimate with the lowest dilution of precision. The DOP-value used is equivalent to the Geometric DOP used in satellite navigation systems and is described in Ref. [20]. The DOP value is a measure for the variance of the north and east components of the ground speed.
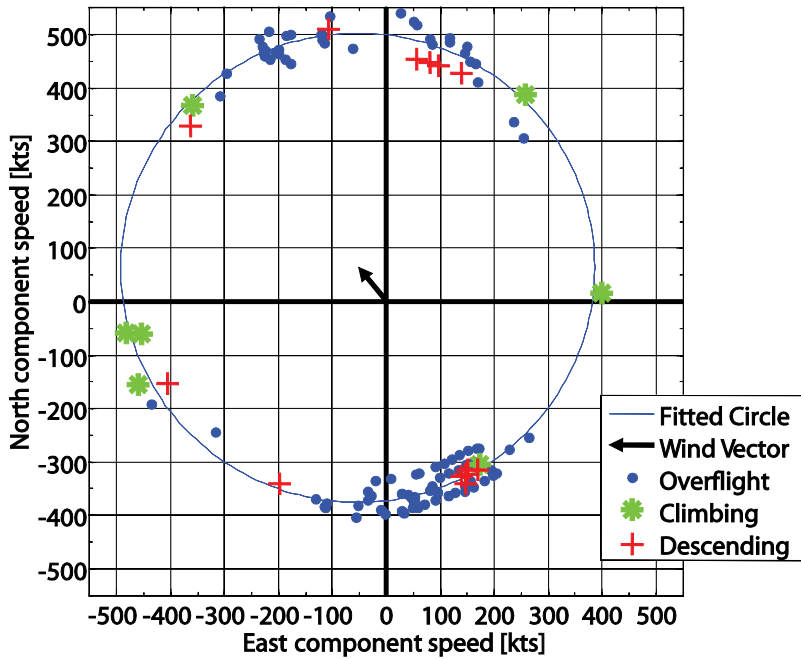
**Figure 2-3 Global estimate for FL300 based on actual ADS-B data
wind direction 310˚ at 83 kts.**

 Figure 2-4 shows the effect of the variance on the estimate for three sets of 100 data points that were simulated. The wind is 20 kts from the west (270 deg). From left to right, the DOP value decreases from 4.4 to 1.2 and finally to 1.0, and the wind estimate converges to the forecast condition.
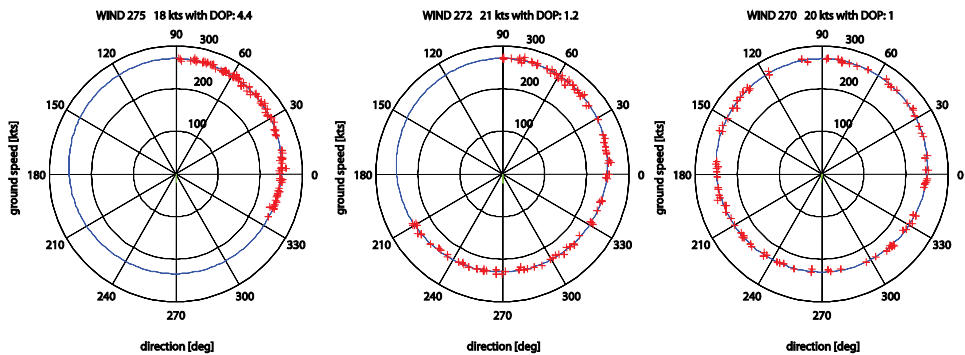
Figure 2-4 Dilution of Precision due to data geometry.

Discrete Kalman Filter

To integrate the noisy wind estimates into a time-varying wind profile, a discrete Kalman filter was used.[21] The linear stochastic difference equation for state *x*, which comprises the wind direction and speed at time-step *k*, is given by:

$$x_k = x_{k-1} + w_k,$$ (2-13)

with measurement:

$$z_k = x_k + v_k.$$ (2-14)

The random variables w_k and v_k represent the process and measurement noise, respectively. The process noise is assumed to be a constant, white, zero mean noise signal with covariance noise matrix Q. The measurement noise is also assumed to be white, zero mean with covariance matrix R.

The Kalman filter is initialized with estimates of the state $\hat{x}_{k-1}$ and error covariance matrix P_{k-1}. The filter estimates the state and then obtains feedback in the form of a new measurement. These two steps are commonly referred to as the time update and measurement update respectively. In the time update the state estimate and error covariance at time step *k-1* are projected to time step *k*:

$$\hat{x}_k^- = \hat{x}_{k-1},$$ (2-15)

$$P_k^- = P_{k-1} + Q.$$ (2-16)

In the measurement update the Kalman gain *K* is computed and used to update the state estimate and error covariance:

$$K_k = P_k^- (P_k^- + R_k)^{-1},$$ (2-17)

$$\hat{x}_k = \hat{x}_k^- + K_k(z_k - \hat{x}_k^-),$$ (2-18)

$$P_k = (1 - K_k)P_k^-.$$ (2-19)

For the measurement noise covariance matrix *R*, the DOP values under which the wind estimates were made are used. Hence, the filter puts more trust in estimates obtained in a low DOP condition, and less trust in estimates when the DOP is high.

Wind Profile

Figure 2-5 schematically shows the wind estimation process. Ground speed and track data are gathered and sorted continuously. At time step *k* a preliminary DOP value is computed for subsets of arriving, departing, and en-route traffic. Based on the DOP values, one or more subsets are selected to estimate the wind at various altitudes. Based on the forecast estimate, the DOP value is then updated. Finally, the data are filtered using the Kalman Filter. The DOP values become inputs to the filter for computing the measurement error covariance matrix.
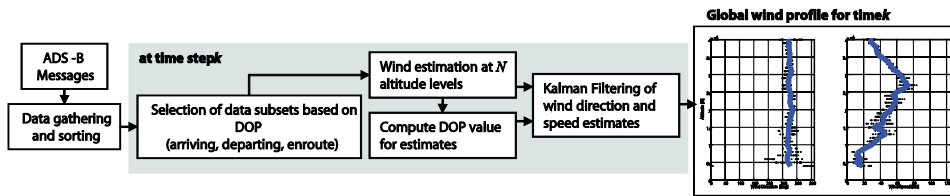
Figure 2-5 Schematic overview of the wind estimation algorithm based on ADS-B data from multiple aircraft.

2.4   Pressure and Temperature Estimation

The air pressure and temperature estimates use the barometric altitude, the difference between the GNSS HAE and the barometric altitude, the hydrostatic equilibrium, and the gas law.

2.4.1 Pressure Estimate

The method to estimate pressure from ADS-B data is illustrated in Figure 2-6. The broadcast barometric altitude is always computed using the International Standard Atmosphere (ISA) pressure datum of 1013.25 hPa. The pressure at the barometric altitude, P_h, follows from:[17]

$$P_h = P_0 \left(\frac{T_0 + \lambda(h - h_0)}{T_0} \right)^{-\frac{g_0 M}{R\lambda}},$$

(2-20)

where P_0 and T_0 are the ISA pressure and temperature at mean sea level h_0, the temperature lapse rate is given by λ, g_0 is the standard gravitational acceleration, M is the molar mass of air, and R the universal gas constant. P_h was measured at the GNSS-height; hence the pressure at the GNSS-height P_{GNSS} is equal to P_h.

Using the difference between the GNSS-HAE and the barometric altitude, the actual GNSS-height of the aircraft can be determined. To obtain a pressure profile, a

polynomial is fitted to the data in a least-squares sense. Equation (2-20) is valid up to the tropopause, which is typically at 36,000 ft. In the stratosphere, the temperature is constant and equals the temperature at the tropopause.[17]
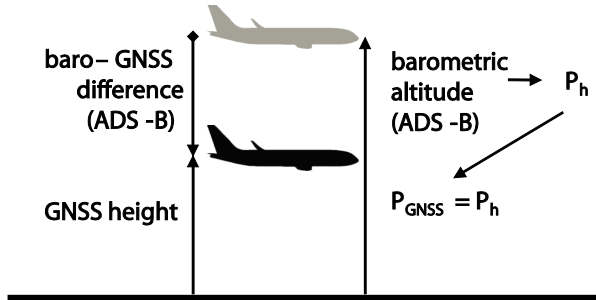
Figure 2-6 Pressure estimate from ADS-B data and ISA.

2.4.2 Air Density and Temperature Estimate

Using the estimated pressure profile and the hydrostatic equilibrium, the density is derived. The hydrostatic equilibrium is given by: [17]

$$\frac{dP}{dh} = -\rho g_0 \text{,}$$

(2-21)

where ρ is the air density. Finally, the temperature is obtained using the gas law:[17]

$$T = \frac{pM}{\rho R}$$

(2-22)

2.5   Validation Setup

To validate the use of the described methods under actual conditions, estimates were made based on ADS-B data collected for a 100 day period. The estimates were compared with Global Forecast System (GFS) forecasts. The GFS is a numerical weather prediction model run by the National Oceanic and Atmospheric Administration.[22]

2.5.1 Global Forecast System

GFS forecasts include wind speed and direction, pressure, and temperature at altitude in grid points. Forecasts for nine grid points in a three-by-three grid were used. Figure 2-7 shows the grid together with the location of Amsterdam Airport Schiphol (AAS) in the approximate center of the grid. The GFS model runs four times a day; estimates were compared to at most a six-hour forecast.

2.5.2 Automatic Dependent Surveillance-Broadcast Data

ADS-B data were collected using three receivers in the Netherlands; see Figure 2-7 for their locations. Data transmitted by aircraft when inside the area enclosed by the eight GFS grid points were used to produce the estimates. On a single day, approximately 450 AAS arrivals and departures and 2750 en route flights were followed, transmitting a total of six million ADS-B messages. Only data with a minimum NUC_p of 6 (amounting to 59% of the messages) for the aircraft position was used in the estimation process.
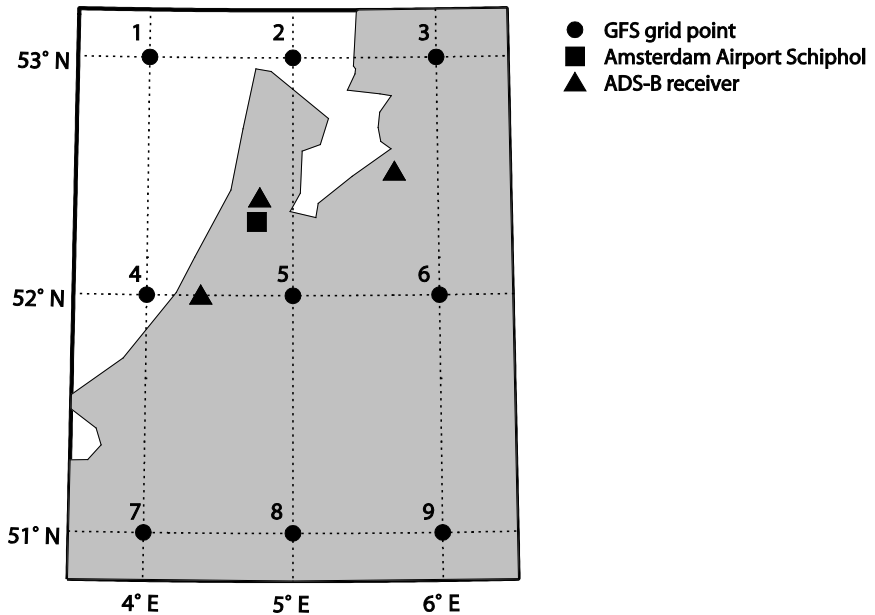
Figure 2-7 Map of the study area enclosed by 8 GFS grid points.

2.5.3 Estimation Process

Wind estimates based on single aircraft were made using flight path data of aircraft that completed a horizontal turn above 4000 ft of at least 45˚. Turns made by aircraft that changed ground speed directly before or after the turn were excluded because of possible violation of the assumption that aircraft do not change airspeed during the turn. For the initial conditions of the non-linear least-squares problem given by Eqs. (2-4, 2-5, 2-6, 2-7), wind estimates were made using the method based on multiple aircraft. The process and estimation covariance matrices were determined by trial and error.

Wind estimates based on multiple aircraft were made every six minutes between 0500 hrs and 2300 hrs local time at every 1000 ft between 4000 ft and 40,000 ft pressure altitude. ADS-B data broadcast up to 30 minutes before the estimate was used. Figure 2-8 gives an example of the estimated wind profile. The dots represent estimates made in the past two hours every 1000 ft. The thick solid line shows the resulting wind profile

after Kalman filtering the estimates. Also the forecast for the center grid point (dashed line) and the adjacent grid points (thin solid lines) are shown. In this example the wind direction forecast does not vary much between the grid points and the estimate is considered a good approximation of the forecast. The wind speed varies considerably between the grid points. At most altitudes the estimate wind speed is within the range of the forecasted wind speed in the grid points.
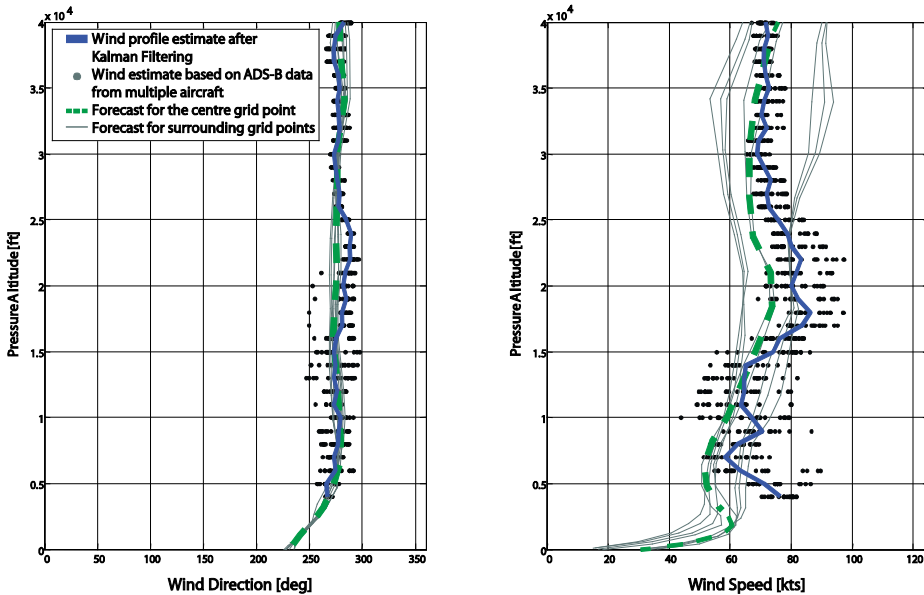
Figure 2-8 Wind profile estimate based on ADS-B data from multiple aircraft compared with GFS Forecast.

Pressure and temperature estimates were made every hour from 0500 hrs to 2300 hrs local time at every 1000 ft between 1000 ft and 36,000 ft pressure altitude. Figure 2-9 gives an example of a pressure and temperature estimate. On the left side the observed, estimated, and forecast pressures are given as the deviation from the ISA pressure. The dots show the pressure computed from the ADS-B messages. The estimate is the result of a polynomial fit to these data (thick solid line) and overlaps with the forecast for the center grid point (dashed line). The temperature estimate is plotted together with the temperature forecast and ISA temperature. Both the pressure and temperature estimate approximate the forecast.
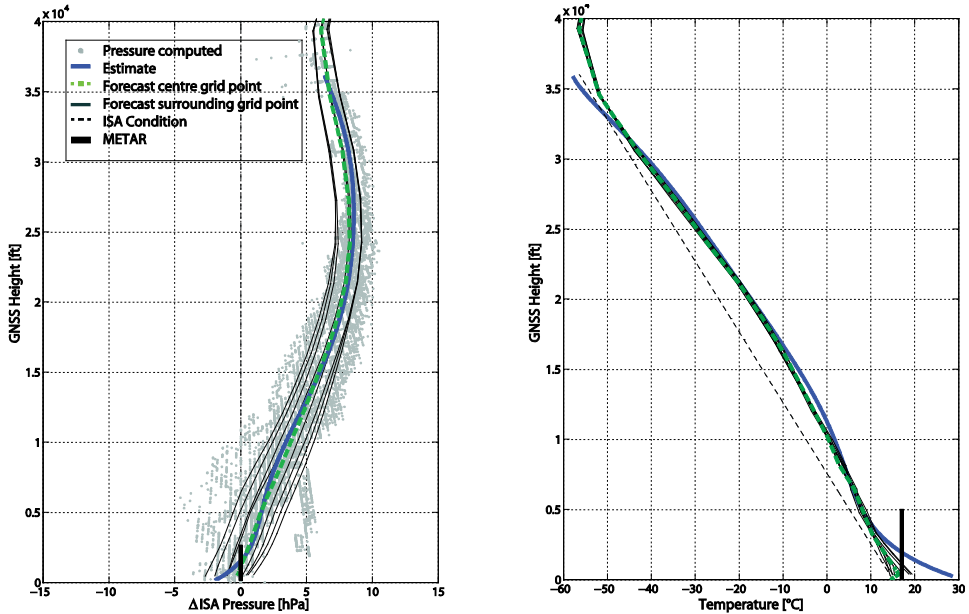
Figure 2-9 Pressure and temperature estimate compared with GFS Forecast.

2.5.4 Comparison with the GFS forecast

Wind estimates from single aircraft were compared to the latest forecast in the closest GFS grid point at the start of the turn. Wind, pressure and temperature estimates based on multiple aircraft made on the hour were compared with the GFS forecasts. It was assumed that the forecast was errorless and acts as our reference.

The metrics defined to assess the accuracy of the estimates were the Mean Error (ME), Mean Absolute Error (MAE), Root Mean Squared Error (RMSE), the correlation between the estimates and forecast, and the correlation between the errors of the estimate and forecast.

2.5.5 Modeling Output Statistics

Model Output Statistics (MOS) is an objective weather forecasting technique which consists of determining a statistical relationship between a prediction and variables forecast by a numerical model.[23] MOS were used to derive a statistical model to reduce the errors of the wind estimates. The MOS system consisted of multiple linear regression equations:

$$\hat{Y} = a_0 + a_1 X_1 + a_2 X_2 + ... + a_n X_n \tag{2-23}$$

The dependent variable *Y*, in this case wind speed or direction, is related to *n* predictors *X*. The regression constant and coefficients were estimated such that:

$$\sum_{j=1}^{n}(Y_i - \hat{Y}_i)^2$$

(2-24)

,

is minimal. To validate the effect of the MOS system on the estimate, ADS-B data and GFS forecasts for an additional 32-day period were used.

2.6 Results

2.6.1 Wind Estimate using a Single Flight Path

In total, 1550 estimates were made for the same number of horizontal turns. For all estimates the left-hand side of Eq. (2-4) was computed. This value is the residual of the least-squares problem and can be used as a quality indicator for the estimate. Figure 2-10 shows the ME and MAE of the wind speed and direction estimates for all estimates with a residual equal or less than the limit value depicted on the horizontal axis. The ME and MAE increase as the maximum residual increases. For the remainder of this analysis it was decided to use only estimates with a residual of 2000 kts^2 or lower. This subset encompassed 1030 of the 1550 estimates made at an average altitude of 9,400 ft and track angle change of 90 deg. The correlation between the GFS forecast is $R = 0.54$ and $R = 0.53$ for the speed and direction estimate, respectively, at a level of $p < 0.01$. The MAE of the speed estimate is uncorrelated with the forecast speed and direction, and altitude. The direction estimate is uncorrelated with the forecast wind direction, but weakly correlated with the forecast wind speed, $R = -0.24$ $p < 0.01$, and the altitude $R = -0.25$, $p < 0.01$.

Figure 2-11 shows the effect of the track angle change during the turn on the MAE of the estimate. For track angle changes up to 200 deg a larger angle change yields a lower MAE of the speed and direction estimates. The MAE of the estimate shows an increase for a full turn.
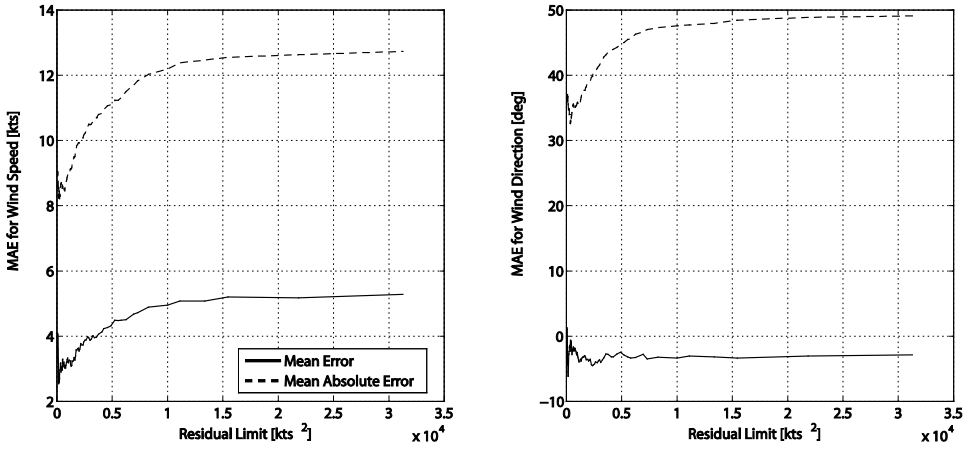
Figure 2-10 Non-linear least-squares residual vs the MAE of 1550 wind estimates, each based on a single flight path.

2.6.2 Wind Estimate for a Larger Area using Multiple Aircraft

Summarized in Table 2-2 are the error measures for all grid points and the correlations between the estimate and forecast. The grid point numbers correspond with numbers in Figure 2-7. The ME of the direction estimate indicates a bias of approximately 3 deg for all grid points. The difference between the MAE and RMSE indicates there is a large variation in the direction errors. The wind speed is overestimated in all grid points with a ME ranging between 3.6 kts and 5.5 kts. The 2-kts difference between the MAE and RMSE indicates that there was some variation in the magnitude of the speed errors, but very large errors are unlikely to have occurred.
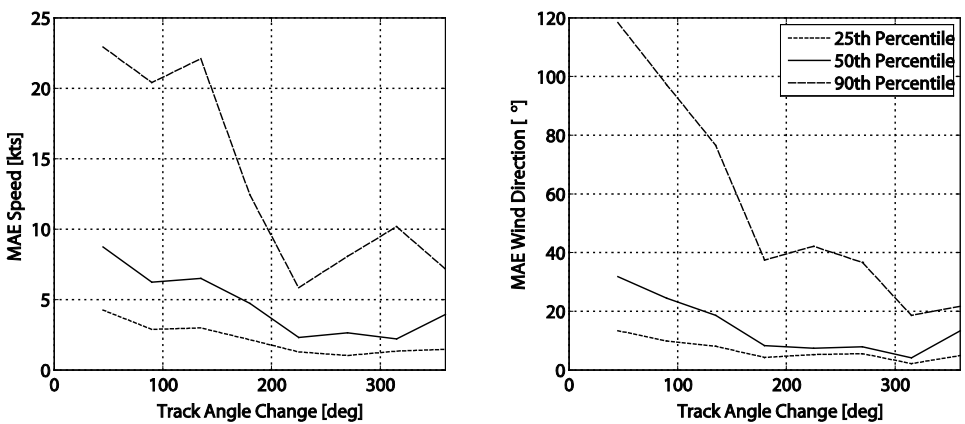
Figure 2-11 Effect of track angle change during turn on the MAE the wind estimate.

A more detailed analysis was performed for the center grid point. Figure 2-12 and Figure 2-13 show the box plots of the error in wind estimates at the center grid point. Between FL40 and FL340 the wind speed is overestimated, especially below FL60. Also the wind direction estimates appear to be more biased at lower altitudes. To explore the possible effects of the forecast wind conditions on the errors, the MAE is plotted for the forecast wind direction and speed in Figure 2-14 and Figure 2-15.

Table 2-2 Error measures for 66,600 wind estimates made every hour between 0500 hrs and 2300 hrs and every 1000 ft between 4000 ft and 40,000 ft in 100 days.

Grid Point	Mean Error	Mean Absolute Error	Root Mean Squared Error	Correlation coefficient R (2-tailed)
1	3.6 kts / -3.6	10.5 kts / 31.3	13.9 kts / 46.8	0.78 / 0.62
2	3.7 kts / -3.2	10.0 kts / 30.5	13.2 kts / 46.4	0.80 / 0.63
3	3.9 kts / -2.0	9.8 kts / 30.4	12.9 kts /46.4	0.80 / 0.62
4	4.1 kts / -3.1	9.6 kts / 29.7	12.5 kts /45.0	0.82 / 0.67
5	4.4 kts / -2.0	9.2 kts / 29.0	12.0 kts / 44.7	0.84 / 0.67
6	4.7 kts / -1.7	9.2 kts / 29.5	12.0 kts / 45.5	0.84 / 0.65
7	4.5 kts / -3.5	9.9 kts / 30.9	12.8 kts / 47.0	0.81 / 0.65
8	4.9 kts / -2.5	9.7 kts / 30.2	12.6 kts / 46.3	0.82 / 0.65
9	5.5 kts / -2.0	10.0 kts / 30.4	12.8 kts / 46.8	0.82 / 0.65

All reported correlation coefficients are significant at a level of $p < 0.01$

Wind direction estimate

The MAE of the wind direction decreases with the forecast wind speed, as can been seen in Figure 2-14. This trend can also be observed from the MAE of the direction estimate vs. the forecast wind direction plotted in Figure 2-15 and the forecast wind speed vs. wind direction plotted in Figure 2-16. The MAE of the direction estimates is higher for those directions where the forecast wind speed is lower. This effect was anticipated and confirmed in the simulation study described in Ref. [9]. The wind direction is computed from the north and east wind speed components. Hence, the direction estimate becomes more sensitive to errors of these components as the wind speed decreases. The non-parametric partial correlation coefficient, controlling for altitude, $R = -0.39$, $p < 0.01$ confirms there is a significant negative correlation between the MAE for the direction estimate and the forecast wind speed.

Figure 2-15 shows the highest MAE for wind from a northerly direction. This effect could not be related to the forecast wind speed, but was caused by the 360-degree discontinuity of the wind direction that was not addressed in the implementation of the Kalman Filter.
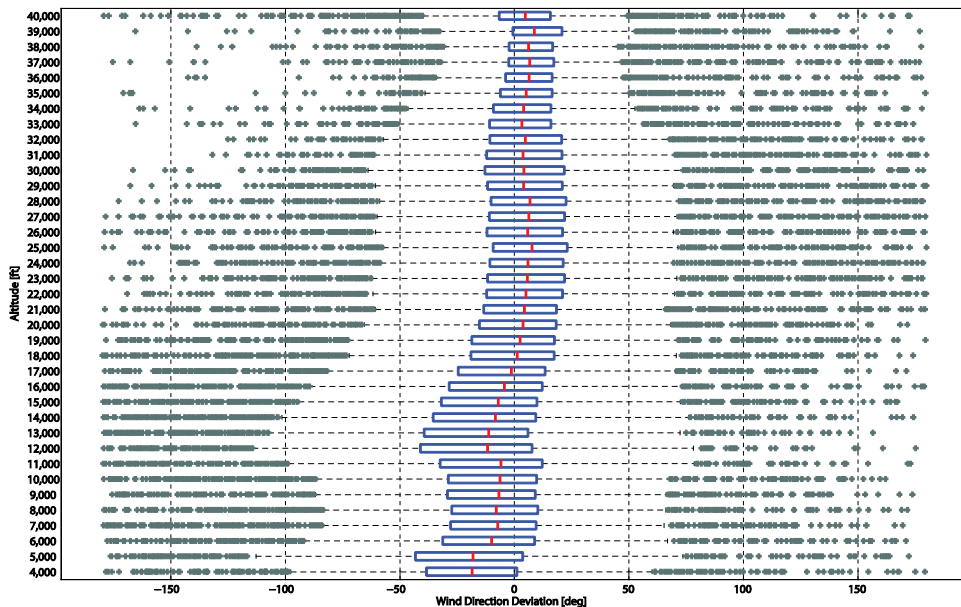
Figure 2-12 Box plot of the error for 1800 wind direction estimates per altitude level made every hour between 0500 hrs and 2300 hrs for 100 days.
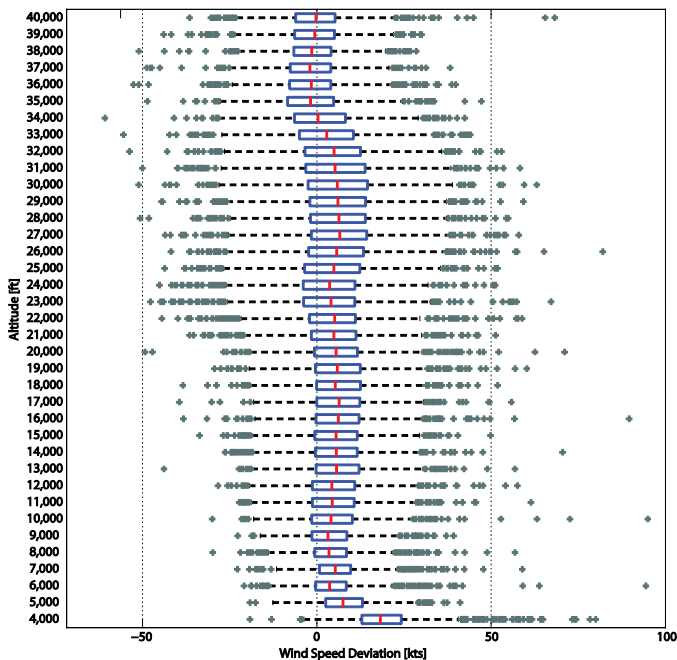
Figure 2-13 Box plot of the error for 1800 wind speed estimates per altitude level made every hour between 0500 hrs and 2300 hrs for 100 days.

Wind speed estimate

Figure 2-14 shows that the MAE for the speed estimate is also higher at lower wind speeds, but independent of the forecast wind direction as shown in Figure 2-15. However, the non-parametric partial correlation coefficient, controlling for altitude, indicates that the forecast wind speed and the MAE of the estimate are uncorrelated, $R = -0.08$, $p < 0.01$. The observed effect is caused by the increase of the MAE at lower altitudes. At lower altitudes the wind speed is generally lower, as can be seen in Figure 2-17. It was suspected that this increase is caused by acceleration and deceleration of arriving or departing aircraft in combination with constant heading changes, therefore violating the assumption that all aircraft fly at equal speed in all directions. Review of data from individual flights at low altitude confirmed the deceleration and acceleration and changing track angle, violating the main assumption.

Model Output Statistics

To improve the estimates, a MOS system consisting of two multiple regression equations was made. Parameters in the equation for the speed estimate were the estimated wind speed and direction, altitude, and the interaction between altitude and estimated wind speed. Parameters in the equation for the wind direction estimate were the wind direction, and interaction between wind speed and altitude. The altitude and wind direction were treated as categorical variables.

To assess the effect of the MOS on the estimates, the MOS was applied to estimates for additional 32 additional days of data. Table 2-3 gives the error measures both with and without the MOS. For the wind speed estimate the ME, MAE, and RMSE all improved. The MAE and RMSE reduced by 9% and 8%, respectively. For the direction estimate, the MOS only reduces the ME. The MAE and RMSE increased by 5% and 3%, respectively.

Table 2-3 Effect of the MOS on control set of 21,312 wind estimates made every hour between 0500 hrs and 2300 hrs and every 1000 ft between 4000 ft and 40,000 ft in 32 days.

Model	Mean Error	Mean Absolute Error	Root Mean Squared Error	Correlation coefficient R (2 tailed)
Original	3.2 kts / -1.8 deg	9.7 kts / 21.5 deg	12.9 kts / 31.5 deg	0.82 / 0.71
+MOS	-1.4 kts / 1.0 deg	8.9 kts / 22.4 deg	11.9 kts / 32.3 deg	0.84 / 0.70

All reported correlation coefficients are significant at a level of $p < 0.01$
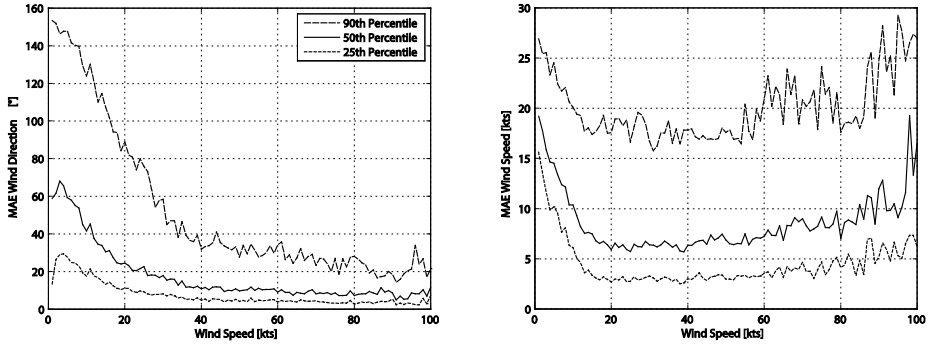
Figure 2-14 Effect of forecast wind speed on the MAE of the wind estimates.
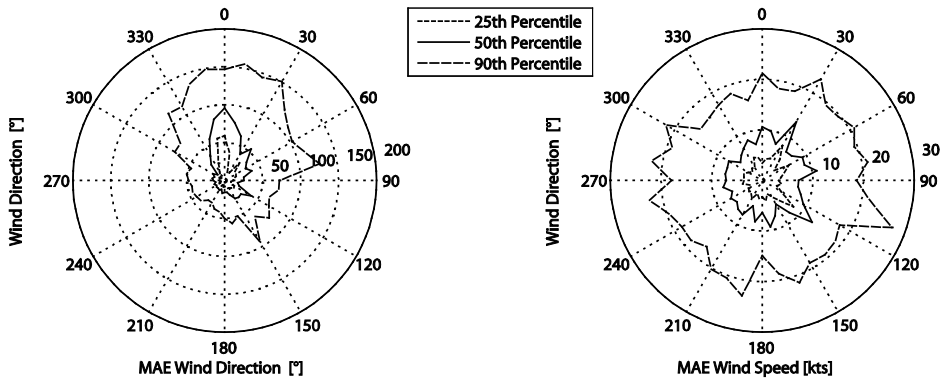
Figure 2-15 Effect of forecast wind direction on the MAE of the wind estimates.
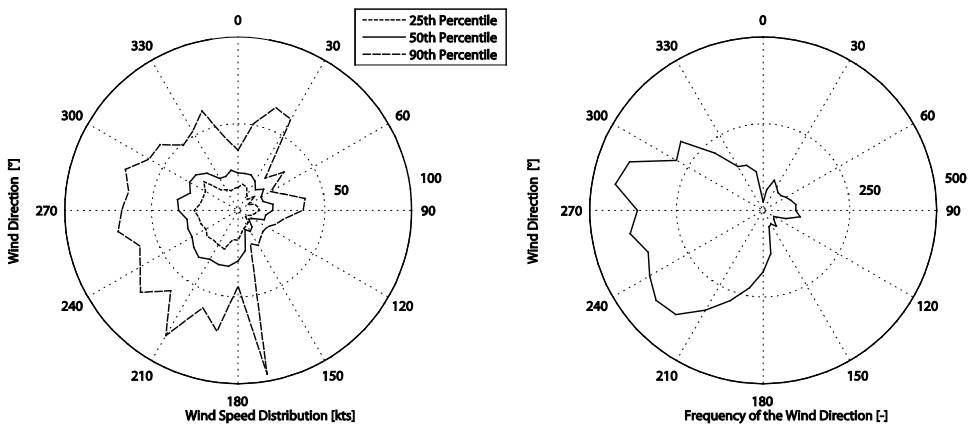
Figure 2-16 Wind direction and speed forecast by the GFS.
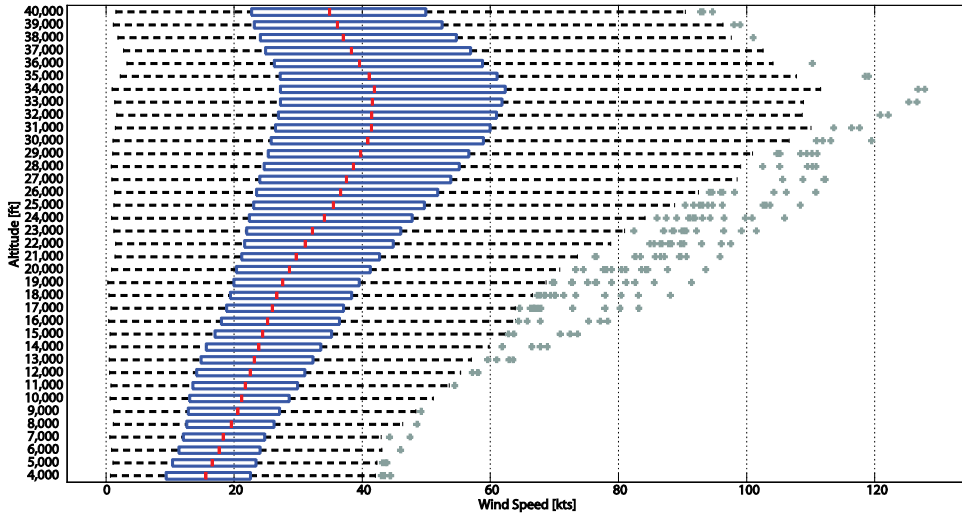
Figure 2-17 Box plot of the wind speed forecast by the GFS between 4000 ft and 40,000 ft between 0500 hrs and 2300 hrs for 100 days.

2.6.3 Pressure and Temperature Estimates

Table 2-4 summarizes the error measures and correlation between the estimates and forecast in the nine grid points. For both the temperature and pressure estimates, performance is best for grid points 4 and 5. These grid points are closest to AAS. Hence more data, especially at lower altitudes, were available from aircraft in the vicinity of these points. The ME for the pressure and temperature estimates ranges between -1.1 hPa and 1.0 hPa and 0.2 K and 1.3 K, respectively. The maximum MAE for the pressure and temperature estimate is 1.5 hPa and 2.4 K, respectively. The differences between the RMSE of both estimates do not indicate that very large errors have occurred.

Figure 2-18 and Figure 2-19 show the errors of the estimates for the center grid point from 1000 ft to 36,000 ft. The error for the pressure estimate is uncorrelated with the altitude, $R = 0.01$, $p < 0.01$. The non-parametric partial correlation coefficients, controlling for altitude, indicate that the ME, ($R = 0.09$, $p = 0.17$) and MAE ($R = -0.10$, $p = 0.95$) are uncorrelated with the forecast pressure.

The distribution of the temperature estimate error is significantly different across categories of the altitude. Below 6000 ft the error decreases with altitude. The non-parametric partial correlation coefficients, controlling for altitude, indicate that the ME, ($R = 0.00$, $p = 0.84$) and MAE ($R = 0.02$, $p < 0.01$) are uncorrelated with the forecast temperature.

Table 2-4 Error measures for 66,600 pressure and temperature estimates made every hour between 0500 hrs and 2300 hrs and every 1000 ft between 1000 ft and 36,000 ft in 100 days.

Grid Point	Mean Error (hPa / K)	Mean Absolute Error (hPa / K)	Root Mean Squared Error (hPa / K)	Correlation Coefficient R (2-tail)
1	1.0 / 1.3	1.5 / 2.4	3.1 / 3.8	1.00 / 0.99
2	0.8 / 1.2	1.2 / 2.3	1.8 / 3.7	1.00 / 0.99
3	0.7 / 1.2	1.1 / 2.3	1.6 / 3.6	1.00 / 0.99
4	0.1 / 0.8	1.1 / 2.2	1.6 / 3.4	1.00 / 0.99
5	-0.1 / 0.8	0.8 / 2.0	1.3 / 3.4	1.00 / 0.99
6	-0.2 / 0.7	0.8 / 2.0	1.2 / 3.4	1.00 / 0.99
7	-0.9 / 0.4	1.5 / 2.1	2.0 / 3.5	1.00 / 0.99
8	-1.0 / 0.3	1.4 / 2.0	1.9 / 3.4	1.00 / 0.99
9	-1.1 / 0.2	1.5 / 1.9	1.9 / 3.3	1.00 / 0.99

All reported correlation coefficients are significant at a level of $p < 0.001$
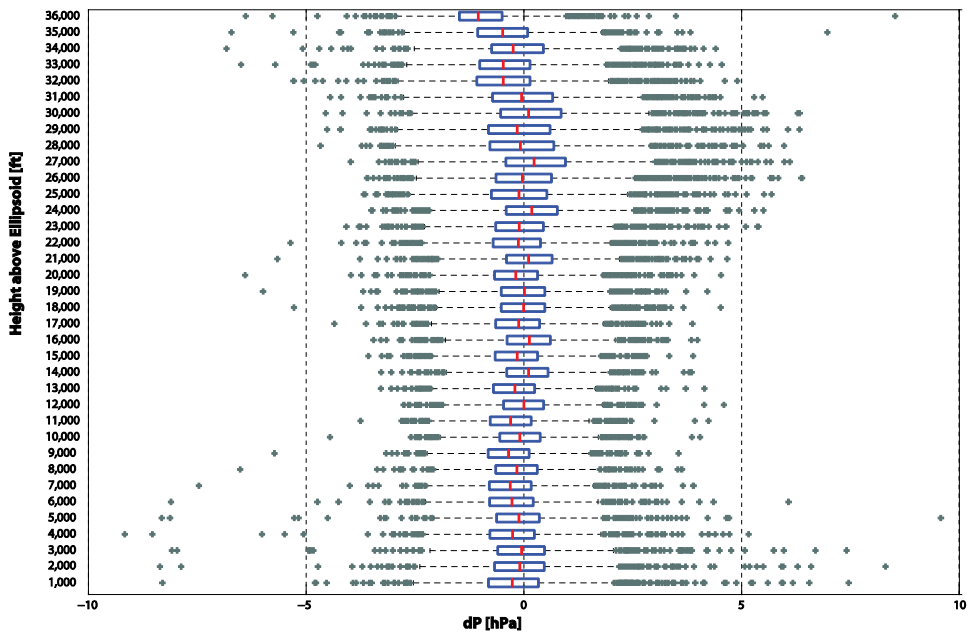
Figure 2-18 Box plot of the error in 1800 pressure estimates per altitude level made every hour between 0500 hrs and 2300 hrs for 100 days.
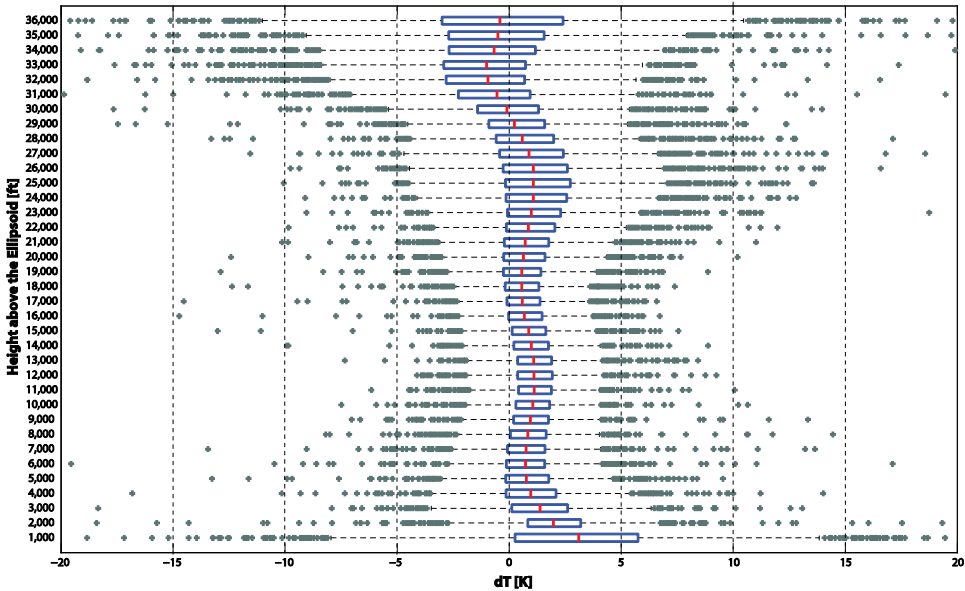
Figure 2-19 Box plot of the error in 1800 temperature estimates per altitude level made every hour between 0500 hrs and 2300 hrs for 100 days.

2.7   Discussion

Methods to estimate wind, air pressure, and temperature from ADS-B data were described and validated using GFS forecasts. The comparison of the estimates with the forecasts shows that the ADS-B system can be used for meteorological monitoring.

Flight path data of either one aircraft or multiple aircraft can be used to estimate wind. However, using only one aircraft resulted in constraints on the flight path as well as a dependency on turning aircraft, which lead to a low number of estimates. Also, a large track angle change was needed to limit the estimation error. This method is therefore not suited to provide wind estimates at fixed time and altitude intervals.

When using multiple aircraft, wind estimates for a larger area could be produced at fixed time and altitude intervals. At lower altitudes the estimates were less accurate. Likely causes are airspeed differences between aircraft and airspeed changes at these altitudes. The wind speed estimate error is uncorrelated with the forecast wind speed and direction. The wind direction estimate error is negatively correlated with the forecast wind speed. At lower wind speeds the wind direction, since it is computed from estimated north and east components, is more sensitive to errors in the estimation of these components. A Modeling Output Statistics system (MOS) was introduced to improve the performance. The MOS reduced the biases of the wind speed and direction

estimates. The mean absolute error and Root Mean Square Error (RMSE) were only reduced for the wind speed estimate.

The pressure estimates showed a strong correlation with the forecast ($R = 1.00$, $p < 0.01$). The error of the pressure estimate was uncorrelated with the forecast conditions. The mean absolute error varied between 0.8 hPa for the center grid point and 1.5 hPa for one of the outer GFS grid points used. These errors are comparable to the 1.0 hPa maximum error reported in Ref. [16] for pressure estimates made using ADS-B data collected in Spain that were also compared to the GFS forecast.

Ref. [16] also discusses a potential source of error in case the preferred GNSS HAE is unavailable onboard the aircraft and the GNSS altitude above mean sea level (MSL) is broadcast. If MSL is used as the reference surface, and MSL and the ellipsoid do not coincide, an error is introduced. To mitigate this problem in the analysis presented in Ref. [16] a minimum NUC_p of 6 was used, because a number of aircraft broadcasting a NUC_p of 5 used MSL as the reference surface. The results presented earlier in this paper are based on data with a minimum NUC_p of 6. Therefore it is expected that ambiguity in the reference surface has not significantly affected the results. The absence of a significant bias in the estimates supports this; MSL and the ellipsoid are approximately 130 ft apart in the study area and would have resulted in a large bias.

The temperature estimates were derived from the pressure estimate, the hydrostatic equilibrium, and the gas law, under the assumption that the air can be considered an ideal gas. The error of the temperature estimate differed significantly with altitude, but the source of this variation could not be identified. Possible explanations are errors in the GFS forecast and deviations of air from the ideal gas.

The comparison of the estimates with the GFS forecasts provides an order of magnitude of the error that can be expected under actual traffic and meteorological conditions. However, an accurate independent measure of true wind, pressure, and temperature is needed to determine the accuracy of the proposed methods. Possible sources that can be used are better meteorological models and aircraft observations. The current results suggest that AMDAR data and estimates made using SSR position and speed data combined with DAP (SSR-DAP) are more accurate. Wind data from the AMDAR program and SSR-DAP in Ref. [24] are of an equal quality. For the SSR-DAP method the observed RMSE for the wind speed is 5 – 8 kts, compared to approximately 12 kts for the ADS-B based method. Also the RMSE of the temperature estimates is larger than for the SSR-DAP estimates in Ref. [24]: 3.5 K and 1-1.5 K, respectively. However, ADS-B data is already being broadcast and reception does not require expensive ground equipment.

Therefore, this technique is likely to be much cheaper and may also be applied onboard 'ADS-B In' equipped aircraft without requiring additional communication protocols.

2.8   Conclusion

Methods to estimate wind, pressure, and temperature from Automatic Dependent Surveillance Broadcast (ADS-B) have been presented and validated using Global Forecast System (GFS) forecasts. Using data from multiple aircraft, wind estimates can be made at fixed time and altitude intervals during the day. The Mean Absolute Error (MAE) for the wind speed and direction estimate is 9.2 kts and 29.0 deg, respectively. The MAE of the wind speed estimate is independent of the actual conditions. The MAE of the wind direction estimate decreases with the actual wind speed. Using a Modeling Output Statistics (MOS) system the MAE of the wind speed estimate can be reduced by approximately 10%. The MOS system did not reduce the MAE for the wind direction estimate.

Pressure estimates can be made using the difference between the barometric altitude and GNSS height above the WGS 84 ellipsoid. Assuming that the air is an ideal gas, the air density and temperature can be estimated as well. The Mean Error for the pressure and temperature estimates ranged between -1.1 hPa and 1.0 hPa and 0.2 K and 1.3 K, respectively. The maximum MAE for the pressure and temperature estimate were 1.5 hPa and 2.4 K, respectively.

2.9   Recommendations

Predicated on the results and conclusions in the previous sections the authors make the following three recommendations: 1) Validation using simulated data, aircraft meteorological observations and more accurate meteorological models is recommended to determine the accuracy and robustness of the proposed methods. 2) ADS-B includes figures of merit for the position and velocity information (Navigational Uncertainty Categories). It is recommended to make use of these parameters to improve the quality of the estimates. 3) It is recommended to extend the proposed methods for wind estimation to identify airspeed changes made by aircraft during the estimation process and to exclude these data from the estimation process.

2.10 Acknowledgments

2.11 References

[1] ICAO, "Technical Provisions for Mode S Services and Extended Squitter", Doc 9871 AN/464, first edition, Montreal, Quebec, Canada, 2008.

[2] Radio Technical Commission for Aeronautics, "Minimum Operational Performance Standards for 1090 MHz Automatic Dependent Surveillance – Broadcast (ADS-B) and Traffic Information Services (TIS-B)", DO-260A, March 2003.

[3] SESAR Joint Undertaking, "SESAR ConOps at a Glance," second edition, July, 2011.

[4] Cole, R.E., Green, S., Jardin, M., Schwartz, B.E., and Benjamin, S.G., "Wind Prediction Accuracy for Air Traffic Management Decision Support Tools," *3rd USA/Europe Air Traffic Management R&D Seminar*, Napoli, June 13-16, 2000.

[5] Mueller, K.T., Bortins, R., Schleicher, D.R., Sweet, D., and Coppenbarger, R.A., "Effect of Uncertainty on En Route Descent Advisor (EDA) Predictions," *AIAA 4th Aviation Technology, Integration, and Operations (ATIO) Forum,* Chicago, Illinois, September 20-22, 2004, No. AIAA-2004-6347.

[6] Coppenbarger, R.A., Mead, R.W., and Sweet, D.N., "Field Evaluation of the Tailored Arrivals Concept for Datalink-Enabled Continuous Descent Approach," *Journal of Aircraft*, Vol. 46, No. 4, 2009, pp. 1200-1209. DOI: 10.2514/1.39795

[7] Stickland, J., and Grooters, A.T.F., "The Global AMDAR Programme," *International Symposium on Remote Sensing of Environment,* Saint Petersburg, Russia, 2005, DOI: 10.1.1.141.2511.

[8] AMDAR Panel, "Aircraft Meteorological Data Relay (AMDAR) Reference Manual," Tech. rep.,World Meteorological Organization, 2003.

[9] Yanovsky, F.J., and Bokal, Z.M., Weather data obtaining and dissemination using ADS-B. *Proceedings of the 9th innovative research workshop & exhibition*, Brétigny-sur-Orge, France, December 7 -9, 2010.

[10] in 't Veld A.C., de Jong, P.M.A., van Paassen, M.M., and Mulder M., "Real-time Wind Profile Estimation using Airborne Sensors," *Proceedings of the AIAA Guidance, Navigation and Control Conference,* Portland, Oregon, August 8 - 11, 2011, No. AIAA 2011-6662.

[11] de Haan, S., and Stoffelen, A., "High resolution temperature and wind observations from commercial aircraft," *Proceedings of the 8th International Symposium on Tropospheric Profiling*, edited by A. Apituley, H.W.J. Russchenberg, W.A.A. Monna, Organizing Committee of the 8th International Symposium on Tropospheric Profiling, Delft, The Netherlands, 2009.

[12] Delahaye, D., and Puechmorel, S., "TAS and wind estimation from radar data," *Digital Avionics Systems Conference 2009,* IEEE, Orlando, FL, 2009, pp. 2.B.5-1 - 2.B.5-16. DOI: 10.1109/DASC.2009.5347547

[13] Hollister, W.M., Bradford, E.R., and Welch, J.D., "Using Aircraft Radar Tracks to Estimate Wind Aloft," *The Lincoln Laboratory Journal*, Vol. 2, No. 3, 1989, pp. 555-565.

[14] de Leege, A.M.P., Mulder, M., and van Paassen, M.M., "Novel Method for Wind Estimation using Automatic Dependent Surveillance-Broadcast," *Journal of Guidance Control and Navigation and Control,* Vol. 35, No. 2, 2012, pp. 648-653. DOI: 10.2514/1.55833

[15] Falk C., Gonzalez J., and Perez J., "Using Automatic Dependent Surveillance-Broadcast Data for Monitoring Aircraft Altimetry System Error," *Proceedings of the AIAA Guidance, Navigation, and Control Conference*, Toronto, Ontario, Canada, August 2–5, 2010, No. AIAA-2010-8165.

[16] Alonso Alarcón, J.F., Sáez Nieto, F.J., and García-Heras Carretero, J., "Aircraft used as a sensor for atmospheric behaviour determination. Practical case: pressure estimation using automatic dependent surveillance-broadcast," *Proceedings of the Institution of Mechanical Engineers, Part G: Journal of Aerospace Engineering*, April 3, 2012. DOI: 10.1177/0954410012442044

[17] Ruijgrok, G.J.J., *Elements of Airplane Performance*, Delft University Press, 1996.

[18] ATC Global, "ATC Global Market Intelligence Reports", http://www.airtrafficmanagement.net/central/attachments/ADS-B_feature_-_Market_Intelligence_Report_I.pdf [retrieved 1 March 2012].

[19] Alessandri, A., Cuneo, M., Pagnan, S., and Sanguineti, M., "A recursive algorithm for nonlinear least-squares problems," *Computational Optimization Applications*, Vol. 38, Issue 2, November 2007, pp. 195-216. DOI: 10.1007/s10589-007-9047-7

[20] Zhu, J., "Calculation of Geometric Dilution of Precision," *IEEE Transactions on Aerospace and Electronic Systems*, Vol. 28, Issue 3, July 1992, pp. 893-895. DOI: 10.1109

[21] Zarchan, P., and Musoff, H., *Fundamentals of Kalman Filtering: A Practical Approach*, Vol. 208 of Progress in Astronautics and Aeronautics, American Institute of Aeronautics and Astronautics, Inc., Reston, VA , 2nd ed., 2005.

[22] NOAA, "Global Forecast System", http://www.emc.ncep.noaa.gov/GFS/ [retrieved April 29 2011]

[23] Glahn, H.R., and Dale A.L., "The Use of Model Output Statistics (MOS) in Objective Weather Forecasting," *Journal of Applied Meteorology*, Vol. 11, Issue 8, December 1972, pp. 1203-1211. DOI: 10.1175/1520 0450(1972)011<1203:TUOMOS>2.0.CO;2

[24] Haan, S. de, "Quality assessment of high resolution wind and temperature observations from ModeS," Tech rep.: WR-200907, Royal Netherlands Meteorological Institute (KNMI), Revised edition, De Bilt, The Netherlands, 2010.

3   A Machine-Learning Approach to Trajectory Prediction

A machine learning approach to trajectory prediction is presented. The trajectory prediction problem is defined as a supervised learning regression problem. The developed approach is applied to a Continuous Decent Operations procedure used at Amsterdam Airport Schiphol. The prediction performance is quantified using the along track error and time error. Finally, the effect of the prediction performance on the runway throughput for Continuous Descent Operations is analyzed.

Abstract

A machine learning approach to trajectory prediction for sequencing and merging of traffic following fixed arrival routes is described and evaluated using actual trajectory and meteorological data. In the approach a model is trained using historic data to make arrival time predictions. Model inputs are the aircraft type, aircraft groundspeed and altitude at the start of the arrival route, surface wind, and altitude winds. A stepwise regression method is used to systematically determine the inputs and functions of inputs that are included in the prediction model based on their explanatory power. For the evaluation of the approach a 45 NM fixed arrival route was used that ends at the runway. Traffic performed a continuous descent operation. At a prediction horizon of 45 NM the model explained 63% of the observed variance in the arrival time. The mean absolute time error was 18 s. Finally, the prediction model was used to determine the required initial spacing interval between aircraft for continuous descent operation and examine the impact on runway throughput and conflicts. Using the prediction model throughput increased by up to 4 aircraft per hour compared to a constant initial spacing.

3.1   Introduction

The performance of many Air Traffic Management (ATM) processes relies on accurate trajectory prediction (TP). Examples include departure and arrival management, conflict detection, flight planning, and flow management. Common approaches to TP are the use of full six degree-of-freedom (6-dof) aircraft models, point mass models, and macroscopic models [1]. The first two approaches model the trajectory through computation of forces, and in case of 6-dof, also moments acting on the aircraft. Macroscopic models describe the aircraft behavior as a function of the aircraft state and environmental conditions. An example of a macroscopic model is the Base of Aircraft Data (BADA) model [2]. These approaches require explicit modeling of the aircraft performance procedures, and airspace. The models and inputs needed might not always be readily available. In addition, some data is commercially sensitive or a data-link to downlink intent information or aircraft state parameters is unavailable. Examples are airline flight planning and aircraft intent information as described in Refs. [3, 4].

In this paper, we propose a machine learning approach to TP. Machine learning is defined by Mitchell in Ref [5] as follows: "*A computer program is said to learn from experience E with respect to some class of tasks T and performance measure P, if its performance at tasks in T, as measured by P, improves with experience E.*" Using machine learning techniques, trajectory predictions can be made without explicit modeling of the aircraft performance, procedures and airspace. Instead, historic trajectory and meteorological data are used to train a predictive model. Only data that is readily

available through surveillance and meteorological systems is used. During training, model parameters are tuned to minimize the prediction error.

Applications of machine learning for aircraft TP found in literature include the prediction of the aircraft vertical speed during climb and traffic flow forecasting [6-8]. These studies demonstrated the potential use of machine learning techniques for TP. However, in these studies the effect of wind on the aircraft was neglected. Wind has a significant impact on the prediction accuracy [1]. Therefore it is expected the TP performance could be improved by including wind in the predictions.

In our machine learning approach, we define TP as a supervised learning regression problem. First the general approach is established. The approach encompasses data gathering, data preparation, algorithm training, and finally TP. Supervised learning regression techniques include Generalized Linear Models (GLMs), Support Vector Regression, and Artificial Neural Networks [9]. All three techniques have been applied to the trajectory prediction problem as part of this research. Application of the GLM and Support Vector Regression techniques resulted in equal trajectory performance. GLM and Support Vector Regression performed marginally better than Artificial Neural Networks. However, in this paper only the results obtained using the GLMs are discussed, because GLM is easier to implement and the models are easier to interpret than the two techniques.

Finally, the prediction model was used to compute the required initial spacing between aircraft for closed-path Continuous Descent Operations (CDO) to gauge the potential operational benefits. The current CDO operations at Amsterdam Airport Schiphol were use for this purpose. In these operations an arrival route defines the aircraft lateral path. The vertical path is free for optimization (e.g., by the flight management system) within the constraints set by ATC. Accurate arrival timing is required to keep aircraft separated and to deliver the capacity required. The TP was used to compute the required aircraft spacing at the start of the procedure. A trade-off was made between the throughput and the number of conflicts to be resolved during the CDO phase. Tactical intervention during the CDO phase is unwanted, because it reduces the aircraft's ability to follow the optimized descent profile. Ren and Clarke proposed a similar approach in their work on the Tool for the Analysis of Separation and Throughput (TASAT) [10, 11]. TASAT computes feasible spacing intervals for CDO offline using a fast-time trajectory prediction tool. These intervals are computed for different probability levels that tactical intervention during the CDO phase for conflict resolution is not required (CDO success rate). The range of spacing intervals and the associated throughput levels and CDO success also present a trade-off. In this research the machine learning based TP will be used instead of the fast-time simulator to generate aircraft trajectory data. The

separation analysis is less complex. It is assumed that the aircraft spacing is minimal when the leading aircraft is at the runway threshold. Also, the air traffic controllers' ability to space at the required initial spacing is not considered.

The remainder of this paper is organized as follows: Section 3.2 provides a discussion of the functional requirements of TP for arrival management (AMAN). In Section 3.3 a description is given of the closed-path CDO procedure that will be used to examine the trajectory prediction performance. In section 3.5 the machine learning approach to TP for AMAN is presented. Section 3.6 presents the results of the TP performance analysis. In section 3.7 the results of analysis to examine the effects of TP performance on throughput are described. The Sections 3.8 and 3.9 contain the discussion and conclusions.

3.2   Trajectory Prediction for Arrival Management

Figure 3-1 shows a typical procedure for CDO with fixed arrival routes. Traffic from different directions is merged, sequenced, and spaced before the start of the CDO. This spacing can be either time-based or distance based at an intermediate fix. The time or distance interval between the aircraft should ensure the safe separation throughout the remainder of the approach, whilst providing the required capacity. Tactical interventions by ATC during the CDO are likely to take the aircraft off the fixed arrival route. In that case the optimized descent profile and associated environmental benefits are (partially) lost.
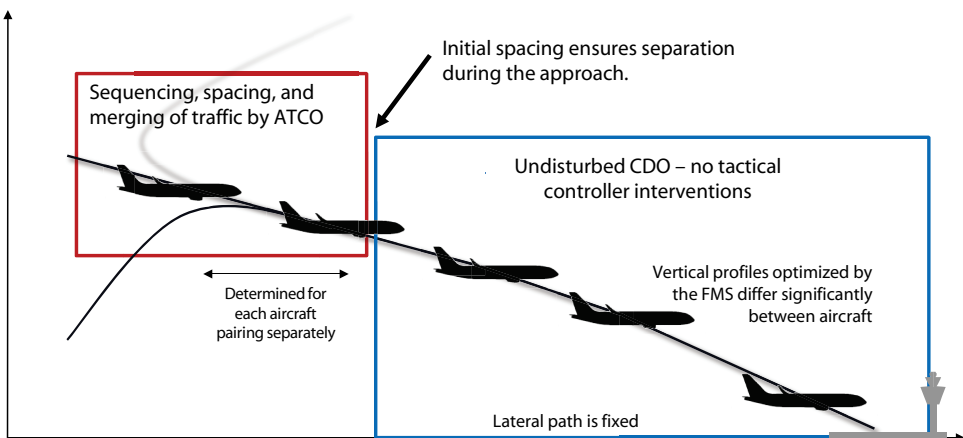
Figure 3-1 General CDO concept.

Without decision support an ATCO cannot accurately determine the required initial spacing and arbitrarily large spacing buffers are used [10, 12]. The required initial spacing can be provided by a decision support tool such as an AMAN [13]. The AMAN determines the required spacing intervals based on the predicted time of the aircraft over significant points along the arrival route. A significant point is typically a waypoint or a point a certain distance from a waypoint or the runway threshold.

3.3 Closed-path CDO procedure

In this research we use data from a closed-path CDO procedure used at Amsterdam Airport Schiphol to build the GLMs. This arrival procedure is used between 2300 hrs and 0640 hrs local time, traffic conditions permitting.

Figure 3-2 shows the arrival procedure based on the approach plates found in Ref. [14]. The arrival procedure starts at the Initial Approach Fix (IAF) ARTIP and ends at the threshold of runway 18R at Amsterdam Airport Schiphol. Along the route, altitude and speed constraints are imposed that shall be respected. Flight crew are expected to establish a continuous descent path.
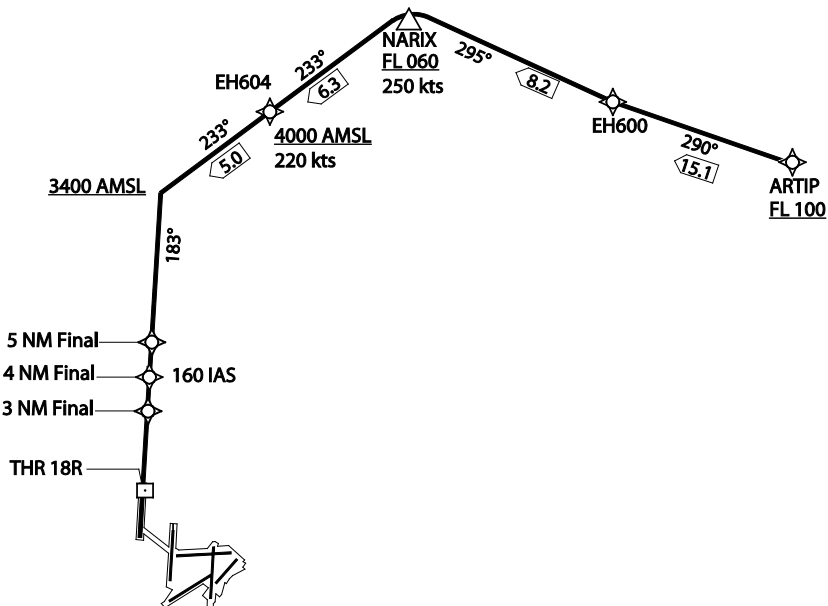
Figure 3-2 Schiphol arrival procedure from ARTIP to runway 18R.

Predictions will be made at significant points along the arrival route. Selected points are waypoints along the arrival route, the runway threshold, and points at 3 NM, 4 NM and 5 NM distance from the runway threshold. The latter three points were selected to support

the spacing task and is discussed in more detail in Section 3.7. Figure 3-3 shows the along track distance from the IAF to the significant points (prediction horizon) and the mean and standard deviation of the flying time from the IAF basic on historic trajectory data.
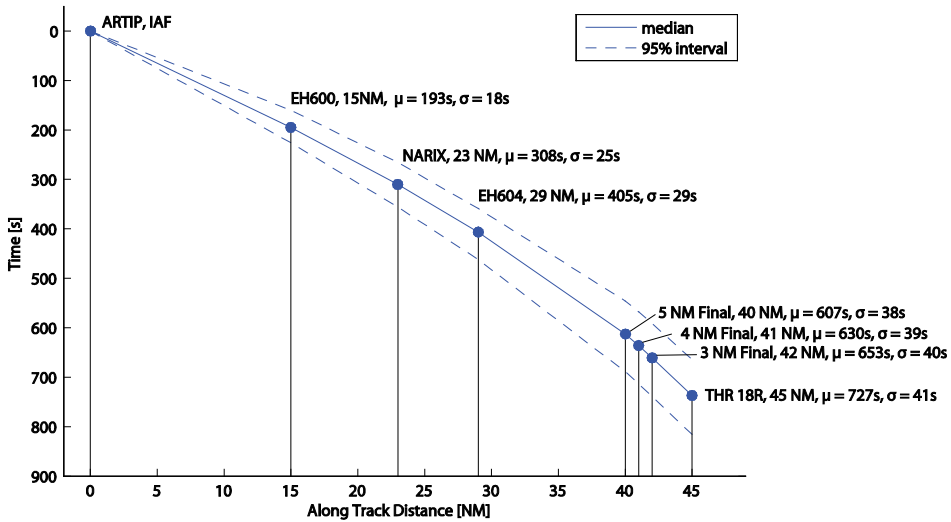
Figure 3-3 Prediction horizon from IAF and trajectory dispersion.

3.4   Aircraft Trajectory Data

Two aircraft types were selected based on the number of trajectories available. The first aircraft are a narrow-body aircraft in the ICAO wake vortex category medium and the second aircraft is a wide-body aircraft in the wake vortex category heavy. The ADS-B trajectory data was collected between February 2011 and April 2012. Trajectories of flights that were vectored off the arrival route or showed signs of speed control were removed from the data set. Ultimately, 928 and 427 trajectories were used in the analysis for the medium and heavy aircraft, respectively. Figure 3-4 shows a breakdown of the trajectories per airline. For both aircraft types, approximately two thirds of the flights were operated by one airline. The remaining thirds were operated primarily by two airlines.

3.5   Machine Learning Approach

Figure 3-5 gives an overview of the proposed approach. For an existing CDO procedure trajectory and meteorological data are collected. This data is used to train the predictive model. Training data consists of pairs of the input and output vectors. The input vector elements shall have statistical significance in explaining the output vector. Examples of such input variables are aircraft state parameters at the start of the CDO procedure and

Medium aircraft   **Heavy aircraft**
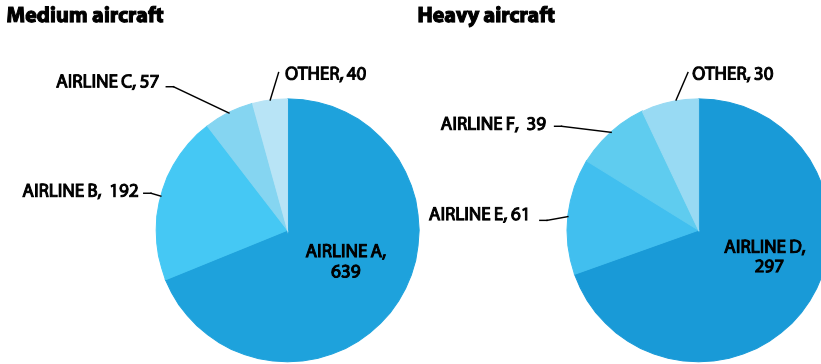
Figure 3-4 Trajectories per airline.

meteorological conditions. The model output consists of the predicted time over points along the fixed arrival route.

The machine learning approach to trajectory prediction can be defined as a supervised learning regression problem. A learning algorithm uses the training data to set the model parameters to minimize the prediction errors. A supervised learning regression technique is GLM. After training of the GLM the model is ready for trajectory prediction in real-time based on surveillance data and the actual meteorological conditions.
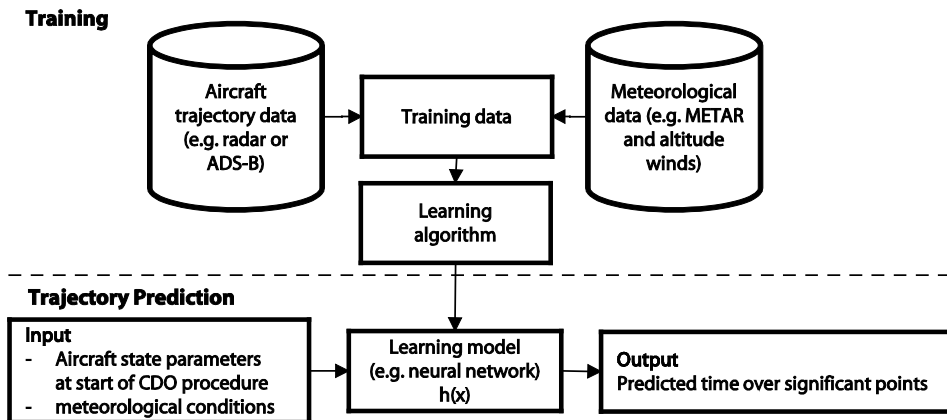
Figure 3-5 Schematic overview of training and trajectory prediction processes.

3.5.1 Generalized Linear Models

GLMs were introduced by Nelder and Wedderburn in 1971 [9]. GLMs can be used to predict output variables that are distributed or assumed to be distributed by an exponential family distribution. GLMs can be considered a generalization of ordinary

linear regression models. The following description of GLMs is based on the discussion of GLMs in Ref. [15] by Fox.

A GLM consist of the three components:

1. A probability distribution of the output variable Y_i. This distribution shall be a member of the exponential distribution family. Among exponential family distribution are the normal, gamma, binomial, and Poisson distributions.

2. A linear predictor of the form:

$$\eta_i = \alpha + \beta_1 X_{i1} + \beta_2 X_{i2} + ... + \beta_k X_{ik} \tag{3-1}$$

The model is linear in the parameters β. The regressors X_{ij} are functions of the model inputs. These functions may include but are not limited to the main effects, interactions between input variables, and transformations of the input variables. The α parameter is the intercept of the linear model.

3. A link function that transforms the expectation of the output variable, $\mu_i = E(Y_i)$, to the linear predictor:

$$g(\mu_i) = \eta_i = \alpha + \beta_1 X_{i1} + \beta_2 X_{i2} + ... + \beta_k X_{ik} \tag{3-2}$$

Common link functions are the identity, log and inverse function. Ideally a link function is selected that renders the regression of Y on X's linear and is compatible with the response variable ranges [15].

Three components in building a GLM are selection of the output variable distribution, of the function that links the linear predictor to the mean of the distribution, regressors, and of the model inputs. The model parameters β are estimated using a maximum likelihood procedure.

3.5.2 Building Generalized Linear Models
The GLM is built to predict the time over the trajectory points of the procedure introduced in Section 3.3. We start with the discussion of the explanatory features because this affects the choice for the link function.

Model Inputs

Criteria for the selection of input variables are the dependency of time over the significant points on the input variable and the availability of the input variables in real-time. For this study the following inputs are considered to be included in the GLMs:

- Aircraft type;
- Aircraft ground speed at the IAF;
- Aircraft altitude over the IAF;
- Surface wind and;
- Altitude winds.

The aircraft ground speed is available from the SSR or ADS-B. Surface wind conditions are part of the METAR. Possible data sources for altitude winds are the AMDAR program or wind forecasts or nowcasts. Alternatively, altitude winds can be derived from aircraft surveillance data such as the SSR and ADS-B as described in Refs [17-20].

Output variable distribution and link function

The exponential family distribution includes the normal distribution. Figure 3-6 shows normality plots of the time of the selected trajectory points. At the center of the distribution the normal distribution appears to be a good fit. At the tails of the distribution, especially the right side, the data deviates from the normal distribution.

Overall, the normal distribution is considered to be a reasonable fit to trajectory data. We select the inverse as the link function. The explanatory features include the aircraft speed and wind speeds. The inverse function renders the regression between the output variable and speed linear.
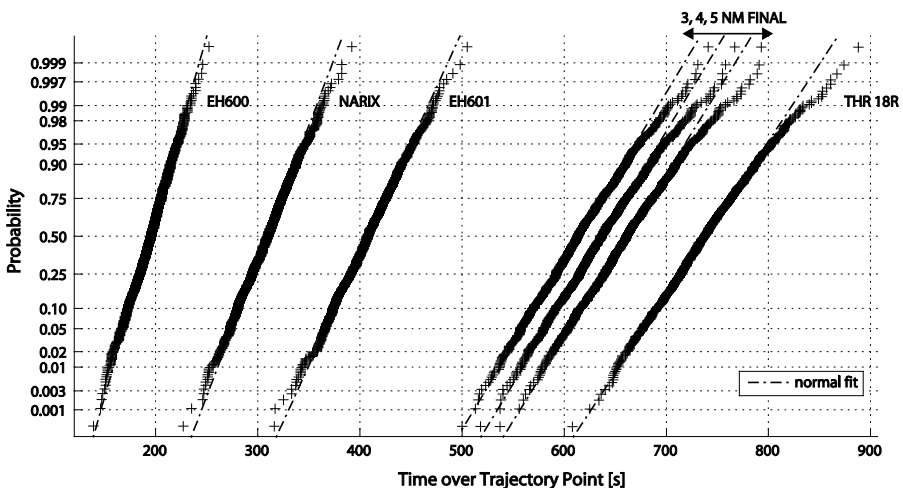
Figure 3-6 Normality plot trajectory data.

Stepwise Regression

To determine which regressors to include in the GLM a stepwise regression approach is applied. Stepwise regression provides a systematic approach to add or remove regressors from the GLM based on their statistical significance in explaining the output variable. A criterion for the explanatory power of the model is the sum of squared errors. In the stepwise regression approach regressors are added or removed from the model based on the change in the model's explanatory power [21].

The stepwise regression approach consists of three steps. The first step is to initialize the model. The model is initialized with an intercept and the linear regressors of each model input. The other two steps determine which regressors are added to or removed from the model.

To determine which regressor to add to the model, the p-value of the F-statistic of the change in the sum of squared errors is used. This change is computed for all regressors that could be added to the model. The regressor with the lowest p-value of the F-statistic below the tolerance level of $p < 0.05$ is added to the model. This step is repeated until no regressor can be found that meets the criteria. In that case the approach goes to the next step that determines which regressor shall be removed from the model.

Again, the p-value of the F-statistic of the change in the sum of squared errors is used to determine which regressor to remove. The regressor associated with the highest p-value above the tolerance level of $p > 0.1$ is removed from the model. After removal of a regressor the approach again tries adding regressors to the model. If none of the p-values exceeds the tolerance level the stepwise regression ends.

3.6 Trajectory Prediction Performance Analysis

The objective of the TP performance analysis was to assess the time and along track errors that can be expected under actual conditions [16]. GLMs were trained following the procedure outlined in Section 3.5.2 and were used to predict the time over the trajectory points selected in Section 3.3. The trajectory predictions and analysis were conducted using Matlab.

3.6.1 Model input variable sets

To assess the impact of the model input variables on the TP performance, four model input variable sets were used. Table 3-1 lists the input sets. The aircraft type is included in every input sets. Subsequently, the aircraft altitude and speed over the IAF, surface wind and altitude winds were added to the input set. The rationale behind the order in which the variables were added, was to first base the prediction on aircraft parameters only. Then add meteorological information that is readily available (e.g., airport surface

wind) and finally include altitude wind information. The latter requires more advanced systems than currently available at most control centers, such as those described in Refs. 17, 19 and Chapter 2 of this thesis. It was expected that TP performance will improve if more input variables are added to the model. In particular, the wind related input variables are expected to impact the TP performance for longer prediction horizons.

Table 3-1 Model input variable sets for trajectory prediction.

Id	Inputs
AC	Aircraft Type
+A&S	Same as previous plus aircraft altitude and speed over the IAF
+SW	Same as previous plus surface wind
+AW	Same as previous plus altitude wind at FL30, FL60, FL90, FL120

3.6.2 Meteorological Data

Meteorological data sources are the meteorological aerodrome report (METAR) for the surface wind at the airport and Global Forecast System (GFS) for the altitude winds. Parameters used in the analysis are the north and east components of the surface winds and altitude winds up to FL120. Prevailing surface winds were from the southwest, with a maximum of 23 kts.

3.6.3 Prediction Performance Metrics

Basic TP performance metrics include the time and along track error [16]. The time error is the difference between the predicted and actual time over a significant point. In this research we define the along track error as the difference between the actual and predicted along track distance when the aircraft is predicted to fly by or fly over a particular reference point. Statistical measures used to quantify the errors are the mean error (ME), mean absolute error (MAE), and root mean square error (RMSE).

3.6.4 Method

Models were trained using 70% of the available trajectory and meteorological data. The remaining 30% of the data were used to examine the TP performance. The data was divided randomly over the training and testing data sets. Four models with different input sets were trained using one data set. Next, the models were used to predict the time over the selected points using the testing data. The final step was to determine the time and along track errors. This process was repeated 100 times with different random training and testing data sets.

3.6.5 Time Error

Figure 3-7 shows the probability density distribution (PDF) estimates of the time error at the selected trajectory points for the different input sets. Independently of the input set, the time error increased with the prediction horizon. Adding more input variables to the

input set reduced the time error significantly. The impact on the TP performance increases with the prediction horizon.
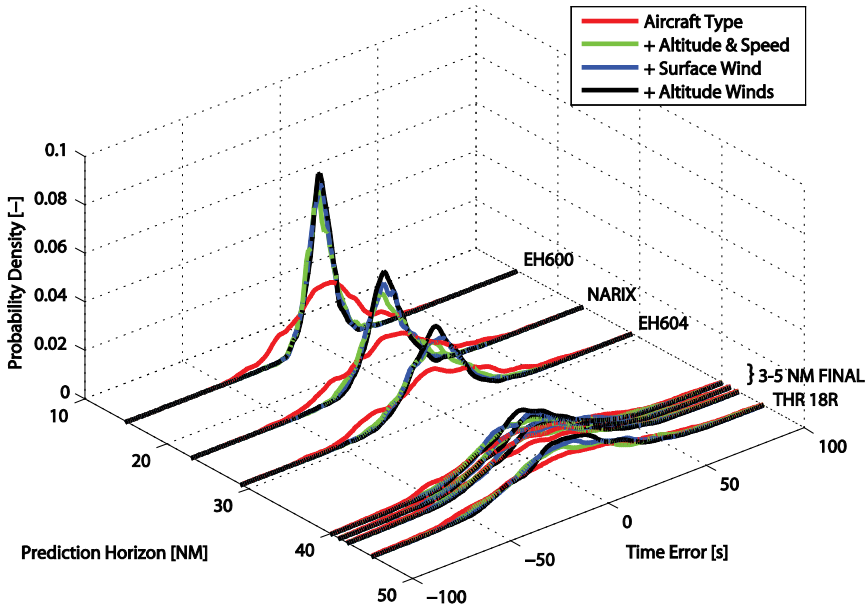
Figure 3-7 Probability density distribution of the time error.

Table 3-2 provides the descriptive statistics of the time error. The ME of the predictions at all trajectory points and for all model input sets was smaller than 1 s. There is no indication of any systematic errors in the predictions. The MAE and RMSE are also plotted in Figure 3-8. Adding more input variables yields smaller prediction errors. Compared to a model with only the aircraft type as input, the MAE for the time over the runway threshold was reduced by 29% when the altitude and speed were added. Adding the surface wind and altitude winds, the MAE reduced by 43% to 18.3 s with an RMSE of 23.4 s. Figure 3-8 also shows that adding wind has a stronger effect on the time error in absolute sense for longer prediction horizons. Figure 3-9 shows the MAE of the predicted time over THR 18R (longest prediction horizon) against the east and north surface wind components for the different feature sets. For models without wind related input variables the MAE was large for surface winds from the southwest. Adding wind related inputs reduced the MAE significantly.

Table 3-3 provides the correlation coefficients between the actual and predicted time over the trajectory points. The model with all input variables explained between 83% and 63% of the variance observed in the actual time over a trajectory point. The MAE, RMSE and correlation coefficients show that for the trajectory points at a relatively short

prediction horizon the aircraft altitude and speed were the main determining factors. Wind related input variables are important for longer prediction horizons.

Table 3-2 Time error descriptive statistics [s].

POINT	Mean Error				Mean Absolute Error				Root Mean Square Error			
	AC	+A&S	+SW	+AW	AC	+A&S	+SW	+AW	AC	+A&S	+SW	+AW
EH600	-0.1	0.0	0.0	0.0	13.0	5.6	5.3	5.1	16.4	7.3	7.0	6.8
NARIX	-0.1	0.0	0.0	0.0	17.7	9.6	8.7	8.0	22.5	12.4	11.3	10.6
EH604	-0.1	0.0	0.0	0.0	20.7	12.6	11.4	10.4	26.4	16.2	14.7	13.6
5 NM FINAL	-0.1	0.0	0.0	-0.1	27.3	20.6	18.6	16.7	34.9	26.4	23.5	21.3
4 NM FINAL	-0.1	0.0	0.0	0.0	27.9	21.4	19.2	17.2	35.7	27.5	24.2	21.9
3 NM FINAL	-0.1	0.0	0.1	0.0	28.4	22.1	19.7	17.5	36.4	28.3	24.8	22.4
THR 18R	0.0	0.1	0.1	0.0	29.2	23.3	20.4	18.3	37.6	30.0	25.8	23.4

Table 3-3 Correlation between the actual and predicted time over a trajectory point.

POINT	Pearson correlation coefficient R^2, (2-tailed)[*]			
	AC	+A&S	+SW	+AW
EH600	0.00	0.80	0.82	0.83
NARIX	0.00	0.70	0.75	0.78
EH604	0.00	0.62	0.69	0.74
5 NM FINAL	0.02	0.44	0.56	0.63
4 NM FINAL	0.02	0.42	0.55	0.63
3 NM FINAL	0.02	0.41	0.55	0.63
THR 18R	0.04	0.39	0.55	0.63

*All reported correlation coefficients are significant at a level of $p < 0.01$
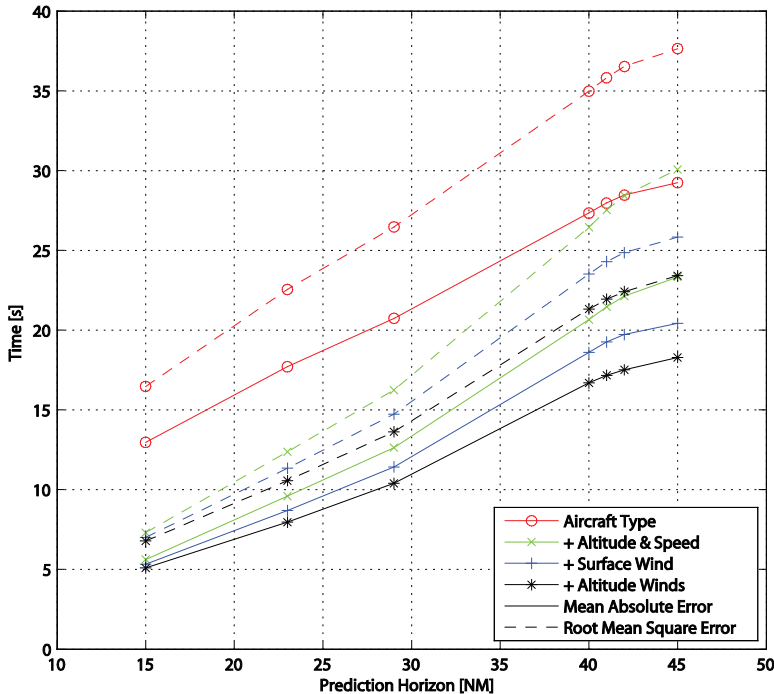
Figure 3-8 Time error as function of the input set and prediction horizon.
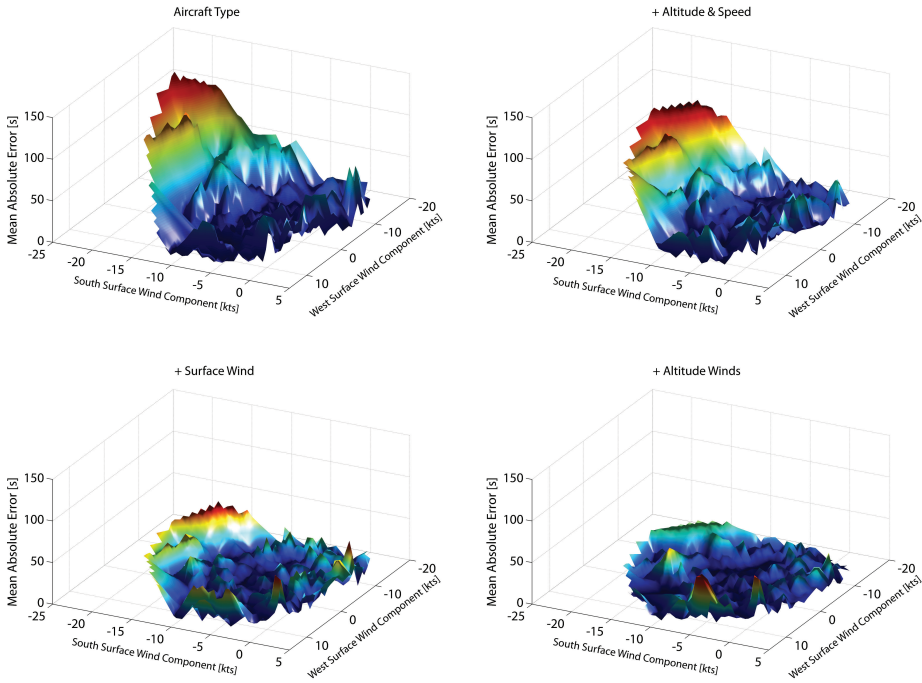
Figure 3-9 Mean absolute time error at the runway threshold vs. surface wind.

3.6.6 Along Track Error

The along track error results are comparable to the time error results. Figure 3-10 shows the probability density distribution estimates. The descriptive statistics are given in Table 3-4. The along track error at the runway threshold was omitted, because the error could only be quantified if the aircraft landed later than predicted. Again no systematic errors were observed. The model with the most input variables performed best. Figure 3-11 shows that the MAE and RMSE reduced. The MAE and RMSE increase with the prediction horizon for the first four points along the route, except when the aircraft type is the only input variable. For the last two trajectory points (4 NM and 3NM Final) the error decreased because the aircraft speed is significantly reduced in this phase of the approach.

Table 3-4 Along track distance error descriptive statistics [NM].

POINT	Mean Error				Mean Absolute Error				Root Mean Square Error			
	AC	+A&S	+SW	+AW	AC	+A&S	+SW	+AW	AC	+A&S	+SW	+AW
EH600	-0.1	-0.1	-0.1	-0.1	1.0	0.5	0.4	0.4	1.3	0.6	0.6	0.6
NARIX	-0.1	-0.1	-0.1	-0.1	1.2	0.7	0.6	0.5	1.6	0.9	0.8	0.7
EH604	-0.1	-0.1	-0.1	-0.1	1.3	0.8	0.7	0.7	1.7	1.1	1.0	0.9
5 NM FINAL	0.0	0.0	0.0	0.0	1.2	0.9	0.8	0.7	1.5	1.2	1.0	1.0
4 NM FINAL	0.0	0.0	0.0	0.0	1.2	0.9	0.8	0.7	1.5	1.1	1.0	0.9
3 NM FINAL	0.1	0.0	0.0	0.0	1.1	0.9	0.8	0.7	1.4	1.1	1.0	0.9
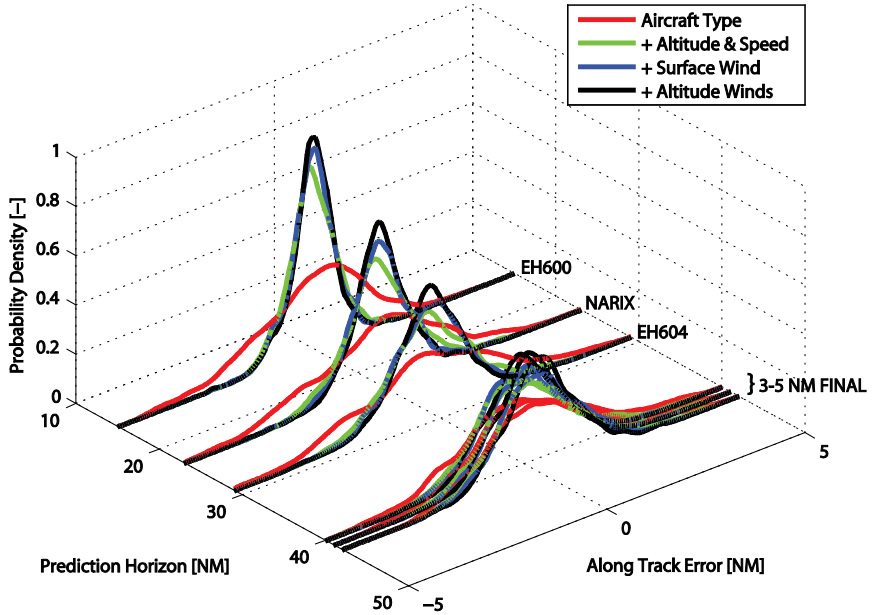
Figure 3-10 Probability density distribution of the along track error.
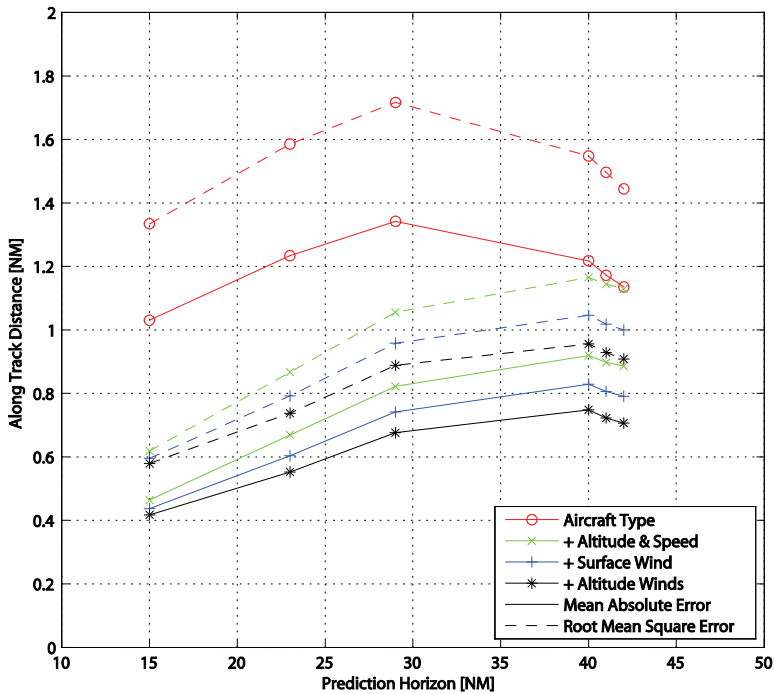
Figure 3-11 Along track error as function of the input set and prediction horizon.

3.7 Spacing for Continuous Descent Operation

Based on the results of TP performance analysis, the GLM with an input comprising of the ground speed, surface wind, and altitude winds was selected to examine the possible use of the TP in spacing aircraft for CDO. In the analysis, the spacing task was to determine the initial spacing between two aircraft to be separated on final. The same approach procedure and data as for the TP analysis were used, see Sections 3.3 and 3.6.

The initial spacing was determined for 5,000 randomly selected aircraft trajectory pairs from the data set. The initial spacing was set such that the expected distance between aircraft on final equaled the applicable separation minimum. The separation minima ranged between 3 NM and 5 NM, depending on the wake vortex categories of the aircraft. Table 3-5 contains the separation minima that were used. In the data set 68% of the traffic falls in the category medium and 32% in the category heavy. The spacing interval was computed from the predicted time over the runway threshold for the leading aircraft, and the predicted time that the trailing aircraft is at 3, 4, or 5 NM distance from the runway threshold.

In a baseline scenario, a constant initial spacing interval was used for all aircraft pairs, as opposed to the dynamic spacing interval used in the TP scenario. In both scenarios a minimum initial spacing requirement of 5 NM was used to adhere to radar separation minima and get more realistic throughput values.

Table 3-5 Separation minima.

Preceding Aircraft	Followed by	Separation minimum
Medium	Medium	3 NM
	Heavy	3 NM
Heavy	Medium	5 NM
	Heavy	4 NM

The analysis was repeated fifteen times with a time buffer on top of required spacing that was determined using the trajectory predictions to account for TP uncertainty. The time buffer was increased from 0 s to 70 s in steps of 5 s.

3.7.1 Throughput vs. Conflicts

Figure 3-12 shows the throughput versus the percentage of conflict free flights. Using the TP an average throughput of 38 AC/H was realized and 55% of the flights remained conflict free. The percentage of conflict free flights was higher than the expected 50% due to the 5 NM radar separation minimum that was applied at the start of the procedure. Increasing the spacing buffer in steps of 5 s from 0 s to 70 s reduced the throughput to approximately 23 AC/H. Simultaneously, the percentage of conflict free flights increased from 55% to 98%.

Compared to the baseline scenario, a higher or equal throughput was realized at an equal percentage of conflict free flights. The throughput was up to 4 AC/H higher. The performance difference follows from the final spacing distribution.
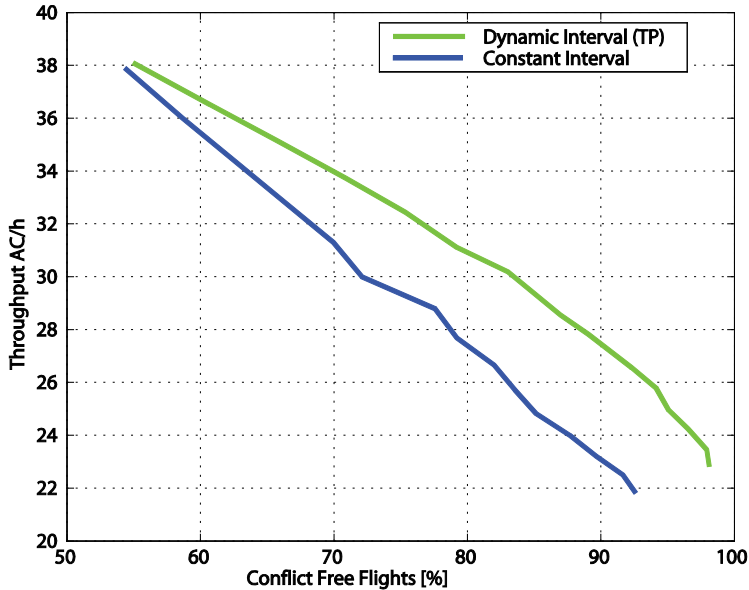
Figure 3-12 Throughput vs. the number of conflict free flights.

In Figure 3-13, the empirical cumulative density function distribution (eCDF) of the difference between spacing at final and the separation minima are plotted for the maximum throughput of 38 AC/H and an arbitrarily selected throughput level of 25 AC/H. At a throughput of 38 AC/H the eCDF's of the two scenarios intersect at 0 NM (i.e., the final spacing equals the separation minimum), hence the percentage of conflict free flights is equal. Increasing the spacing buffer moves the eCDF plotted in Figure 3-13 to the right. The variance of the eCDF for the dynamic interval case is lower than for the constant interval case. The result is that the percentage of conflict free flights is higher in case dynamic intervals are used.

3.8 Discussion

A machine learning approach to TP was developed and tested. Based on a limited set of input variables that are readily available through current surveillance systems, arrival time predictions were made for aircraft following fixed arrival routes in combination with CDO. The performance analysis results show that a model input comprising of only the aircraft type has very limited explanatory power. Adding the aircraft altitude and
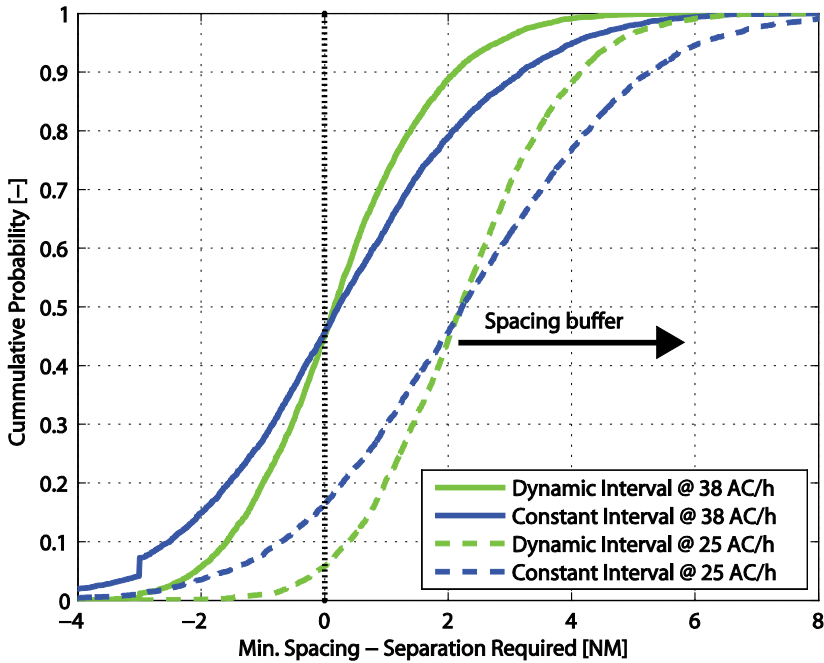
Figure 3-13 Empirical cumulative density function of final spacing.

groundspeed at the start of the CDO procedure to the model resulted in a model with significant explanatory power. The model could be further improved by including the surface and altitude winds. The latter two parameters particularly benefited the prediction performance at longer prediction horizons.

For further improvement of the TP performance additional inputs with significant explanatory power of the aircraft trajectory are needed. Likely candidates are the aircraft weight and aircraft intent information. However, the availability of additional parameters is limited when considering current surveillance system capabilities and data link availability. Also, some data are considered commercially sensitive, making it unlikely that these will be transmitted in the future. Possibly more aircraft state parameters and aircraft intent can be inferred from the surveillance system data as was done for the wind speed and direction [17-19].

The results of the spacing analysis suggest that on a short term, runway throughput for CDO can be increased if the required initial spacing is tailored to each aircraft pair using the TP. However, depending on the required throughput, a percentage of the aircraft need to be vectored off the fixed arrival routes for conflict resolution. Hence, not all

aircraft will fly the optimized descent. Ren and Clarke came to a similar conclusion in their work on the Tool for the Analysis of Separation and Throughput (TASAT) [10, 11].

The required aircraft spacing computed using the TP should be presented to the air traffic controller in such a way that he or she can formulate and execute a strategy such that all aircraft are spaced accordingly. This could be done using an arrival manager tool that supports the air traffic controller in setting up the sequence for CDO. After setting up the sequence, the spacing during the CDO phase has to be monitored. Also during this phase a form of controller support might be needed that provides information about whether an aircraft pair will remain separated and or whether conflicts might occur. This should avoid unnecessary tactical interventions and allow for timely conflict resolution. TP will also play an important role in such a support tool.

3.9   Conclusions

A machine learning approach to trajectory prediction was proposed. Historic aircraft trajectory and meteorological data was used to train predictive models. A stepwise regression approach was used to systematically determine which input variables to include predictive models based on their explanatory power. Trajectory prediction performance was examined using surveillance data and meteorological data for a 45 NM long closed-path continuous descent operation procedure. The aircraft time over seven points along a fixed arrival route were predicted. The prediction horizon ranged from 15 NM to 45 NM (runway threshold). At 15 NM the Generalized Linear Models explained 83% of the variance in the time over the trajectory points. The mean absolute error was 5 s with a root mean squared error (RMSE) of 7 s. At 45 NM the model explained 63% of the variance in the time over the threshold. The mean absolute error was 18 s with a RMSE of 24 s.

The trajectory prediction accuracy is expected to be sufficient to enhance runway throughput for closed-path Continuous Descent Operations on a short term. However, depending on the required throughput level some aircraft might be vectored and can no longer follow the optimized descent path.

3.10 Recommendations

Predicated on the results and conclusions in the previous sections the authors make the following four recommendations: 1) Extending the proposed method to predict the 2D trajectory to the full 4D trajectory of the aircraft. 2) Compare the trajectory prediction performance with other trajectory prediction methods that make use aircraft performance models. 3) To assess the impact of adding aircraft state parameters, aircraft

intent information, and environment information on the TP accuracy and 4) to explore methods to acquire this data.

3.11 References

1.   Mondolini, S., "Aircraft Trajectory Prediction Errors: Including a Summary of Error Sources and Data , FAA/Eurocontrol Action Plan 16," Version 0.2, July 2006.

2.   Anon., "User Manual for the Base of Aircraft Data (BADA), Revision 3.6," EUROCONTROL Experimental Center, Brussels, Belgium, September 2004.

3.   Coppenbarger, R.A., "En Route Climb Trajectory Prediction Enhancement Using Airline Flight-Planning Information." *AIAA Guidance Navigation and Control Conference*, 1999.

4.   Bronsvoort, J., McDonald, G., Paglione, M., Garcia-Avello, C., Bayraktutar, I., and Young, C.M., "Impact of missing longitudinal aircraft intent on descent trajectory prediction," *IEEE/AIAA 30th Digital Avionics Systems Conference*," Seattle (WA), USA, pp. 3E2-1 - 3E2-14, December, 2011. DOI: 10.1109/DASC.2011.6096062

5.   Mitchell, T., *Machine Learning,* McGraw-Hill, 1997.

6.   Le Fablec, Y., and Alliot, J.M., "Using Neural Networks to predict aircraft trajectories, " *Proceedings of the International Conference on Artificial Intelligence,* IC-AI '99, June 28 - July 1, 1999, Las Vegas, edited by Arabnia, H.R., CSREA Press, 1999, Vol 2., pp. 524-529.

7.   Cheng, T.C.T., Cui, D.C.D., and Cheng, P.C.P., "Data mining for air traffic flow forecasting: a hybrid model of neural network and statistical analysis." *Proceedings of the 2003 IEEE International Conference on Intelligent Transportation Systems*, IEEE, 2003, Vol 1, pp. 211-215. DOI: 10.1109/ITSC.2003.1251950

8.   Kun, W.K.W., and Wei, P.W.P., "A 4-D trajectory prediction model based on radar data,"*Proceedings of the 27th Chinese Control Conference July 16-18 2008*, 2008, pp. 591-594. DOI: 10.1109/CHICC.2008.4605732

9.   Nelder, J.A., and Wedderburn, R.W.M., "Generalized Linear Models," *Journal of The Royal Statistical Society Series A General*, Vol. 135, 1972, pp. 370–384. DOI: 10.2307/2344614

10. Ren, L., and Clarke, J.-P.B., "A Separation Analysis Methodology for Designing Area Navigation Arrival Procedures," *Journal of Guidance, Control, and Dynamics*, Vol. 30, No. 5, 2007, pp. 1319-1330. DOI: 10.2514/1.27067

11. Ren, L., and Clarke, J.-P.B., "Flight-Test Evaluation of the Tool for Analysis of Separation and Throughput," *Journal of Aircraft*, Vol. 45, No. 1, 2008, pp. 323-332. DOI: 10.2514/1.30198

12. Reynolds, H.J.D., Reynolds, T.G., and Hansman, R.J., "Human Factors Implications of Continuous Descent Approach Procedures for Noise Abatement in Air Traffic Control," *6th USA Europe Air Traffic Management RD Seminar Baltimore USA*, 2005.

13. SESAR, European ATM Master Plan, 2nd edition, October, 2012.

14. Anon., Aeronautical Information Package Netherlands, Air Traffic Control The Netherlands, [retrieved March 2012 www.ais-netherlands.nl].

15. Fox, J., *Applied Regression Analysis and Generalized Linear Models*, Second Edition, Sage Publications, 2008, pp. 379-387.

16. Mondoloni, S., Swierstra, S., and Paglione, M., "Assessing Trajectory Prediction Performance - Metrics Definition", 24th Digital Avionics Systems Conference, Washington, DC, 2005.

17. de Leege, A.M.P., Mulder, M., and van Paassen, M.M., "Novel Method for Wind Estimation using Automatic Dependent Surveillance-Broadcast," *Journal of Guidance Control and Navigation and Control,* Vol. 35, No. 2, 2012, pp. 648-653. DOI: 10.2514/1.55833

18. de Leege, A.M.P., Paassen, M.M. Van, and Mulder, M., "Using Automatic Dependent Surveillance-Broadcast for Meteorological Monitoring," *Journal of Aircraft*, Vol. 50, No. 1, 2013, pp. 249-261. DOI: 10.2514/1.C031901

19. de Haan, S., and Stoffelen, A., "High resolution temperature and wind observations from commercial aircraft," *Proceedings of the 8th International Symposium on Tropospheric Profiling*, edited by A. Apituley, H.W.J. Russchenberg, W.A.A. Monna, Organizing Committee of the 8th International Symposium on Tropospheric Profiling, Delft, The Netherlands, 2009.

20. Delahaye, D., and Puechmorel, S., "TAS and wind estimation from radar data," *Digital Avionics Systems Conference 2009,* IEEE, Orlando, FL, 2009, pp. 2.B.5-1 - 2.B.5-16. DOI: 10.1109/DASC.2009.5347547

21. Anon., Statistics Toolbox User's Guide R2012b Matlab, The Mathworks, Natick (MA), USA, Version 8.1, pp. 9-141 - 9-175.

4   Self-Spacing during the Continuous Descent Operation

Monte-Carlo simulations are performed to assess the feasibility of self-spacing to enable continuous descent operations in high-density traffic. Arrival streams of eight aircraft are simulated in a relative distance-based or absolute time-based self-spacing environment. These self-spacing concepts are used in combination with the three-degree decelerating approach that gives control over the speed-profile of the descent to perform the spacing task. Simulation results include the runway throughput, arrival delay, and the number of separation losses. For the relative distance-based spacing concept a sensitivity study is performed to assess the effects of operational aspects and arrival time uncertainty of the performance.

Abstract

Trajectory unpredictability of aircraft performing continuous descent operations results in reduced runway capacity, because more spacing is applied. A possible solution to this problem is self-spacing - the transfer of the spacing task from the controller to the pilot. Using a fast-time simulation tool the performance differences between distance- and time-based self-spacing in high-density traffic in terms of runway capacity and separation are quantified for the Three-Degree Decelerating Approach. Distance-based self-spacing is the most promising concept. The average runway capacity is 39 aircraft per hour (40% heavy, 60% medium aircraft). Runway capacity in case of time-based self-spacing is 3 aircraft per hour lower, due to spacing margins applied to lower the separation violation rate to the level of distance-based spacing. A sensitivity analysis was carried out for distance-based self-spacing. One of the results is that accurately determining the starting time and subsequently arriving at this time benefits the TDDA performance. TDDA performance is also affected by the initial speed and altitude as they affect the TDDA's control space.

4.1   Introduction

Continuous Descent Approach (CDA) is a cost effective mean to reduce aircraft noise, emissions, flight time, and fuel burn [1-4]. Aircraft continuously decelerate while on these approaches, which leads to trajectory unpredictability from the standpoint of a controller who is monitoring inter-aircraft spacing based on periodic radar updates of aircraft position.   As such, controllers apply larger spacing to prevent vectoring instructions that would conflict with the CDA. Larger spacing between aircraft reduces runway capacity down to 50% when compared to conventional approaches [5-8].

A possible solution to this problem is the use of in-trail self-spacing [6, 7]. The spacing task is transferred from the controller to the pilot. Self-spacing is proposed because of the availability of precise aircraft performance information and the control strategy onboard the aircraft. The maneuverability of an aircraft while executing a CDA is limited and driven by the aircraft performance, the control strategy, and wind conditions. Information about wind conditions the aircraft is likely to encounter during descent can be made available as described in [9]. The flight crew can plan and execute, with the help of onboard systems, a CDA to remain safely separated [10-12].

This paper discusses research into the performance of the Three-Degree Decelerating Approach (TDDA) in high-density arrival streams in a distance- or time-based self-spacing environment. The TDDA is a CDA that lies within the boundaries of present approach procedure limitations and gives the pilot control over the descent path to fulfill the spacing task [6, 9-13]. In a distance-based self-spacing environment the aircraft actively adapts its speed profile to the speed profile of the aircraft flying directly in front.

This requires that the aircraft predicts the trajectory of this leading aircraft. Using the relative state of the leading aircraft to predict the trajectory can give rise to transient motions in the arrival stream, hereafter referred to as the "slinky effect," resulting in spacing problems [14]. In this research intent-based trajectory prediction is introduced for the TDDA to prevent the slinky effect in case of distance-based self-spacing. Another solution to circumvent the slinky effect is a time-based self-spacing procedure, which does not require trajectory prediction of the leading aircraft during the TDDA. Its performance was compared with the more common distance-based procedure. In the time-based environment the aircraft receive a Required Time of Arrival (RTA) for the runway threshold point. The RTAs are set prior to the start of the TDDA with the aim to keep the aircraft safely separated during approach. A fast-time simulation tool was developed to investigate the differences in performance between distance- and time-based self-spacing in terms of capacity, and loss of separation.

4.2   Three-Degree Decelerating Approach

The TDDA is a straight-in approach, with a constant 3° geometrical path angle [13]. Figure 4-1illustrates the TDDA together with a conventional step-down approach. The approach procedure starts when the aircraft intercepts the fixed descent path at an altitude (7,000-10,000 ft) well above the altitude the aircraft intercepts the instrument landing system's glide slope. Initially the aircraft maintains a constant Indicated Airspeed (IAS).
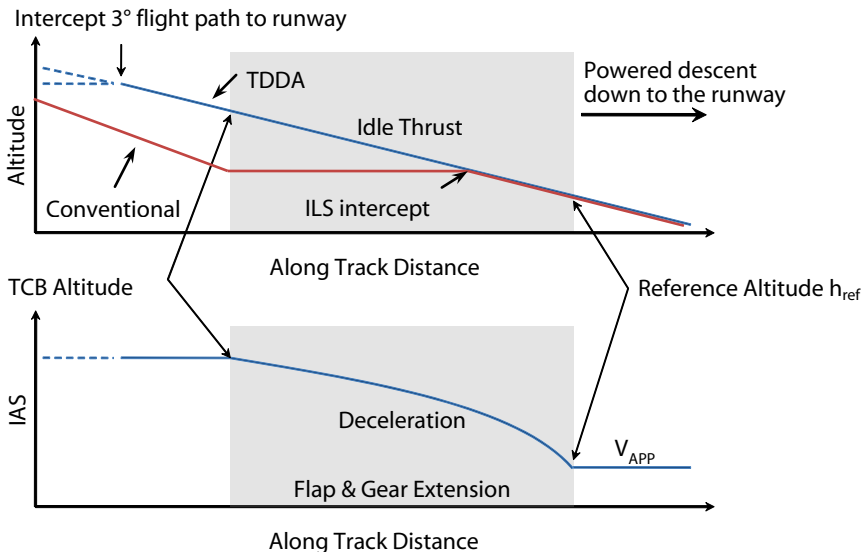
Figure 4-1 The Three-Degree Decelerating Approach profile.

To perform the spacing task, control over the descent is required. The TDDA gives the pilot two controls. The first control option is the thrust cutback (TCB) altitude, where engine thrust is set to idle and the aircraft starts to decelerate. Moving the TCB altitude up results in a slower descent and moving the TCB altitude down speeds up the descent. Second control option available after the TCB is flap scheduling. After the TCB the aircraft starts to decelerate. By changing flaps speeds the pilot controls the deceleration of the aircraft along the flight path. During the TDDA the pilot performs two tasks. One task is the spacing task in a distance-based or time-based self-spacing environment. Second task is to bring the aircraft in a stabilized landing configuration at the 1,000 ft reference altitude, h_{ref}, at approach speed V_{APP} for safety reasons. Below h_{ref} the aircraft maintains V_{APP}. Reaching V_{APP} above h_{ref} is not desired because engine thrust has to be reapplied, negating noise and fuel benefits.

4.2.1 Self-Spacing Task

The aim of the self-spacing task is to control the aircraft such that the minimum distance to the leading aircraft equals the minimum safe separation. In this situation the highest runway capacity is achieved for a fixed sequence. The separation minima used in this research are listed in Table 4-1. The self-spacing tasks in a distance-based and time-based self-spacing environment are different.

Table 4-1 Separation Minima in NM by weight category.

	Trailing Aircraft		
Leading Aircraft	*Heavy*	*Medium*	*Light*
Heavy	4	5	6
Medium	4	4	5
Light	2.5	2.5	2.5

Distance-Based Self-Spacing

Input for the self-spacing task in distance-based self-spacing is the predicted minimum distance between the own aircraft and the leading aircraft and the separation minimum. If this prediction indicates that the separation minima will be violated, the approach of the own aircraft has to be slowed down such that the minimum distance between the aircraft equals the separation minimum. If necessary the aircraft may decelerate to V_{APP} before reaching h_{ref}. If the predicted minimum exceeds the separation minimum, a faster approach profile should be selected if available. From a safety point of view, no approach should be selected where V_{APP} is reached below h_{ref}, even if this would close the spacing gap between the aircraft. In a distance-based self-spacing environment the pilot has two performance goals: First, the minimum distance to preceding aircraft should equal the applicable separation minimum, hereafter referred to as the separation goal. Second, the aircraft should reach to V_{APP} when at h_{ref}, hereafter referred to as the noise goal.

Time-Based Self-Spacing

In the time-based self-spacing environment the aircraft in the arrival stream adhere to a RTA for the runway threshold point. The RTA is computed before the aircraft starts the TDDA and is based on early predictions of the TDDA trajectories of the own aircraft and leading aircraft. The RTA is fixed during the TDDA. The RTA can be provided by the air traffic service provider but could also be calculated onboard the aircraft. Section V describes the methodology used in the simulations to compute the RTA. In the time-based concept the pilot has two performance goals. First, to cross the runway threshold at the RTA (time goal) and second the noise goal that is also applies in the distance-based environment. Figure 4-2 gives a schematic overview of both self-spacing concepts.
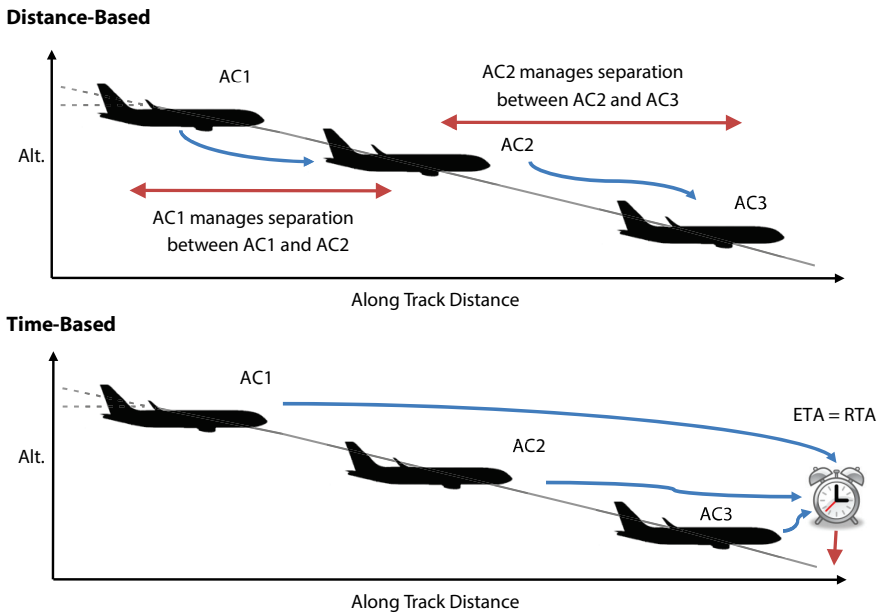
Figure 4-2 Distance- and Time-based spacing concepts.

TDDA Pilot Support Algorithms

Previous research showed that it is difficult for pilots to determine the correct TCB altitude and flap schedule [10, 11]. Therefore the pilot is supported by TCB altitude and flap scheduling optimization algorithms fed by wind and trajectory predictions to meet the noise goal, and separation or time goal [9-11]. Figure 4-3 gives an overview of the algorithms used to provide the pilot with a TCB altitude and flap schedule in the distance-based self-spacing environment.
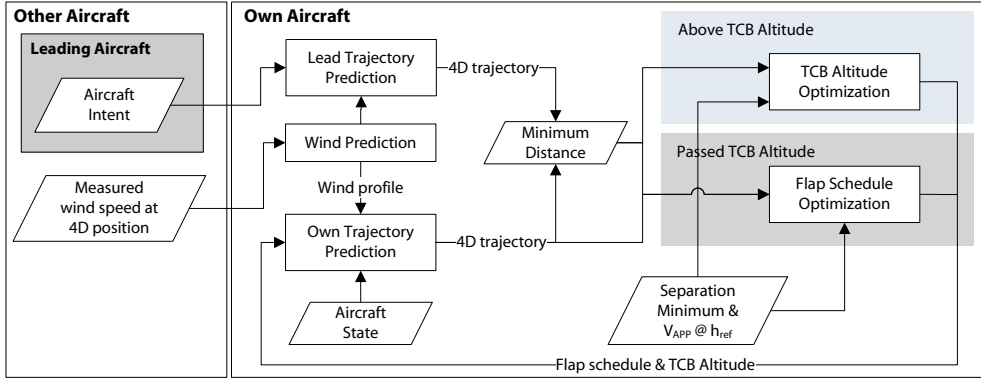
Figure 4-3 Structure of TDDA algorithm for distance-based self-spacing.

Shown on the left are the three algorithms that provide the input for the TCB altitude and flap schedule optimization algorithms at the right. The wind prediction algorithm used in this research is the Advanced Wind Prediction Algorithm described in [9]. The output is a wind profile the aircraft is likely to encounter during descent. The algorithm is driven by Automated Meteorological Data Relay (AMDAR) observations received from aircraft in the vicinity. The observations are stored, ordered, and filtered to obtain a wind prediction. Trajectory prediction of the own aircraft uses an onboard performance model. Inputs are the current state of the aircraft, planned TCB altitude, flap schedule, and the wind prediction. Trajectory prediction of the leading aircraft uses an aircraft intent based prediction model that is addressed in Section 4.3. In addition to an aircraft intent description of the leading aircraft, the wind prediction is used. From the trajectory predictions the minimum distance between the aircraft is derived.

The minimum distance is compared with separation goal (the separation minimum). The trajectory prediction of the own aircraft is also used to determine the altitude where V_{APP} is reached to check against the noise goal. When the aircraft position is still above the last computed TCB altitude, TCB optimization continues until all performance goals are met. The separation goal has priority over the noise goal when the minimum separation between the aircraft is less than the separation minimum. The noise goal has priority over the separation goal when the minimum separation between the aircraft exceeds the separation minimum. Once below the TCB altitude, flap schedule optimization is started. The flap scheduler is based on the scheduler developed by de Prins et al. [10]. The flap scheduler uses a binary search algorithm to determine the optimal schedule. The scheduler only optimizes for the noise goal is only if the separation goal is met, thus giving priority to the separation task.
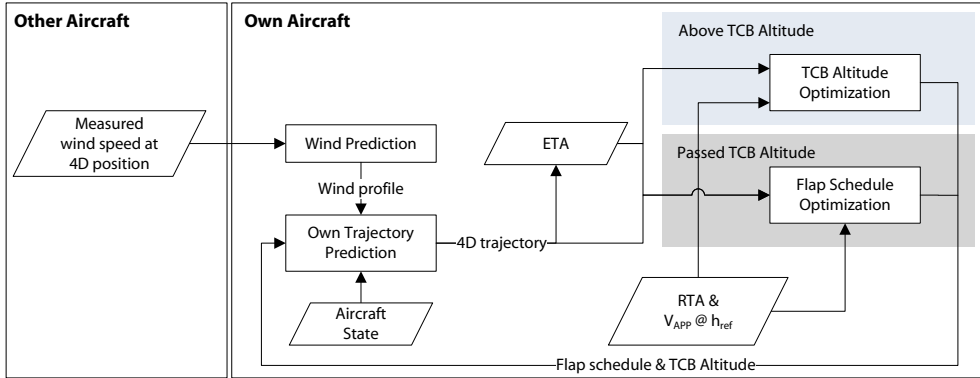
Figure 4-4 Structure of TDDA algorithm for time-based self-spacing.

The TDDA algorithm structure for time-based self-spacing is similar to the structure used for distance-based spacing, see Figure 4-4. The minimum distance between the aircraft is no longer computed and is replaced by the Estimated Time of Arrival (ETA), which is checked against the RTA. In the TCB altitude and flap schedule optimization algorithms the time goal is treated in a similar way as the separation goal.

4.3 Aircraft Intent-Based Trajectory Prediction

To prevent the slinky effect during of distance-based self-spacing aircraft intent is used to predict the trajectory of the leading aircraft. Captured in the intent is the outcome of optimization of the trajectory by the TDDA algorithms onboard the leading aircraft. If an aircraft descent profile is disturbed, for instance by a wind change or delayed pilot action, the TDDA algorithm optimizes the trajectory. The new trajectory is described in aircraft intent that may be different from the previous intent information, because of the optimization process. The intent is exchanged using a data-link. Predictions only based on previous states do not account for the ongoing optimization process. This can cause unnecessary control actions from the trailing aircraft that can propagate through the arrival stream resulting in the slinky effect.

4.3.1 Aircraft Intent Description of the TDDA

Aircraft intent is an unambiguous description of how the aircraft is to be operated within a timeframe. The intent information is the input to a trajectory predictor [15]. The TDDA procedure can be expressed in terms of aircraft intent and consists of three segments:

- Descent along the glide slope with constant IAS down to the TCB altitude.
- Descent and deceleration along the glide slope down to the altitude where V_{APP} is reached, normally 1,000 ft above the runway. During this segment the flaps and landing gear are extended.

- ▪ Descent along the glide slope with constant IAS (V_{APP}) down to the runway threshold.

Before continuing with the design of the trajectory predictor based on aircraft intent, the relevance of the leading aircraft prediction has to be analyzed.

4.3.2 Point of Minimum Separation

When the relative ground speed of the trailing aircraft is higher than the leading aircraft, the separation reduces. For two aircraft on CDA this is generally the case and minimum separation takes place when the leading aircraft passes the runway threshold. One exception is when the leading aircraft is locked into its own approach speed while the trailing aircraft is still decelerating to meet its approach speed and the ground speed of the trailing aircraft has dropped below the leading aircraft. A headwind component that increases with altitude can have the same effect. Simulations of arrival streams of aircraft performing a TDDA under actual wind conditions indicated that the minimum separation takes places when the leading aircraft has passed h_{ref} and maintains a constant IAS [16].

4.3.3 Intent-Based Trajectory Prediction

A prediction of the last constant speed segment is sufficient to determine the minimum separation. This segment can be predicted independent of the other segments using the leading aircraft ETA, V_{APP}, and descent path angle as illustrated in Figure 4-5.
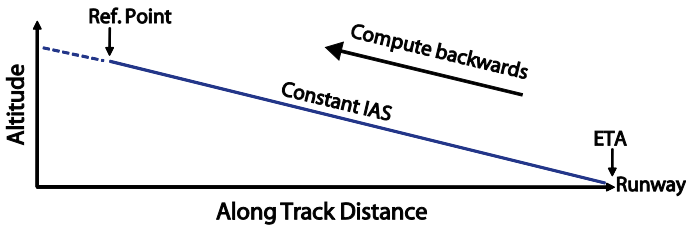
Figure 4-5 Intent-based trajectory prediction.

The speed and flight path angle are constant during the last stage of the final approach. Only aircraft intent information is needed for the prediction. The predictor starts at the runway threshold where the aircraft is at the ETA with speed V_{APP} and computes the trajectory up to the reference altitude. Because the aircraft maintains a constant IAS, no aerodynamic performance model of the leading aircraft is required. A wind prediction is supplied by the wind predictor.

4.4 TDDAs in Arrival Streams

An arrival stream consists of aircraft aligned to land on the same runway. The aircraft in the stream vary in type and weight and have different aircraft performance characteristics. This imposes constraints on the initial separation between aircraft at the start of the TDDA. These constraints are determined by size of the TDDA control space and the separation minimum or RTA. The control space is defined as the time interval between the earliest and latest possible arrival for a given starting time.

4.4.1 Factors that Affect the TDDA Control Space

The boundaries of the TDDA's control space are a function of the aircraft type, weight and wind conditions. Figure 4-6 gives the control spaces under three wind conditions for a Boeing 737NG-like aircraft. The boundaries are the TDDA with the shortest and longest duration. To get the shortest duration all flaps are extended at their maximum speed, resulting in a fast but late deceleration and the lowest possible TCB altitude. The longest duration is achieved by extending flaps at their minimum speed resulting in a gradual and early deceleration and the highest possible TCB altitude.
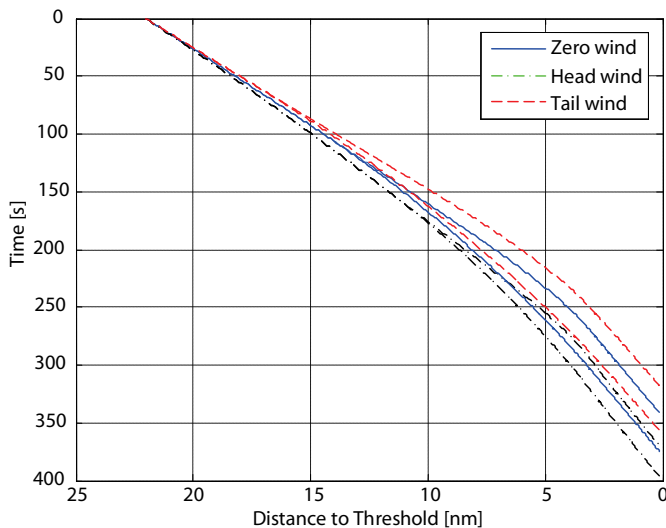
Figure 4-6 Control space time vs. distance for three wind conditions.

From Figure 4-6 the minimum and maximum time-to-fly can be derived. Alternatively the control space can be expressed in terms of the TCB altitude, as shown in Figure 4-7. The figure shows the range of TCB altitudes for which the noise goal can be met. A headwind increases the duration of the TDDA and lowers the TCB altitudes, but also makes the control space smaller. A tailwind has the opposite effect.
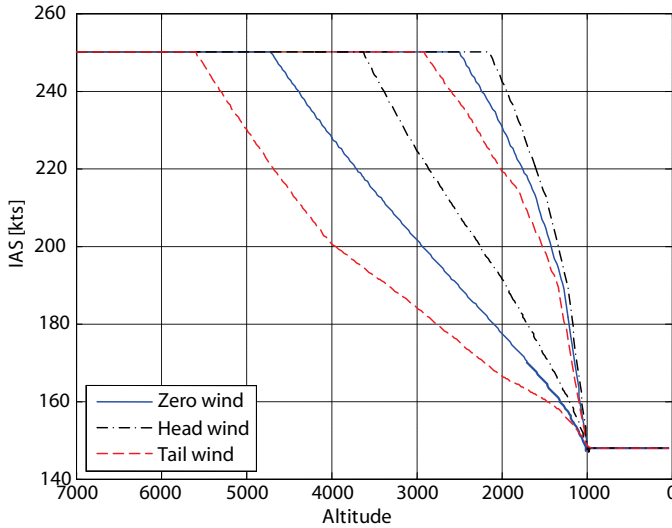
Figure 4-7 Control space IAS vs. altitude for three wind conditions.

4.4.2 Effect of Initial Separation on TDDA

Figure 4-8 shows a TDDA control space for three different initial separations behind a leading aircraft in a distance-based self-spacing environment. The separation goal is visualized by offsetting the leading aircraft trajectory prediction over the required separation away from the runway (separation boundary). The separation boundary gives the minimum allowable distance to the runway threshold.

For the upper control space the initial separation is too small. The separation boundary crosses the full control space. The aircraft must reduce speed to V_{APP} before the aircraft passes h_{ref} otherwise there will be a loss of separation. If the separation boundary does not cross the control space, which is the case for the lower control space, there will be spacing gap with a negative effect on the runway capacity. The aircraft is not able to fly the TDDA fast enough to close this gap.
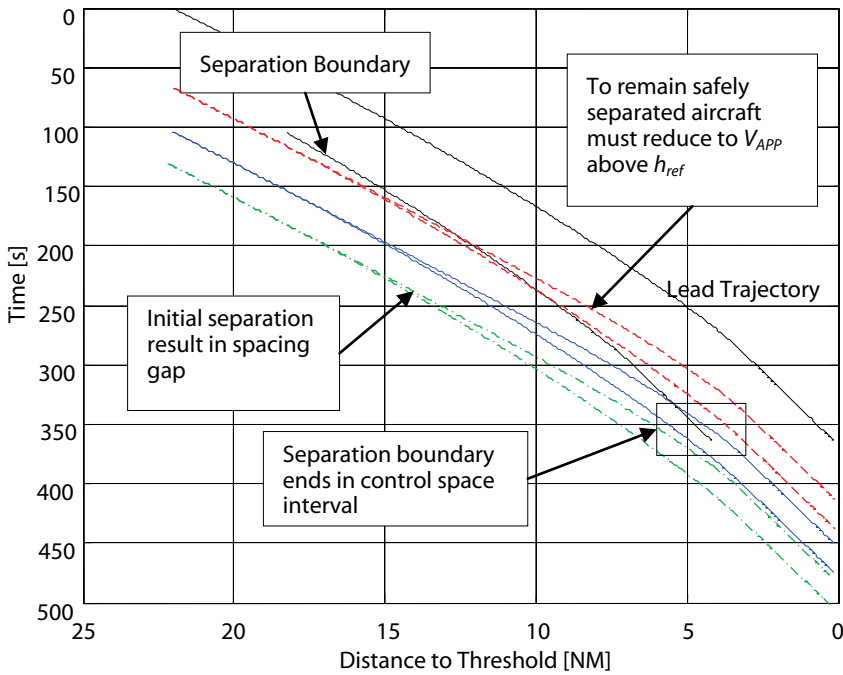
Figure 4-8 Effect of initial separation on TDDA performance

Only when the separation boundary ends in the control space a TDDA is possible that meets the performance goals. Figure 4-9 and Figure 4-10 show two possible trajectories for TDDAs with the highest and lowest possible TCB that meet the performance goals. A high TCB altitude is preferred because of the positive effect on the aircraft noise, fuel use, and less flap wear. For time-based self-spacing the separation is replaced by the RTA.
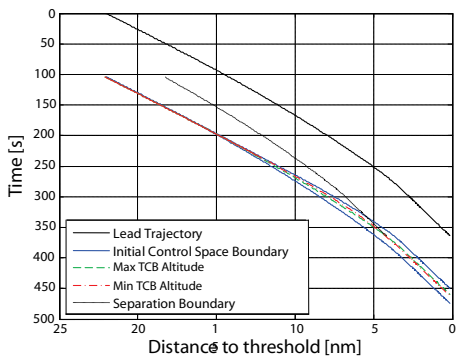
Figure 4-9 Feasible TDDA Trajectories.
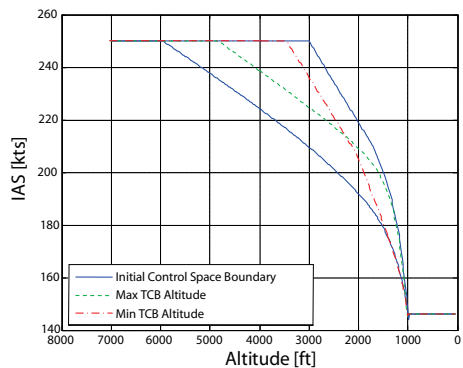
Figure 4-10 Feasible TCB Altitudes.

4.4.3 Initial Separation Constraints - Distance-Based Self-Spacing

Using the control space and separation boundary the initial separation constraints can be determined. Figure 4-11 illustrates how these constraints are determined for distance-based self-spacing. The control space boundaries are positioned such that the minimum separation equals the minimum safe separation; hence the minimum and maximum initial separation are visible.
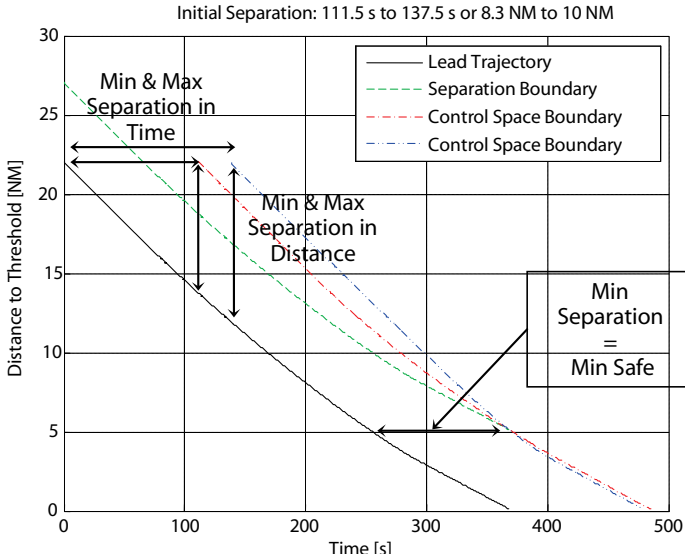
Figure 4-11 Min. and max. initial separation for distance-based spacing.
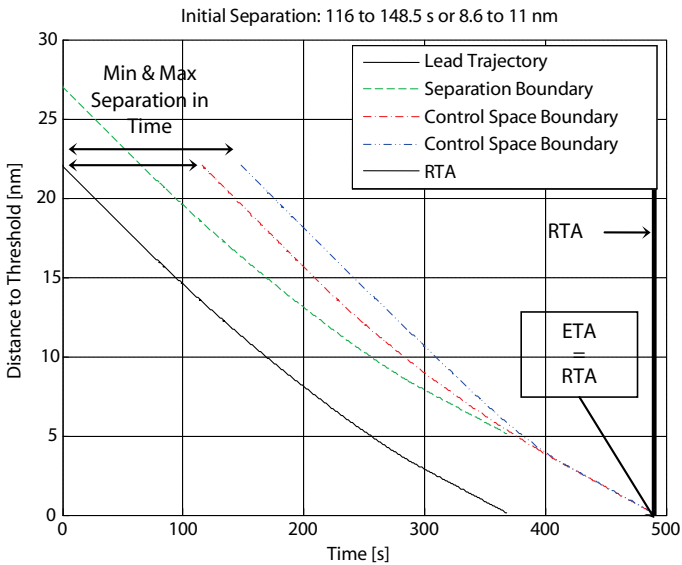
Figure 4-12 Min. and max initial separation for time-based spacing

4.4.4 Initial Separation Constraints - Time-Based Self-Spacing

The initial separation constraints in case of time-based spacing are determined in a similar way. The arrival time of the control space boundaries is set equal to the RTA from where the entry time interval is determined, see Figure 4-12. For sake of reference the separation boundary is drawn, hence the minimum separation between the aircraft should not be violated.

4.5 Fast-Time TDDA Simulation Tool

The fast-time simulation tool simulates arrival streams of aircraft executing the TDDA in a distance- or time-based self-spacing environment under actual wind conditions. Implemented in the simulator is the TDDA with the optimization and scheduling algorithms depicted in Figure 4-3 and Figure 4-4.

4.5.1 Aircraft Model

For the aircraft trajectory simulation and trajectory prediction, point mass models are used that approximate the following aircraft: Boeing 747-400, 777-300, 737-400, 737-800, and the Airbus 321. The models resemble the performance differences between different aircraft types and sizes, which for this research is more important than a very precise modeling of the aircraft performance. The equations of motion are derived using Figure 4-13 and Figure 4-14.
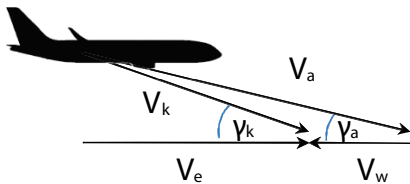
Figure 4-13 Kinetic Diagram.   **Figure 4-14 Force Diagram.**
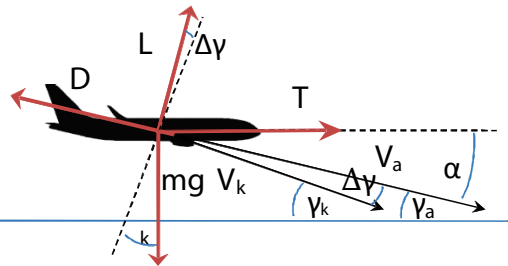
For small angles of attack (α) and assuming that the geometric path angle equals the aerodynamic path angle ($\gamma_k = \gamma_a$) the equations of motion in the kinematic reference frame F_k, along the fixed flight path are:

$$\sum F_Z : 0 = L - mg \cos \gamma_k \qquad (4\text{-}1)$$

$$\sum F_X : m\ddot{x}_k = T - D + mg \sin \gamma_k \qquad (4\text{-}2)$$

The mass is assumed to remain constant during the simulation and is used to determine the required lift force L and resulting drag. Subsequently the aerodynamic coefficients C_L and C_D and thrust are computed. The approach speed V_{APP} is 1.3 times the stall speed in the landing configuration plus 10 kts. Maximum flap extension speeds are obtained from the aircraft manufacturer or operator. Minimum speed for an aircraft configuration is 1.3 times the stall speed for that configuration.

4.5.2 Pilot Response Time and Wind

The pilot response time for flap and gear deployment is modeled using the Pilot Response Delay Model described in [5]. The model consists of a normal distribution fitted to pilot response time data collected during an experiment to investigate the variables that influence the performance of noise abatement procedures. AMDAR observations have been used to create 54 time-varying wind profiles of approximately one hour. For simulation of the aircraft trajectory the observations are used. For the wind prediction algorithm noise is superimposed on the observations to simulate measurement errors.

4.5.3 Setting the RTA and Initial Separation

The RTA and starting time for an aircraft are set 600 s before the leading aircraft starts the TDDA. Use is made of the prediction algorithms described in Section II to compute the control space boundaries and initial separation constraints. A 0.2 NM buffer is added to the separation minima to account for uncertainties in the predictions and changing wind conditions. The size of the buffer was determined using trial and error. To set the RTA the procedure to determine the initial separation constraints for distance-based self-spacing is followed. The RTA is set to the latest crossing of the control space boundaries with the time axis to account for trajectory deviations. The starting times position the aircraft exactly in between the initial separation constraints.

4.6 Distance- and Time-Based Self-Spacing Performance

Using the simulation tool 5,000 arrival streams consisting of eight aircraft have been simulated for both self-spacing environments. The aircraft type was selected randomly from the five available aircraft models. Per aircraft type three different weights were assigned randomly to the aircraft: the Operating Empty Weight (OEW), the Maximum Landing Weight (MLW), and mean of the OEW and MLW. The TDDA starts at 7,000 ft with 230 kts IAS. The performance of the TDDA in high traffic density arrival streams in the two self-spacing environments was assessed using the formulated noise, separation, time goal, and the runway capacity.

4.6.1 Noise Goal

The noise goal is met if V_{APP} is reached at h_{ref}. Figure 4-15 shows the average altitude where V_{APP} was reached, hereafter referred to as $h_{V_{APP}}$, per position in the arrival stream. As expected for time-based self-spacing no trend between the position of the aircraft and $h_{V_{APP}}$ could be identified (*R = 0.01, p = 0.29, Pearson 2-tailed*). On average $h_{V_{APP}}$ lies 20 ft above h_{ref}. When taking tolerances used by algorithms into account it is concluded that on average the noise goal is met. For the distance-based scenario a positive correlation between $h_{V_{APP}}$ and the position in the stream can be identified (*R = 0.15, p < 0.001, Pearson 2-tailed*). The noise reduction deteriorates towards the end of the arrival stream. From the median and 5th to 95th percentiles it can be concluded that the number of aircraft that fail the noise goal remains almost constant but that the deviation from h_{ref} increases, see Figure 4-16.

Deterioration of the noise reduction is caused by accumulation of delays (slowdown effect) in the arrival stream. If there is delay in the arrival stream all trailing aircraft in the stream are affected by this delay. Aircraft in the end of arrival stream are confronted with longer delays than the aircraft in the beginning of the arrival stream. To remain safely separated, aircraft increase the TCB altitude to the upper bound of their control space. If this is not sufficient, flap extension is advanced but this will result in failure to meet the noise goal. In case of a delayed arrival there is a significant correlation between h_{ref} and the magnitude of the delay (*R = 0.67, p < 0.001, Pearson 2-tailed*). When an aircraft arrives earlier than initially planned, no effect on the noise goal can be identified (*R = 0.06, p < 0.001, Pearson 2-tailed*).
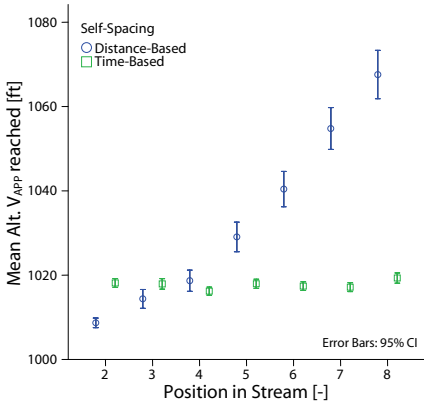
Figure 4-15 Altitude V_APP reached.
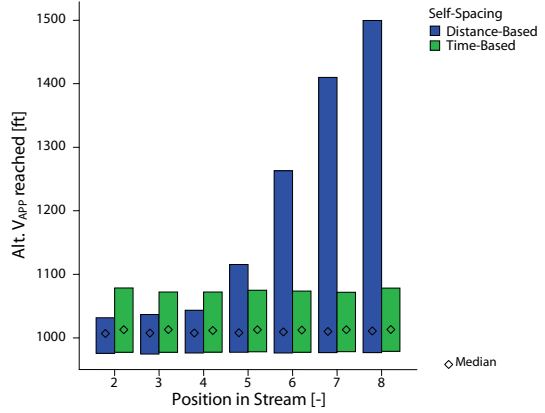
Figure 4-16 Median and 5th to 95th Percentile of Altitude V_APP reached.

Deterioration of the noise reduction due to accumulating time delays was suppressed by increasing the initial separation between the aircraft in the end of the arrival stream. The 0.2 NM buffer was increased for the last four aircraft to 0.5 NM. The aircraft first use the additional spacing when confronted with a delay before starting to move the TCB. The result is that the aircraft still reach V_{APP} at h_{ref}, see Figure 4-17. A positive correlation between $h_{V_{APP}}$ and the position cannot be identified *(R = 0.04, p < 0.001, Pearson 2-tailed)*.

4.6.2 Separation

Table 4-2 shows the deviation of the RTA for time-based self-spacing. All aircraft arrived within 49.5 s from the RTA and 99% of the aircraft arrived within 6.5 s of the RTA.

Table 4-2 Absolute Deviation from the RTA in Percentiles.

	Percentile					
	1	25	50	75	99	100
Deviation [s]	0.0	0.0	0.5	1.0	6.5	49.5

The two self-spacing concepts are compared using the separation margin. The separation margin is defined as the actual minimum separation minus the minimum allowable separation; hence a positive margin yields a spacing gap and a negative margin a separation loss. Visible in the histograms in Figure 4-18 are the 0.2 NM buffer applied in case of time-based self-spacing and the 0.2 NM and 0.5 NM buffers for the distance-based scenario. In both self-spacing environments separation violations do occur, see Table 4-3. Under distance based self-spacing there was a separation loss between 0.32% of the aircraft pairs. This percentage is comparable to go-around percentages reported by two major UK airports: London Heathrow 0.24% and London Gatwick 0.31% of the total annual arrivals [17, 18]. At this stage of the research this is deemed to be an acceptable reference level. Furthermore, other possible measures to bring this percentage down (e.g., the use of speed brakes) have not been evaluated because of limitations of the fast time simulator.
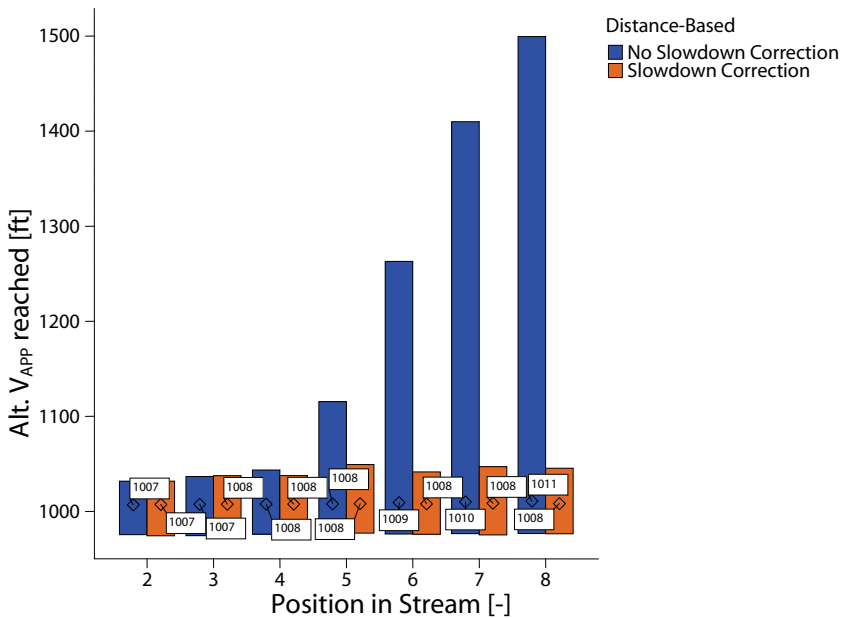
Figure 4-17 Effect of slowdown correction on median and 5th to 95th percentile of altitude V_{APP} reached.

In case of time-based self-spacing the separation violation percentage is 1.42%. To lower the violation rate for time-based spacing to the level of distance-based spacing, the separation buffer was extended by 0.3 NM to 0.5 NM. As a result, the separation violation percentage dropped to 0.27% and the separation margin increased, see Table 4-3.
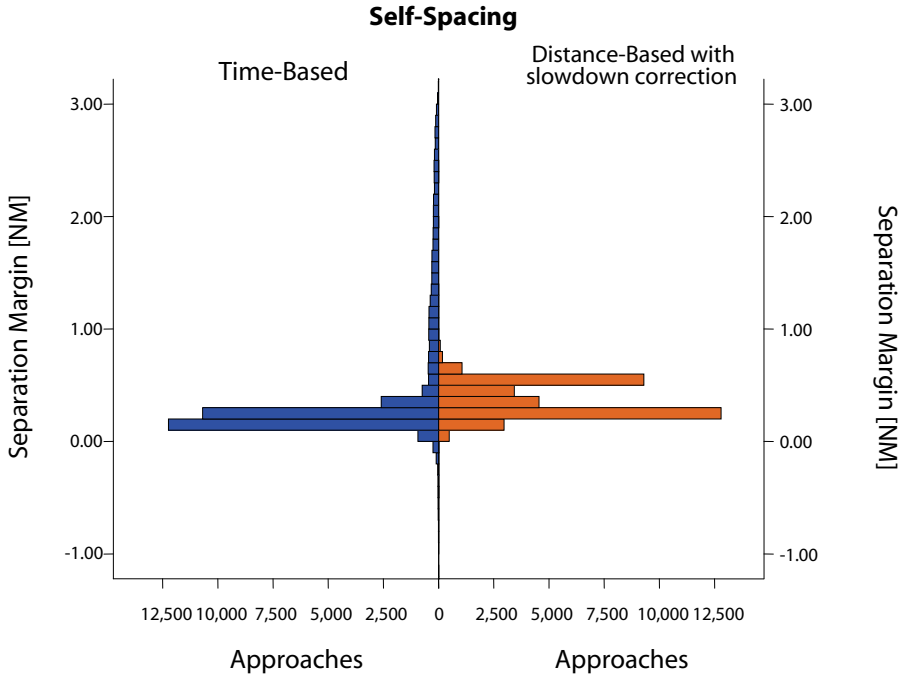
Figure 4-18 Separation Margin.

Table 4-3 Separation Violations Compared.

Self-Spacing	Mean	Median	Separation Violations
Time-Based	0.47 NM	0.22 NM	1.42%
Distance-Based	0.37 NM	0.31 NM	0.32%
Time-Based (0.5 NM buffer)	0.76 NM	0.52 NM	0.27%

4.6.3 Capacity

For evaluation of the runway capacity the time-based scenario with the extended separation buffer is used, such that the separation violation percentage is similar. For the distance-based self-spacing use is made of the arrival stream initially described in Section VI with the slowdown correction. The capacity figures are based on 5,000 randomly created arrival streams per self-spacing concept. Figure 4-19 shows the histograms of the capacity expressed in aircraft per hour (AC/H) for both forms of self-spacing. Independent of the self-spacing concept there is some spread in the runway

capacity, because the traffic mix (on average: 40% heavy, 60% large) is determined randomly, variation in the runway capacity can be expected.

Use of distance-based spacing results in a higher runway capacity than time-based spacing; as expected due to the 0.5 NM separation buffer used for time-based spacing. For distance-based self-spacing the separation buffer was also extended to 0.5 NM, but only for the last four aircraft. Furthermore, this buffer is used to absorb delays. For the time-based scenario the average runway capacity is 35.7 aircraft per hour (σ = 3.3 AC/H); when using distance-based spacing for eight aircraft in the arrival stream the average capacity is 39.2 aircraft per hour (σ = 3.6 AC/H). More descriptive statistics are summarized in Table 4-4. To determine significance of the difference in runway capacity, an Analysis of Variance test (ANOVA) is used *(F = 2560, p < 0.001).*
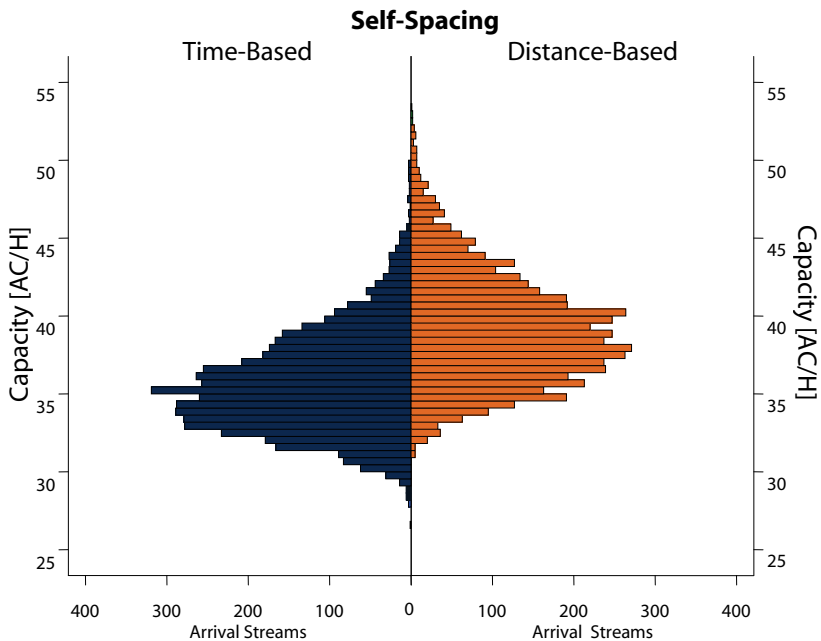
Figure 4-19 Runway Capacity.

Table 4-4 Capacity descriptive statistics in AC/H

Self-Spacing	Mean	Median	Std.	Min	Max	Range
Time-Based	35.7	35.3	3.3	26.7	49.7	23.0
Distance-Based	39.2	38.8	3.6	30.9	53.3	22.3

A simulation tool for arrival streams executing a conventional approach is not available; this makes an exact capacity comparison impossible. The runway capacity figures are analyzed using a packing factor. The packing factor *PF* is defined as:

$$PF = \frac{\sum_{i=2}^{k} S_{allowed}}{\sum_{i=2}^{k} S_{actual}} \forall S_{actual} \geq S_{allowed} \qquad (4\text{-}3)$$

where *k* is the number the aircraft in the arrival stream, S_{actual} is the actual separation minimum between two aircraft, and $S_{allowed}$ the minimum safe separation. Separation violations are not included in the *PF* calculation. If *PF = 1* the runway capacity equals the theoretical maximum. As expected from results discussed earlier the *PF* for distance-based spacing is higher than for time-based spacing: 0.90 and 0.81, respectively. Both self-spacing scenarios increase runway capacity significantly when compared to runway capacity figures for current CDA operations [4, 6].

Using conventional approach procedures the *PF* will also be less than 1. The runway capacity observed in the distance-based simulations is a least 90% of the runway capacity when using conventional approach procedures.

4.7   Sensitivity Analysis

Time-based and distance-based self-spacing perform comparable except for the runway capacity where the distance-based scenario has a three AC/H advantage. Runway capacity is one of the major issues with CDAs in high-density traffic; in that respect distance-based self-spacing is the most promising option. Therefore a sensitivity analysis was carried out for the distance-based self-spacing scenario with the slowdown correction. The goal of this study was to investigate the effects of ATM performance, top of descent altitude, predictions based on erroneous weight information, and initial speed on the TDDA performance. The main effects are described; possible interactions are the subject of ongoing research.

4.7.1 Initial Control Space Prediction

In the simulations the starting time of the TDDA for an aircraft was set 600 s before the preceding aircraft starts the TDDA to give the controller and the aircraft sufficient time to let the aircraft arrive at the computed entry time. The required time is subject of ongoing research. To assess the effect of this time period (lead time to start) on the TDDA performance, the lead time to start is reduced to 0 s in 3 equal steps of 200 s. In case the lead time to start is 0 s, the control space used to determine the starting times for the trailing aircraft are computed when the leading aircraft start the TDDA.
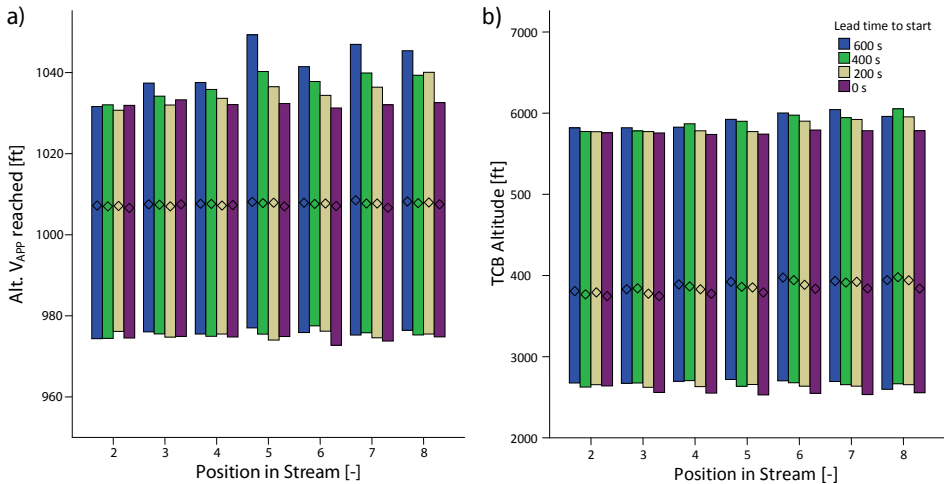
Figure 4-20 Median and 5th to 95th percentile of altitude V_{APP} and TCB altitude.

From Figure 4-20 it is concluded that the lead time to start affects the TDDA noise goal performance and TCB altitude, especially those of the last four aircraft in the arrival stream. The noise goal performance and TCB altitude become less dependent on the position of the aircraft in the arrival stream. The Predictions over a shorter time horizon benefit the performance of the TDDA. The number of separation violations and the runway capacity (39.1 AC/H ±0.1, PF= 0.90) are not affected.

The slowdown effect is not visible when the lead time to entry is 0 s, hence the correction is no longer needed. Without the slowdown correction, the capacity would increase to 40.6 AC/H (0.34% separation violations) and only a 5 ft deterioration of the noise goal is visible. Time-based spacing is still being outperformed by distance-based spacing in case the shortest time period would be feasible, both in terms of capacity (-2.4 AC/H) and separation violations (+1.38%).

4.7.2 Initial Separation Distribution

In the previous sets of simulations the TDDA starting time was such that the aircraft were positioned in the middle of their control space. It is expected that in reality a distribution will be observed around the computed starting time. A new set of simulations was made in which the aircraft were initially positioned around computed starting time using a normal distribution with the standard deviations σ ranging from 1 to 6 s.
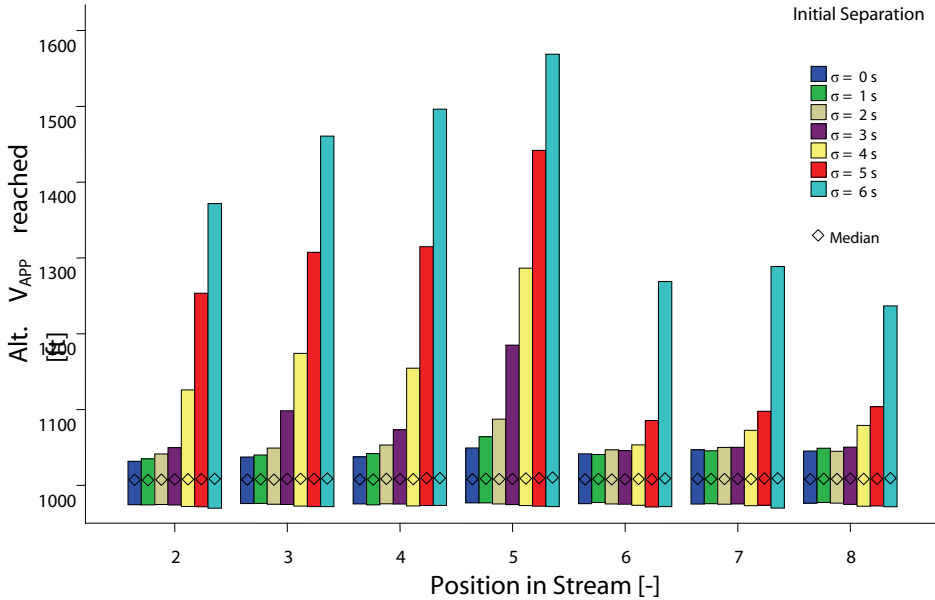
Figure 4-21 Median and 5th to 95th percentile of altitude V_{APP}.

Noise Goal

Figure 4-21 shows the median and 5th to 95th percentile of $h_{V_{APP}}$ per position for each initial separation distribution. The noise reduction deteriorates with the increase of the standard deviation σ, but the impact is limited when the standard deviation is below or equal to 3 s. The 3 s standard deviation means that 95% of the aircraft are positioned within 6 s of the middle of the control space, creating a 12 s interval. This interval is equivalent to the smaller control spaces. A bigger standard deviation causes aircraft to be positioned outside the initial separation constrains, making it impossible to fly a TDDA and remain safely separated as was shown in Figure 4-8. Because of the additional initial separation applied in the end of the arrival stream, the effect is less strong there.

Separation Violations and Capacity

The separation violation percentage increases almost exponentially with the standard deviation, see Figure 4-22. No significant effect on the runway capacity could be identified *(F = 1.859, p=0.084)*.

Thrust Cutback Altitude

The initial separation distribution affects the TCB altitude. This is logical because TCB altitude is related to the control space and initial separation. The mean of the TCB altitude shows a negative trend. The TCB altitude lies approximately 100 ft lower for σ = 6 s when compared to σ = 0 s. An ANOVA confirms the effect of the initial separation on

the TCB Altitude *(F = 9.847, p < 0.001)*. The effect depends on the position of the aircraft in the stream *(F = 104.548, p < 0.001)*.
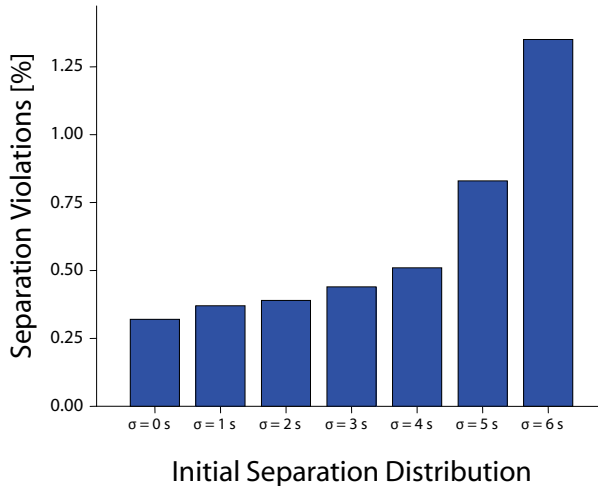
Figure 4-22 Effect of initial separation on separation violations.

Starting Altitude

The starting altitude of the TDDA procedure sets the length of the TDDA and the maximum achievable TCB altitude. A higher altitude allows for higher TCB altitudes, see Figure 4-23. The median of TCB altitude increases slightly. The increase of the 95th percentile indicates that only a number of flights with a TCB altitude above the median benefit from the increased starting altitude. The median altitude where V_{APP} is reached remains constant, but the 95th percentile increases indicating that the deviations from the reference altitude become bigger. A higher starting altitude and thus a longer TDDA leads to an increase of the number separation violations, see Table 4-5.

Table 4-5 Effect of starting altitude on % of arrivals with separation violation.

Starting Altitude	Separation Violations [%]
8,000 ft	0.48%
7,000 ft	0.32%
6,000 ft	0.26%

Figure 4-23 Median and 5th to 95th percentile of altitude V_{APP} and TCB Altitude.

4.7.3 Initial Speed

Figure 4-24 shows the effect of the initial speed on the noise goal performance and the TCB altitude. A lower speed results in a lower TCB altitude but also shrinks the control space. The smaller control space limits the aircraft in their power to account for the slowdown effect. A speed of 230 kts IAS is the maximum possible speed; beyond 230 kts the acceleration along the glide path cannot be stopped for all aircraft types due to flap limits (speed brakes are not included in the simulation).

Figure 4-24 Median and 5th to 95th percentile of altitude V_{APP} and TCB Altitude.

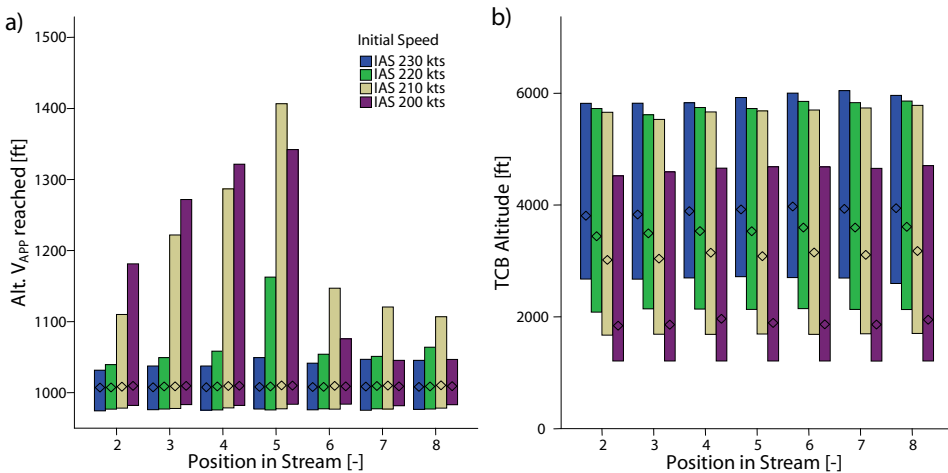
Figure 4-24 Median and 5th to 95th percentile of altitude V_{APP} and TCB Altitude.

No effect on the runway capacity was expected because the approach speeds were unchanged, this is confirmed by an ANOVA *(F = 0.627, p < 0.645)*. The lower IAS has a negative effect on the control space of the aircraft with a negative effect on the number of separation violations, see Table 4-6.

Table 4-6 Effect of initial speed on separation violations.

Initial Speed	Separation Violations [%]
230 kts	0.32%
220 kts	0.53%
210 kts	1.26%
200 kts	2.00%

4.7.4 Aircraft Weight

The aircraft weight is one of the factors that determine the aircraft performance. In the simulations performed thus far it was assumed that the weight of the aircraft used by the TDDA algorithms equals the actual weight of the aircraft. Because of the use of standard passenger and baggage weights, it is expected that the computed weight and the actual weight differ. To investigate the effect of differences between the computed and actual weight on the TDDA performance an error as percentage of the payload was introduced. Three simulations were set up with payload errors up to 0%, ±5%, ±10%. The actual percentage per aircraft in the arrival stream was selected using a uniform distribution. No significant effects on the TDDA performance could be identified.

4.8 Discussion

The aim of this research was to evaluate the performance of the TDDA in high-density traffic arrival streams in a distance- and time-based self-spacing environment. Distance-based self-spacing concepts may suffer from instability of arrival streams, if predictions of the leading aircraft trajectory are based on previous aircraft states. In this research prediction of the leading aircraft trajectory solely based on intent was introduced in the TDDA. No signs of the slinky effect have been found in the simulated arrival streams. In case of time-based spacing the trailing aircraft trajectory is not adjusted as a reaction to changes in the leading aircraft trajectory, hence the slinky effect is by definition not possible.

Application of the TDDA in arrival streams imposes constraints on the initial separation between aircraft. The initial separation interval expressed in time or distance follows from the control space that is a function of the aircraft type and weight, and the wind conditions.

Under distance based self-spacing there was a separation loss between 0.32% of the aircraft pairs. To lower the violation rate for time-based spacing to the level of distance-based spacing, the separation buffer to set the RTA was extended by 0.3 NM to 0.5 NM.

For the time-based scenario the average runway capacity is 35.7 AC/H, when using distance-based spacing the average capacity is 39.2 AC/H. The runway capacity under distance-based self-spacing is 90% of the theoretical maximum capacity. Because distance-based self-spacing outperformed time-based self-spacing in terms of runway capacity, distance-based self-spacing is considered to be the most promising option.

To further evaluate the performance of the TDDA in a distance-based self-spacing environment a sensitivity study was carried out. Reducing the time between computing the TDDA starting time and the actual starting time improves the performance of the TDDA. However, this also gives the pilot and controller less time to take actions to let the TDDA start on time. The sensitivity analysis also shows that it is crucial for the aircraft arrive to start the TDDA at the set starting time. When aircraft are positioned outside their control space, the performance degrades. The initial conditions of the TDDA affect the performance. A higher initial speed results in a larger control space, which benefits performance. A higher starting altitude results in higher TCB altitude but also increases the number separation violation. The trajectory becomes longer, which increases the uncertainties. Trajectory predictions based on erroneous aircraft weight with errors up to 10% of the payload did not have a significant effect on the performance.

4.9   Conclusion

Distance-based self-spacing has a three AC/H runway capacity advantage over time-based self-spacing when the number of separation violations between aircraft is comparable. Runway capacity is one of the major factors limiting the use CDAs; in that respect distance-based self-spacing is the most promising option. The observed runway capacity is 90% of the theoretical maximum. A sensitivity analysis for distance-based self-spacing showed that accurately determining the starting time and the ability to arrive at the starting time with great precision benefits the TDDA performance.

4.10 References

1.   Wilson, I., and Hafner, F., "Benefit assessment of using continuous descent approaches at Atlanta, *"The 24th Digital Avionics Systems Conference Proceedings*, Institute of Electrical and Electronics Engineers, Vol. 1, Washington, DC, 2005, pp. 2.B.2- 2.1-7, DOI: 10.1109/DASC.2005.1563318.

2. Dinges, E., "Determining the Environmental Benefit of Implementing Continuous Descent Approach Procedures," USA/Europe Air Traffic Management Research and Development Seminars, Paper 17, July 2007.

3. Coppenbarger, R.A., Mead, R.W., and Sweet, D.N., "Field Evaluation of the Tailored Arrivals Concept for Datalink-Enabled Continuous Descent Approaches," AIAA Paper 2007-7778, 2007.

4. Wubben, F.J.M., and Bussink, J.J., "Environmental Benefits of Continuous Descent Approaches at Schiphol Airport Compared with Conventional Approach Procedures," National Aerospace Laboratory, TR NLR-TP-2000-275, Amsterdam, The Netherlands, May 2000.

5. Tan Ho, N., and Clarke, J.-P.B.,"Mitigating Operational Aircraft Noise Impact by Leveraging on Automation Capability", AIAA Paper 2001-5239, 2001.

6. Ren, L., Clarke, J.-P.B., and Tan Ho, N., "Achieving Low Approach Noise Without Sacrificing Capacity," *Proceedings of the 22nd Digital Avionics Systems Conference,* Institute of Electrical and Electronics Engineers,Vol. 1, Piscataway, NJ, 2003, pp 1.E.3- 1.1-9, DOI: 10.1109/DASC.2003.1245810.

7. Abbott, T.S., "Speed Control Law for Precision Terminal Area In-Trail Self Spacing," Tech. rep., NASA Langley Research Center, Hampton, VA, July 2002, NASA/TM-2002-211742.

8. Ren, L., and Clarke, J.-P.B., "Flight-Test Evaluation of the Tool for Analysis of Separation and Throughput," *Journal of Aircraft*, Vol. 45, No. 1, Jan-Feb 2008, pp. 323-332. DOI: 10.2514/1.30198

9. de Gaay Fortman, W.F.M., van Paassen, M.M. ,Mulder, M., in 't Veld, A.C., and Clarke, J.-P.B., "Implementing Time-Based Spacing for Decelerating Approaches," *Journal of Aircraft*, Vol. 44, No. 1, January-February 2007, pp. 106-118, DOI: 10.2514/1.22253.

10. de Prins, J.L., Schippers, K.F.M., Mulder, M., van Paassen, M.M., in 't Veld, A.C., and Clarke, J.P.B., "Enhanced Self-Spacing Algorithm for Three-Degree Decelerating Approaches," *Journal of Guidance, Control & Dynamics,* Vol. 30, No. 5, Mar-Apr 2007, pp. 576-590, DOI: 10.2514/1.24542.

11. in 't Veld, A.C., van Paassen, M.M., Mulder, M., and Clarke, J.-P.B, "Pilot Support for Self-Separation during Decelerating Approaches," AIAA Paper 2004-5102, 2004.

12. de Beer, B.A.F., Mulder, M., van Paassen, M.M., and in't Veld, A.C., "Development of an Ecological Interface for the Three-Degree Decelerating Approach," AIAA Paper 2008-7108, 2008.

13. Clarke, J.-P.B., *A Systems Analysis Methodology for Developing Single Event Noise Abatement Procedures*, Ph.D. dissertation, Massachusetts Institute of Technology, 1997.

14. Slater, G.L., "Dynamics of Self-Spacing in a Stream of In-Trail Aircraft," AIAA paper 2002-4927, 2002.

15. Vilaplana, M.A., Gallo, E., Navarro, F.A., and Swierstra, S., "Towards a formal language for the common description of aircraft intent," *The 24th Digital Avionics Systems Conference Proceedings*, Institute of Electrical and Electronics Engineers, Vol. 1, Washington, DC, 2005, pp. 3.C.5 - 3.1-9. DOI: 10.1109/DASC.2005.1563351

16. de Leege, A.M.P., *Three-Degree Decelerating Approaches in Arrival Streams*, Unpublished MSc. thesis, Delft University of Technology, September 2007.

17. BAA Heathrow, "Flight Evaluation Report 2007," British Airports Authority, 2007, http://www.baa.com/assets//B2CPortal/Static%20Files/Noise%20Booklet.pdf [retrieved 31 January 2009].

18. BAA London Gatwick, "Flight Evaluation Report 2007," British Airports Authority, 2007, http://www.baa.com/assets/B2CPortal/Static%20Files/FEU%20Report%202006-07.pdf, [retrieved 31 January 2009].

5 A Time-Space Diagram based Controller Support Tool

The Time-Space Diagram (TSD) support tool is presented. The interface was designed following the principles of ecological interface design to make the constraints and complexity of the continuous descent operations perceptually evident and provide tools and information to the air traffic controller to be an active problem solver. The interface design is evaluated using the concept of visual momentum to make integration of information presented on the TSD and conventional plan view display easier. Also direct manipulation interfaces are introduced for typical air traffic controller instructions, such as speed control. The direct manipulation interfaces should enable the air traffic controller to rapidly plan and execute actions. A human-in-the-loop experiment is setup to assess the effects of the new interface elements on the air traffic controller performance, workload, and situation awareness.

Abstract

Tactical control during a closed path continuous descent operation is unwanted since it reduces the aircraft's ability to follow the optimized descent profile. To prevent tactical control, air traffic controllers apply arbitrarily large spacing buffers to ensure separation throughout the descent. A controller support tool is required for early de-confliction, spacing, and sequencing to facilitate these operations without the need to apply large buffers. The Time-Space Diagram decision support tool was developed previously to make the constraints and complexity of a continuous descent operation perceptually evident and provide tools and information to the controller to be an active problem solver. This paper addresses the further development and validation of the interface. The concept of visual momentum was applied to enhance the efficiency of working the multi-display interface that consists consisting of the plan view display and time-space diagram. Direct manipulation tools were developed to enable the controller to plan and implement actions, such as speed and altitude control. A controller-in-the-loop-experiment was set up to validate the interface. In the experiment subjects used either the Time-Space Diagram support tool or –as a baseline– a stack list that provided the required spacing and the time to lose or gain. Both interfaces enabled the subjects to space the aircraft safely and efficiently. Compared to the baseline, the Time-Space Diagram interface freed time to plan traffic ahead using the direct manipulation interfaces, which according to all subjects worked intuitively. The number of instructions per aircraft was decreased by 35%. Early accurate speed control was applied and use of heading vectors was no longer necessary in most scenarios. As a result, aircraft commenced their continuous descent at a higher altitude and greater distance from the runway. Controller workload was significantly reduced and; situation awareness increased.

5.1 Introduction

Continuous Descent Operation (CDO) has been identified by ICAO, Single European Sky Air traffic Management Research (SESAR) and NextGen to improve the environmental performance of air transport.[1-3] Aircraft on CDO descend from an optimal position with minimum engine thrust. Demonstrated benefits include reduced noise footprints, fuel-consumption, and emissions when compared to conventional approaches.[3] Closed path CDO procedure designs enable optimization of the vertical profile by the aircraft flight management system for the environmental performance. However, tactical control procedures by Air Traffic Control (ATC) often take aircraft off the closed path reducing the ability to fly the optimized CDO. In that case the economic and environmental benefits are (partially) lost. Tactical control to separate aircraft is not needed if the spacing between aircraft at the start of the procedure ensures separation throughout the entire descent.[4, 5] This requires tailoring of the inter-aircraft spacing at the start of the

procedure for each aircraft pair, based on the aircraft trajectories during the remainder of the approach. From the Air Traffic Controller's (ATCO's) perspective these trajectories are unpredictable, because of the absence of non-transitional periods in the descent and the long prediction horizon.[6] To avoid tactical control, ATCOs apply arbitrarily large spacing buffers at the cost of capacity.[7,8] A controller support tool is needed that enables the ATCO to formulate and execute a control strategy that would ensure the separation throughout the CDO while minimizing and eventually removing the need for additional buffers.

Refs. [9]-[11] describe the use of a Time-Space Diagram (TSD) as an ATCO support tool for CDO. The TSD is presented on a second display next to the Plan View Display (PVD). The PVD shows the current aircraft position in a spatial reference frame, see Figure 5-6. The TSD gives a graphical representation of the current and future traffic situation in the time-space reference frame. Tielrooij et al. implemented the TSD in a real-time simulator and tested the initial concept of the TSD as a support tool.[9, 10] ATCOs reported that the TSD prompted a change in the arrival strategy from a first-come first-serve sequence to the sequence predicted by the TSD and a shift from tactical conflict avoidance to strategic metering. The ATCOs also raised problems with the presentation of information on the TSD. Secondly, the ATCOs indicated difficulties assessing the impact of a certain instruction on the traffic situation and suggested solution guidance.

In 2009 Van der Eijk et al. continued the development of the TSD.[11] The layout of the TSD was made more clear and self-explanatory. Static what-if tools were developed that show the effect of typical tactical instructions on the TSD to provide solution guidance. Validation of the enhanced interface confirmed the results from the initial validation and indicated a reduction of the controller workload and the number of instructions compared to a scenario without any controller support. However, the ATCOs' feedback on the what-if tools was mixed. Not all ATCOs were convinced of the usefulness of the tools. Two of out of the eight ATCOs never used the tools and three out of eight commented the tools made the interface harder to use. No significant effects of the what-if tools on the performance were found. ATCOs suggested to work on a better integration of the PVD and TSD, a comment similar to what was reported in experiments evaluating a 4D trajectory planning tool, which also uses the PVD and TSD.[12] In all these evaluations, ATCOs reported difficulties integrating information displayed on the PVD and TSD in one mental picture and started to put all their attention to the TSD. This situation is unwanted, because the TSD does not provide the information to build a complete mental picture.

This paper addresses the further development of the PVD-TSD interface to make working with the multi-display interface easier, and tests the PVD-TSD interface against a

more conventional solution to support the ATCO. To prevent focus on the TSD only and to enhance the efficiency of working with the multi-display interface, the principle of visual momentum was applied. Furthermore, to replace the what-if tools, which proved cumbersome in the previous version, Direct Manipulation Interfaces (DMIs) were developed. A controller-in-the-loop experiment was set up to test the new interface elements and to test the PVD-TSD against a more conventional stack list visualization to support the ATCO. In the experiment six subjects controlled arriving traffic inbound to one or two Initial Approach Fixes (IAFs) using either the PVD-TSD interface or PVD in combination with the stack list (PVD-STL). Subjective ratings of workload and situation awareness were collected and aircraft trajectories, controller instructions, and the use of the interfaces were analyzed. The impact of the TSD on the controller interface is significant. The TSD shows the traffic in a different reference frame and requires a significant amount of screen real estate. The use of a stack list would require minimal changes to the existing interface and is closer to current systems. The stack list provided the required inter-aircraft spacing and the time to gain or lose to meet the spacing requirement. This paper is structured as follows: Section 5.2 presents the general operational concept to facilitate closed path CDO that was used in this research. In addition an analysis of the variability of the required inter-aircraft spacing using real flight-data is presented, urging the need for a support tool. Section 5.3 introduces the TSD and discusses the layout and information that can be derived from it. Section 5.4 describes the changes made to the interface to enhance visual momentum, followed by a description of DMIs in Section 5.5. The setup of the experiment is discussed in Section 5.6. Sections 5.6.3, 5.7, and 5.7.6 contain the results, discussion and conclusions.

5.2   ATC for Closed-Path Continuous Descent Operation

5.2.1   Continuous Descent Operation

Two main design options for CDO procedures are open and closed path designs.[13] In open-path procedure designs, vectoring is used during the entire or a part of the approach. Vectoring in combination with speed control gives ATC the flexibility to separate and expedite traffic during the CDO in high density traffic. However, the resulting CDO is often suboptimal in terms of the environmental benefits that are achieved. Open path CDOs can be readily implemented, but there is a trend towards closed path designs to improve the ATM system's environmental performance and efficiency as can be seen from the SESAR Lines of Changes in Ref. [14]. In a closed-path procedure design the lateral path is fixed. The altitude and speed profile can be optimized using the aircraft onboard systems for minimum fuel burn, emissions, and noise within the constraints set by ATC. However, closed-path procedures provide

insufficient capacity to be used in high-density traffic. The TSD is targeted to closed path designs. In the remainder of this paper the term CDO refers to a closed path CDO.
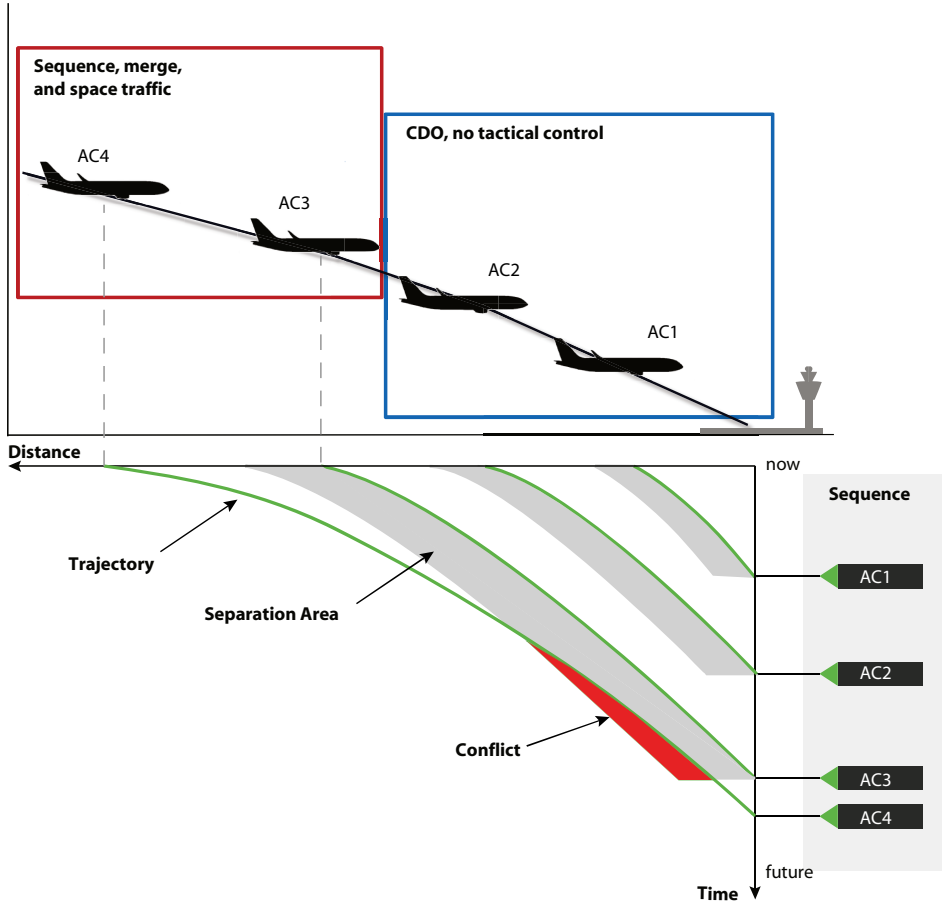
Figure 5-1 Typical CDO concept and schematic view of the TSD interface.

5.2.2   Air Traffic Control for CDO

The left part of Figure 5-1 gives a schematic overview of a generic concept of operations to facilitate CDO. The ATCO de-conflicts by sequencing and spacing the aircraft before the start of the CDO. During the CDO tactical control is avoided. Therefore, aircraft have to be accurately spaced on an intermediate metering fix. The spacing between aircraft at the intermediate fix should ensure separation throughout the CDO and efficient traffic handling. Depending on the location of the intermediate fix, the ATCO can be in an en-route, area control, or terminal maneuvering area controller position.
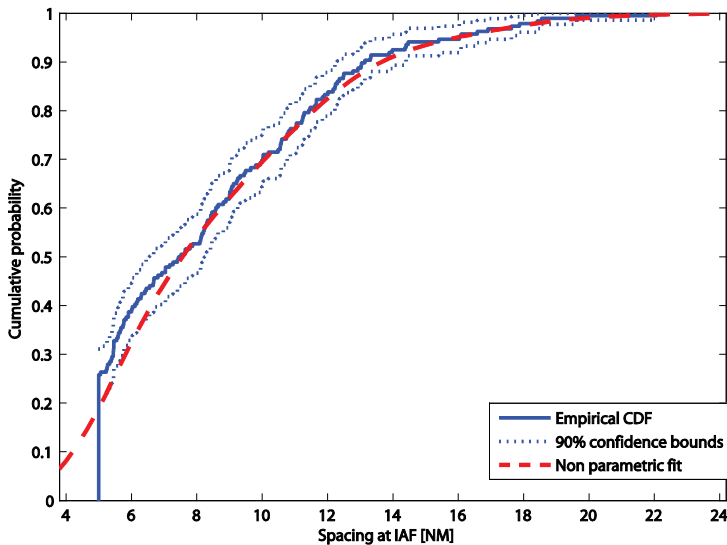
Figure 5-2 Cumulative probability of required spacing at IAF based on flight data.

The required spacing at the intermediate fix varies per aircraft pair, because of differences in the speed and altitude profiles between aircraft. To illustrate the differences between aircraft pairs, Figure 5-2 shows the observed distribution of the required spacing for a fix (IAF) at 63 NM distance to go (DTG) to the runway. The distribution was created using flight data of aircraft on approach to Amsterdam Airport Schiphol, the Netherlands. All aircraft followed the nightly CDO procedure from the same IAF. To rule out possible ATC interventions, only aircraft that landed without another landing 10 minutes prior or after the own landing were considered. Aircraft pairs were formed of aircraft that landed within 60 minutes of each other to limit the influence of atmospheric conditions.

The 95% interval of the required spacing ranges from 5 NM to 16 NM, depending on the aircraft pairing and weather conditions. Hence, the use of a fixed interval that ensures an undisturbed CDO for most aircraft pairings (i.e., 16 NM) will incur a significant capacity penalty. Tailoring of the inter-aircraft spacing based on the expected trajectories is needed. The required inter-aircraft spacing is however not readily available to the ATCO responsible for spacing of the traffic for CDO. A controller support tool is required that provides the ATCO with the information and tools needed to accurately space aircraft for CDO.

5.3   The Time-Space Diagram as a Controller Support Tool

Time-space diagrams are commonly used to investigate transportation related problems, where traffic shares a common path.[15] For example, in traffic and highway engineering it is a visual tool for engineers to analyze a coordination strategy and modify timing plans for traffic signals.[16] In airport planning and management it is used to estimate runway capacity.[17] In the research described in this paper the diagram is used to support the controller in sequencing, merging, and spacing of aircraft from different directions for CDO (see Figure 5-1), such that tactical interventions to ensure separation or merge traffic are not needed during the CDO phase. The TSD shows the time-distance lines for both phases depicted in Figure 5-1, but control using the TSD is only applied during the sequencing, merging, and spacing phase. In line with the ecological interface design (EID) approach, the TSD provides tools and information that allow the ATCO to be an active problem solver.[18]

5.3.1   Time-Space Diagram Layout

The TSD gives a graphical representation of the current and future traffic situation in addition to the information provided on the PVD. Figure 5-1 shows four aircraft on approach (left) and the representation of these aircraft on the TSD (right). The vertical axis in the diagram is the time-axis. Aircraft labels are shown on the axis at the Estimated Time of Arrival (ETA) at the runway threshold. The time axis, together with the aircraft labels, resembles a typical arrival manager interface. The labels from top to bottom show the arrival sequence. The DTG to the runway threshold is drawn on the horizontal axis. Plotted in the diagram are trajectory predictions. Presentation of the aircraft requires that all trajectories have at least one point in common. For arriving traffic on a single runway this condition is always met; the runway threshold is the common point.

Added to the interface is task-relevant information such as separation minima and conflicts. Separation minima are visualized using shaded areas, referred to as the separation areas. Both time-based and distance-based separation minima can be visualized. The separation areas are constructed by offsetting the trajectory of the leading aircraft in the direction of the time- or distance axis over the required separation

interval (e.g., 3 NM or 2 minutes). The separation areas are only drawn when the aircraft are in proximity or when the leading aircraft is on final approach.

If a trajectory crosses a separation area and the aircraft are not separated by altitude there is a conflict. To visualize a conflict, the area enclosed by the trajectory of the trailing aircraft and separation area is colored red. This representation also embodies information about the duration and distance of the conflict. The location on the TSD shows the time and DTG to resolve the conflict. The task of selection, decision making, and implementation of resolving actions is left to the ATCO. Once an action is implemented (e.g., a speed instruction is given) the TSD is updated.

5.3.2 Trajectory Prediction

Accurate trajectory prediction is a key enabler for the PVD-TSD interface. An unambiguous trajectory from the current position to the runway threshold is required to plot the trajectory on the TSD and assess the impact of instructions and clearances give. For the development and validation of the PVD-TSD a trajectory predictor was developed based on the Aircraft Dynamics Model for the FAA Target Generation Facility and the workstation based fast-time aircraft simulator for noise abatement approach procedure study described by Ren et al.[19, 20] For aircraft performance data and computations use was made of EUROCONTROL's Standard Aircraft Modeling Interface (SAMI) and Base of Aircraft Data (BADA) models.[21-23]

5.4   Visual Momentum

The PVD and TSD are presented on separate displays and provide information in different frames of reference. To improve information integration from the multi-display PVD-TSD, the interface has been evaluated using the concept of visual momentum and changed accordingly.

5.4.1 Concept of Visual Momentum

The definition of visual momentum used by Woods is: "*a measure of the user's ability to extract and integrate information across displays*" Ref [24, pp. 231]. When visual momentum is high, successive views support the rapid comprehension of data following the transition to a new display. In case the visual momentum is low, reorientation from scratch is needed when moving across displays. Two of Woods' techniques to improve visual momentum have been implemented: 'long shots' and 'perceptual landmarks'.

5.4.2 TSD as Long shot

Long shots help the user to step back from the details of the monitored process to assess the overall system status and to decide where to look next. Therefore a long shot

shall provide summary status data and an overview of the display structure. The summary data must be distilled and abstracted and enable "check reading".

In the PVD-TSD interface the TSD provides the long shot. The TSD provides a summary on the status of the task of spacing, sequencing, and merging traffic. The separate lines show the aircraft under control. The separation areas and the overlap (conflicts) or space between the separation areas show where spacing has to be increased or decreased. This information is abstracted from lower level information: the aircraft under control, trajectory predictions, the airspace structure and procedures and presented in a recognizable form using lines, areas and different colors. No changes were made to the interface.

The display structure of the PVD-TSD interface consists of the PVD and TSD that are displayed in parallel. There is no display structure that requires navigation through a menu or map; hence no changes were made to the interface to provide an overview of the display structure.

5.4.3   Perceptual Landmarks in the PVD-TSD

Perceptual landmarks are distinctive features that are recognizable in different views and allow integration of data over those views (i.e., the geographical versus time-space representation). The interface did not provide these landmarks and were added. In the PVD-TSD interface these features are triggered by the selection and deselection of aircraft, conflicts, or separation areas. These actions are interpreted as a decision by the ATCO on the next action to take (e.g., which aircraft to control). On selection of an aircraft in either display its trajectory is plotted in the PVD. When involved in a conflict, the conflict and the trajectory of the conflicting aircraft are also plotted. On the TSD the color of conflicts in which the selected aircraft is not involved are darkened. On selection of a conflict area, the trajectories of the aircraft involved in the conflict are plotted in the PVD. Similarly, on selection of a separation area, the trajectories of the associated aircraft are plotted. Finally, consistent use of colors is made, e.g., for the color of the label indicating the aircraft control status. Using this feature the controller is provided with both a status summary of a particular aircraft or conflict – a long shot – and support to quickly integrate the data in the two different reference frames.

5.5   Direct Manipulation Interfaces

The TSD of Ref. [11] included a function to show the effect of possible actions on the traffic situation beforehand. It is proposed to replace these static what-if tools with DMIs. The motivation is twofold. First, the what-if tools show the effect of computer-selected actions. These actions are not necessarily in accordance with the actions the ATCO would like to see and cannot be tailored to the specific situation. This limits the

usefulness of the tools. Secondly, the display of various possible actions cluttered the display. Overall, the use of DMIs is expected to enhance situation awareness.[25]

5.5.1   Direct Manipulation Interfaces

Direct manipulation is a human-computer interaction style with the following properties:[26] 1) Continuous representation of the object of interest; 2) Physical actions or labeled button presses instead of complex syntax, and 3) Rapid incremental reversible operations whose impact on the object of interest is immediately visible.

DMIs are suggested to have the following virtues: 1) Novices can learn basic functionality quickly; 2) Experts can work extremely rapidly to carry out a wide range of tasks, even defining new functions and features; 3) Knowledgeable intermittent users can retain operational concepts; 4) Error messages are rarely needed, and 5) users can see immediately if their actions are furthering their goals, if not, they can simply change the direction of their activity.

5.5.2   Direct Manipulation Interfaces for ATC

For the PVD-TSD interface, DMIs were developed for the following controller instructions: speed, altitude and heading control, direct-to waypoint instructions, and route clearances. The type of instruction is selected by the controller. Subsequently, properties of the instruction (e.g., the aircraft speed in case of speed control) can be manipulated in the PVD and/or TSD. The impact of an instruction can be directly perceived in either display and entered into the system. The use of the DMI can be stopped at any moment. The following subsections discuss the DMIs per controller action, using two aircraft in a conflict to clarify the new tools.

5.5.3   Speed Control using a Direct Manipulation Interface

Figure 5-3 shows the PVD-TSD and DMI for speed control. On the TSD the trajectory and label based on current clearances are faded. The control that can be exercised using speed is visualized by the shaded area, see ① in Figure 5-3. Two labels on the right of the TSD mark the upper and lower bounds, ②. The labels give the minimum and maximum speed. The middle label can be moved up and down by the ATCO within the speed limits by dragging the label in TSD or using the mouse wheel, ③. The speed changes in 5 kts increments.

When the label is moved the traffic situation is updated on the PVD and TSD and the associated speed is displayed in the labels on the PVD and TSD, ④. Once the ATCO has set the speed, and the instruction is given the interface is updated. The DMIs for altitude control use an equivalent control mechanism and graphical representation.

5.5.4 Direct-to instructions using Direct Manipulation Interface

Figure 5-4 shows the DMI for a direct-to-waypoint instruction. The ATCO can set the direct-to waypoint by clicking in the PVD. The nearest waypoint becomes the direct-to waypoint, ① in Figure 5-4. Alternatively, the ATCO can use the mouse wheel to scroll along all the subsequent waypoints on the aircraft anticipated route. The selected fix is also shown in the labels, ②.

5.5.5 Heading Vectors through Direct Manipulation Interface

Figure 5-5 shows the DMI for heading vectors. The aim is to resolve the conflict by setting the trailing aircraft on a heading and let the aircraft intercept the route once the conflict is resolved. The heading and length of the heading segment are controlled by dragging the heading vector, ①. The cursor ② marks the planned position where the aircraft will be instructed to intercept the route. The waypoint the ATCO is planning to let the aircraft intercept the route is marked with a triangle, ③. This point can be changed by selecting a waypoint. The TSD shows the conflict will be resolved by the planned actions, ④.

Once the heading instruction is given, the TSD shows the traffic situation, assuming the aircraft would immediately intercept the route at the waypoint selected by the ATCO. The length of the heading segment that was set by the ATCO is ignored. This choice was made because heading vectors are an "open loop" technique. That is, the lateral path is not unambiguously fixed until the instruction to intercept the route is given. If this instruction is given at a different time than anticipated by the interface, this might lead to unexpected situations. By constantly assuming a direct intercept of the route, the conflict shown on the TSD will gradually become smaller and finally disappear once the aircraft is at the position where currently the cursor is located, ①. At that moment the aircraft can be instructed to intercept the route at the waypoint that was selected.

5.5.6 Route clearances through Direct Manipulation Interfaces

The DMI for route clearances allows the user to select the route the aircraft is expected to proceed on. The selected route is highlighted. The first route to be highlighted is selected by the interface based on the aircraft position and clearances the aircraft has already received. The route can be changed by clicking near a route segment in the PVD.

Figure 5-3 Speed control support.

Figure 5-4 Direct-to support.
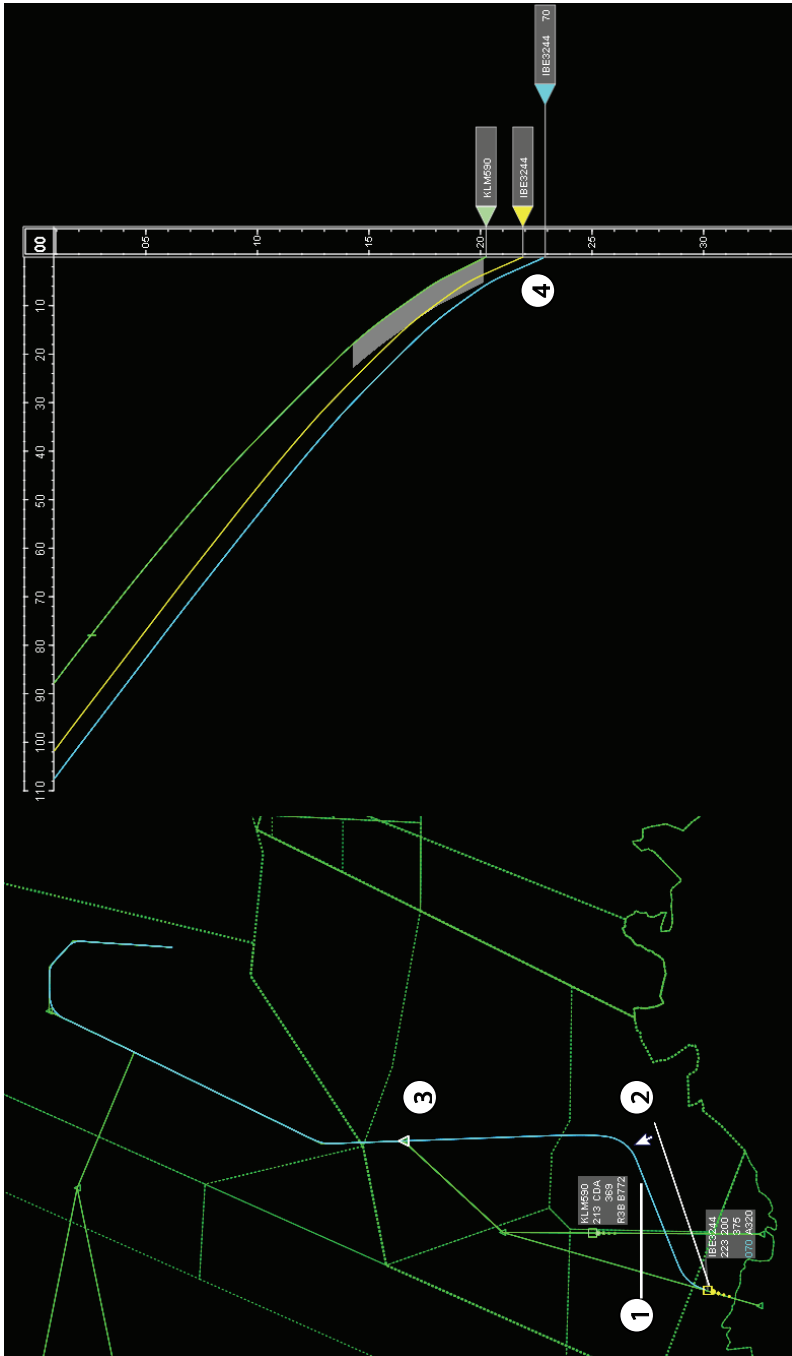
Figure 5-5 Heading vector support.

5.6   Experiment

A controller-in-the-loop experiment was set up to test the new PVD-TSD interface elements and to test the TSD against the stack list visualization (STL). The experiment was performed using a real time ATC research simulator. Two display configurations were used: the PVD-TSD interface and the PVD-STL interface. Subjects controlled traffic for either one or two IAFs. Adding the second IAF added to the task complexity, because traffic arriving from different directions had to be merged during the CDO.

From the experiment design the individual effects of the DMI and changes to enhance visual momentum could not be quantified. This would have required at least one more display configuration resulting in multi-day training and a multi-day experiment per subject that could not be completed within the available time. Preference was given to test the TSD against the stack list while asking the subjects explicitly about any issues they encountered with the integration of information and the acceptability and intuitiveness of the direct manipulation interface. This experiment was deemed the more relevant for further development and operational use of the TSD.

5.6.1 PVD-STL Interface

Figure 5-6 shows the PVD-STL interface, our baseline. The STL is an inset on the PVD. It computes the required time over the IAF for a conflict free and gapless arrival sequence based on the predicted aircraft trajectory after the IAF.

The leftmost column gives the planned arrival sequence. The top aircraft is planned to arrive first. The order can be changed by the ATCO. The second column gives the IAF of the aircraft. The third column gives the call sign for the preceding aircraft that is on the same IAF, if available. The fourth column provides the required spacing with respect to the leading aircraft at the IAF expressed in NM. The fifth column gives the time to lose or gain at the IAF to meet the spacing requirement in steps of 10 seconds. A positive number indicates that the aircraft is late and should speed up. A negative number (in red) indicates that the aircraft will arrive too early at the IAF, resulting in a conflict. The sixth column was added to show the propagation of delay and bunching. The time an aircraft has to lose or gain is added to the total delay, except in situations where the aircraft arrives too early and the total delay is positive. In that case the total delay is set to the time the aircraft needs to lose.

In the stack list in Figure 5-6 the second, third, fourth, and sixth aircraft in the arrival sequence are predicted to arrive late at the IAF resulting at the IAF will being larger than required. The delay accumulates as can be seen in the last column. The fifth aircraft is 90 s early. The accumulated delay is also set to -90 s. Aircraft number six is in fact 110 s late with respect to the fifth aircraft.

Taking into account the -90 s delay of aircraft five, aircraft six is only 20 s late. The seventh aircraft arrives -80 s with respect to the sixth aircraft and again the accumulated delay is set to -80 s. Aircraft eight and nine arrive 50 s early and 20 s late, respectively. Taking into account the 80 s that have to be lost upstream both aircraft have to be delayed.

AC	IAF	LEAD	NM	DT	TIAF
BAW444	SUGOL				
TRA5136	RIVER				
TRA052	SUGOL	BAW444	19.5	30	30
CPA034	SUGOL	TRA052	13.0	20	50
DAL248	SUGOL	CPA034	5.5	20	70
KLM744	SUGOL	DAL248	8.5	-90	-90
KLM1220	RIVER	TRA5136	48.0	110	20
MPH084	SUGOL	KLM744	27.5	-80	-80
AFR240	RIVER	KLM1220	22.5	-50	-130
				20	-110

Figure 5-6 PVD - Stack list interface to support CDO.

5.6.2 Method

Subjects and Experience
Six subjects were invited to participate in the experiment, see Table 1. The subjects had a strong background in ATM research or in fact worked as professional ATCO. All subjects were male and their ages ranged from 26 to 58 years.

Independent Variables
The two within-subject independent variables are: the controller interface INTERFACE with two levels (PVD-STL and PVD-TSD) and IAF with two levels (one IAF and two IAFs). In total there were four experiment conditions.

Table 5-1 Overview of Subjects.

ID	Age	Relevant Experience
S1	44	Basic air traffic controller course and subject in many ATC interface experiments
S2	58	ATCO Tower/Approach for 25 years
S3	27	Interface design for inbound planning and managing 4D trajectories
S4	26	Basic air traffic controller course and aviation consultant
S5	26	Virtual ATC and subject in various ATC interface experiments
S6	35	Basic air traffic controller course and subject in various ATC interface experiments

Airspace and Routes and Procedures
The airspace and route designs were based on the Dutch airspace and arrival procedures for Amsterdam Airport Schiphol, the Netherlands. Figure 5-7 shows the airspace with two area control sectors in the West and South and the Terminal Maneuvering Area (TMA). Traffic entered the sectors at four entry points. At each entry point a Standard Arrival Route (STAR) started that ended at one of the IAFs (waypoints SUGOL or RIVER). At the IAFs transitions to the runway threshold started. The minimum and maximum altitudes over the IAFs were set to Flight Level (FL)100 and FL180, respectively. The South area control sector was used in all experiment conditions. The West sector was only active for the experiments conditions with two IAFs.

Traffic Scenarios
Four traffic scenarios were created, each containing 14 aircraft that were evenly distributed over the inbound routes. In all scenarios, traffic was redistributed, but starting distances to the runway were equal to ensure equal traffic complexity. The aircraft type and weight assigned to a starting distance were fixed. Aircraft of the type Airbus A320 (4), Airbus A330 (1), Boeing 777 (1), Boeing 747 (2), Boeing 737 (5) and Fokker 70 (1) were used. Between the scenarios the call signs were varied to mask the similarities between the scenarios. The approximate traffic level was 35 aircraft per hour and could be handled in the sectors and by the runway.
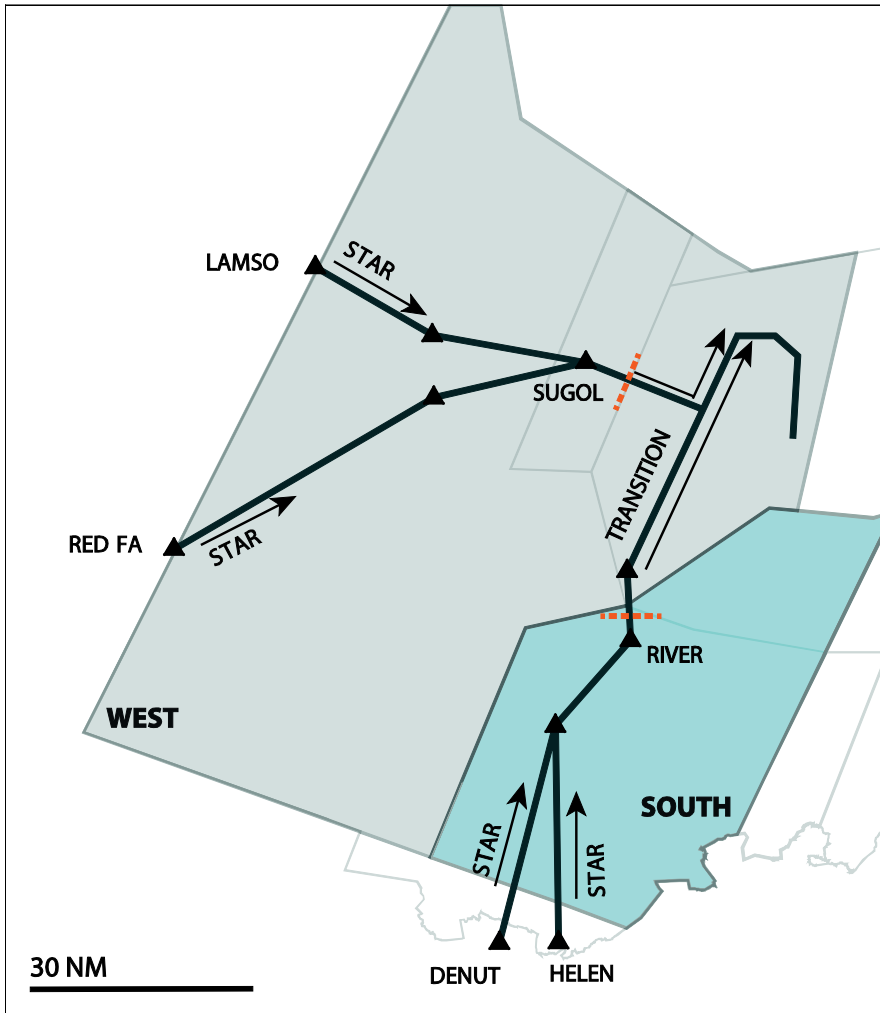
Figure 5-7 Experiment airspace based on the Dutch airspace.

Instructions

Subjects controlled traffic on the South and West area control sector and were instructed to expedite and maintain an orderly flow of traffic and to accurately space the aircraft on the IAF for a CDO. On the initial call by the aircraft, the aircraft had to be taken under control. The aircraft were already cleared direct to the entry point and descending to FL230 or FL240 depending on the entry point. For aircraft under control that were still in the adjacent sector, the subject was instructed not to issue instructions that would change the lateral path. Once in the own sector the subject was free to control both the lateral and vertical paths of the aircraft and apply speed control. Subjects were advised

to keep 250 kts as a minimum speed. Within the own sector 5 NM lateral or 1000 ft vertical separation had to be maintained. Also, subjects were instructed to clear the aircraft for CDO as soon as possible. Once cleared for the CDO no further instructions were allowed. Finally, the traffic was handed-off when approaching the IAF.

Apparatus

The ATC simulator ran on a single workstation. Two identical 20" LCD monitors (1600 x 1200 pixels) were used to visualize the PVD and TSD. The subject was positioned in front of the left monitor showing the PVD. The right monitor showing the TSD screen was positioned adjacent to the left screen at a small angle. Input devices were a standard keyboard and a two-button mouse with a mouse wheel. Text-to-speech software was used to provide audio feedback for aircraft calls and read back of the instructions to the subjects.

5.6.3   Dependent measures

The following dependent measures were used for validation:

Workload

An Instantaneous Self-Assessment (ISA) and the NASA Task Load Index (TLX) questionnaire were used to assess subjective workload.[27, 28] The ISA was due every 60 seconds, with the subjects being asked to indicate the experienced workload using a color bar shown on the PVD and TSD. After each simulation run the subjects completed the NASA Task Load Index (TLX) questionnaire. Subjects were asked to evaluate, by pair-wise comparison, the contribution of each of the six subscales (mental demand, physical demand, temporal demand, effort, performance, and frustration level) to their workload. Thereafter, they had to rate each task based on the six subscales. Finally, the combined weights and ratings resulted in a weighted rating of each subject for each experimental run.

As different subjects exhibit different rating behavior, most notably leniency and central tendency, the workload ratings were first corrected for inter-subject differences. This correction was performed by calculating Z-scores for every subject.[29]

Situation Awareness

After each run, subjects completed the EUROCONTROL Situational Awareness for Solutions for Human Automation Partnerships in European ATM (SASHA) questionnaires.[30] The questionnaire provides a first insight into the impact of a new system on the level of situation awareness. The questionnaire consists of six statements that must be rated on a scale from 0 to 6. Although treating ordinal rather than interval data, the method prescribes that the SASHA score is the averaged rating of the six

statements. Results are to be interpreted in a relative way, in terms of differences in the scores obtained for the four experiment conditions.

5.6.4 Controller Instructions

All aircraft instructions were logged to determine the number of instructions per aircraft, the type of instructions issued and timing.

Aircraft trajectories

Aircraft trajectories were used to analyze the effect of the display configurations on the vertical and horizontal aircraft paths.

Separation and Spacing

Aircraft trajectories were analyzed for any separation violations. In addition the final spacing at the runway threshold was computed.

Capacity

The runway throughput was computed from the average landing interval.

Use of the Interface

All controller inputs on the PVD and TSD were logged, including the selection of aircraft, conflicts and separation areas, and the use of the DMIs.

Final Questionnaire

Subjects were asked to rate to what extent they agreed with a number of statements on a 5-level Likert scale: "strongly disagree", "disagree", "neither agree nor disagree", "agree", and "strongly agree". Four statements focused on the availability, integration, and complementarity of information. Seven statements were specific to the PVD-TSD interface. These statements focused on the use of the interface for planning and implementing actions and intuitiveness of the DMIs. In addition, ten further statements asked the subjects to rate the level of experienced difficulty to identify conflicts, solutions to conflicts, gaps in the sequence, knock-on effects, and control of aircraft for both interfaces separately. Again the Likert scale for these statements had 5 ratings: "very difficult", "difficult", "neither easy nor difficult", "easy", and "very easy".

In addition, subjects were asked about the control strategy they used and suggestions to improve either interface. Finally, subjects were given the opportunity to provide any comments on the simulator and the experiment.

5.6.5 Experiment Design

The experiment started with the briefing of the subject and demonstration of the interfaces. To train the subject in using the simulator and the interfaces a series of short videos were used. Also two practice runs were done in the simulator with a focus on controlling the aircraft and simulator. Four training runs followed, in which each experiment condition was trained once. The experiment itself also consisted of four runs per subject. To eliminate practice and boredom effects a Latin square design was used. Also, the four traffic scenarios were swapped between the experiment conditions for different subjects.

5.6.6 Procedure

Each training and measurement run started with the simulation in pause. The subject was given the time to familiarize with the traffic situation, adjust the display settings, and arrange the aircraft labels. After the last instruction the simulation advanced at high speed until all aircraft had landed. The NASA TLX and SASHA sheet had to be completed after each run. Directly after completion of the last run the subject had to complete the final questionnaire. Typically, the training and experiment were completed in six hours excluding breaks in two days.

5.6.7 Experiment Hypotheses

It was hypothesized that subjects would be able to handle traffic safely and efficiently in terms of throughput with both interfaces *(H1)*, because both provide the required information to tailor the spacing at the IAF(s) for a conflict free and gapless arrival sequence. However, it was also expected that with the PVD-TSD interface workload would be lower at a higher level of situation awareness *(H2)*, because the PVD-TSD was designed following ecological interface design principles other than the PVD-STL interfaces and includes DMIs.[18, 26] As a result it was expected that adding a second IAF would have a smaller effect on the performance when using the PVD-TSD interface *(H3)*. Regarding the CDO it was expected that the PVD-TSD interface would increase the distance and altitude at which the aircraft was cleared to commence the CDO *(H4)*, as from earlier experiments it was observed that instructions were given earlier.[11]

5.7 Results

In the analysis of the experiment results, use is made of Analysis of Variance (ANOVA) and Generalized Estimating Equations (GEE). Before conducting the ANOVA, the assumptions of normality of variance that an ANOVA analysis undertakes were tested using the Kolomogorov-Smirnov or Shapiro-Wilk tests for all continuous dependent measures in order to opt for this parametric test or for the non-parametric Friedman's ANOVA test.29 Follow-up tests for the ANOVA and Friedman's ANOVA (t-tests and Wilcoxon-signed rank tests) were used if the overall effect was significant.

GEE is a method to estimate regression models.31 A linear scale response model of the following form was used:

$$S = \sum \beta_i X_i \qquad (5\text{-}1)$$

The model response was one of the dependent variables that were defined. Potential model parameters are the independent variables and waypoints. Only statistically significant (*p<0.05*) model parameters were included in the model. The parameter estimates give the marginal effect of the model parameter on the model response.

5.7.1 Workload

The graph of Figure 5-8 shows the box plot of the ISA scores after transformation in z-scores. Workload for the PVD-TSD interface is lower than for the PVD-STL interface. Adding a second IAF resulted in an increase of the workload for both interfaces. The effects of the INTERFACE and IAF on the ISA Score were further analyzed using the GEE approach.[31]The response of the model was the ISA score. Model predictors were the INTERFACE, IAF, and subject. Table 5-2 shows the parameter estimates and hypothesis tests. The subject, model intercept, and non-significant parameters, subjects, and the intercept were removed from the table.
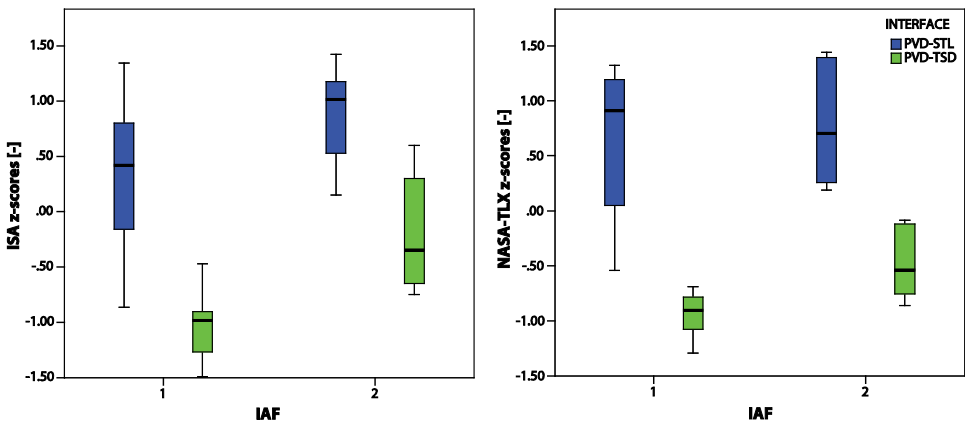
Figure 5-8 NASA TLX and ISA workload z-scores.

From Table 5-2 it was concluded that the main effects of the INTERFACE and IAF on the workload are significant. The ISA Score for the PVD-STL interface was higher (+0.109) than for the PVD-TSD interface. The ISA score for one IAF was lower than the score for two IAFs (-0.054). The effect of the INTERFACE on the ISA Score was twice the size of the effect of the IAF. The model explained 35% of variance of all recorded ISA Scores, ($r_s = 0.59, p < 0.01$).

Table 5-2 Parameter estimates and hypothesis tests ISA score model.

Parameter	β	Std. Error	95% Confidence Interval		Hypothesis Test		
			Lower	Upper	Wald χ^2	df	Sig.
[IAF=1]	-.054	.0133	-.080	-.028	16.236	1	< 0.001
[IAF=2]	0^a	.	.	.	.	.	.
[INT=PVD-STL]	.109	.0133	.083	.136	67.652	1	< 0.001
[INT=PVD-TSD]	0^a	.	.	.	.	.	.
^{a}Set to zero because this parameter is redundant							

NASA TLX

The right panel of Figure 5-8 gives the box plots of the NASA-TLX scores after the transformation into z-scores. The results show a correlation with ISA-scores after z-transformation, ($r = 0.74$, $p < 0.01$). A repeated measure ANOVA of the NASA-TLX scores with a Bonferroni correction for the critical level of significance indicated a significant main effect of the INTERFACE on the NASA-TLX score, ($F_{1,5} = 154$, $p < 0.01$). The contrast indicated a very strong effect, ($r = 0.98$). The medians of the scores for the PVD-STL and PVD-TSD interface were 34 and 14, respectively. To assess the sources of the change in workload, the six subscale scores were analyzed. A repeated measure ANOVA of the six subscales showed a significant decrease of the required effort, ($F_{1,5} = 22.07$, $r = 0.90$, $p < 0.01$). Also the mental demand decreased significantly, ($F_{1,5} = 61.45$, $r = 0.96$, $p < 0.01$). The performance, physical demand, and frustration subscales did not change significantly. The IAF main effect did not significantly affect the NASA TLX score, ($F_{1,5} = 1.46$, $p = 0.28$). Also, the INTERFACE and IAF interaction did not have a significant effect on the NASA TLX scores, ($F_{2,5} = 0.26$, $p = 0.63$).

5.7.2 Situation Awareness

Figure 5-9 shows the estimated marginal means of the SASHA scores. The mean SASHA scores for the PVD-TSD were higher than the mean scores for the PVD-STL interface, indicating a higher level of situation awareness for the PVD-TSD. The impact of the adding a second IAF seemed to be larger for the PVD-STL than the PVD-TSD interface. The Kolmogorov-Smirnov test indicated that the data for the four experiment conditions did not differ significantly from a normal distribution ($p > 0.05$). A repeated measure ANOVA of the SASHA z-scores indicated a significant main effect of the INTERFACE on the SASHA score, ($F_{1,5} = 21.41$, $p < 0.01$). Also the main effect of IAF was significant ($F_{1,5} = 6.69$, $p < 0.05$). The INTERFACE * IAF interaction was not significant, despite the observed trend.

5.7.3 Controller Instructions

Figure 5-10 shows box plots for the number of controller instruction per experiment condition, disaggregated to the type of instruction. The CDO clearance and handoff are omitted since these instructions were independent of the experiment conditions. For the total number of instructions the results of repeated measures ANOVA are given in

Table 5-3. The main effects and interaction of the INTERFACE, IAF are all significant at the $p < 0.05$ level.

Use of the PVD-TSD interface lead to 35% less instructions on average, ($t = -6.95$, $p < 0.01$). In scenarios with two IAFs 17% more instructions were given, ($t(5) = 3.75$, $p < 0.01$). For the PVD-STL interface adding a second IAF lead to a significant 23% increase ($t(5) = 4.56$, $p < 0.01$), but for the PVD-TSD there was non-significant 11% increase, ($t(5) = 1.79$, $p = 0.13$).
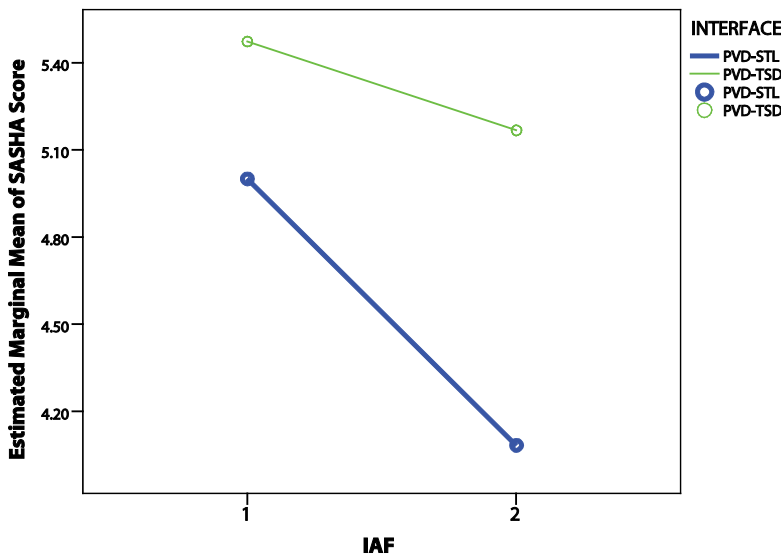
Figure 5-9 Estimated Marginal means of SASHA scores.

Table 5-3 Total number of instructions, tests of within-subject effects.

Source	Type III Sum of Squares	df	F	Sig.
INTERFACE	3650.7	1	29.9	.003
IAF	486.0	1	15.3	.011
INTERFACE * IAF	170.7	1	16.8	.009

The above analysis was repeated for speed instructions, heading instructions, route clearances, direct-to-waypoint instructions, and altitude clearances separately. The number of speed instructions changed significantly between the experiment conditions ($\chi^2(3) = 13.80$, $p < 0.01$). The number of speed instructions compared to the PVD-STL was reduced by 50% when using the PVD-TSD interface for, both one IAF and two IAFs, ($T = 0$, $r = -0.64$, $p < 0.05$). Also the number of heading instructions changed significantly between the experiment conditions ($\chi^2(3) = 13.53$, $p < 0.01$). Heading instructions were

no longer used when controlling traffic for one IAF using the PVD-TSD interface. When controlling traffic for two IAFs the number of heading instructions decreased by 75% when using the PVD-TSD interface compared to the PVD-STL interface, ($T = 0$, $r = -0.64$, $p < 0.05$).

The number of heading instructions significantly increased with the number of IAFs when controlling the traffic using the PVD-STL interface, ($T = 15$, $r = 0.64$, $p < 0.05$). No significant effects were found when controlling traffic using PVD-TSD interface. The number of direct-to instructions varied significantly between the experiment conditions ($\chi^2(3) = 11.15$, $p < 0.05$). However, no further significant effects within the INTERFACE and IAF were found. The number of route and altitude clearances did not change significantly between the experiment conditions.
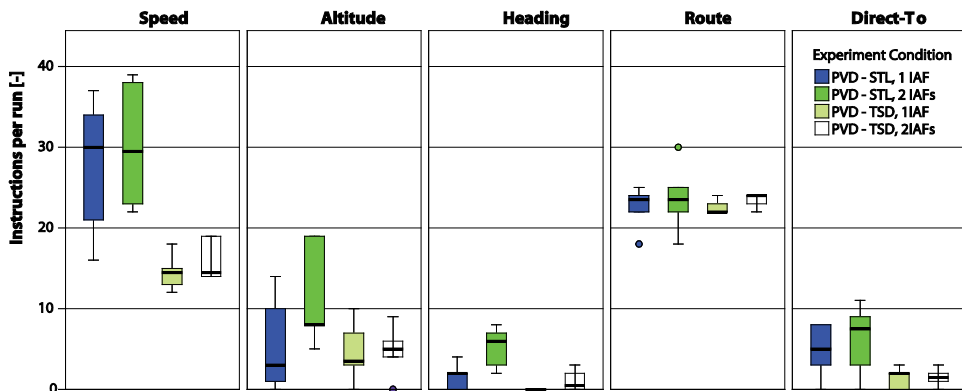
Figure 5-10 Average number of instructions per simulation run and experiment condition (14 aircraft).

5.7.4 Timing of Controller Instructions

The timing of the controller's instructions was analyzed using the time intervals between the aircraft initial call and the first and last instructions that were given. The last instruction was the CDO clearance. Figure 5-11 shows the box plots of the time intervals. A Kolomogorov-Smirnov test indicated that some data was significantly different from a normal distribution ($p > 0.05$). The Friedman's ANOVA indicated a significant effect of the experiment conditions on the time between the initial call and first instruction, ($\chi^2(3) = 10.83$, $p < 0.05$). On average the first instruction was given 9 s earlier when using the PVD-TSD compared to the PVD-STL, ($z = -2.23$, $p < 0.05$). Adding a second IAF lead to an increase of the average time to the first instruction by 10 s, ($z = -3.13$, $p < 0.01$).

A Friedman's ANOVA also indicated a significant effect of the experiment conditions on the time between the initial call and last instruction, ($\chi^2(3) = 48.68$, $p < 0.01$). A linear

scale response model as described in Section VII-A was used with the interval between the initial call and last instruction as the response variable. The results of the test of the model effects are summarized in Table 5-4. All three main effects were significant. Also the interactions between IAF * ENTRY POINT and INTERFACE * ENTRY POINT were significant and were included in the model.
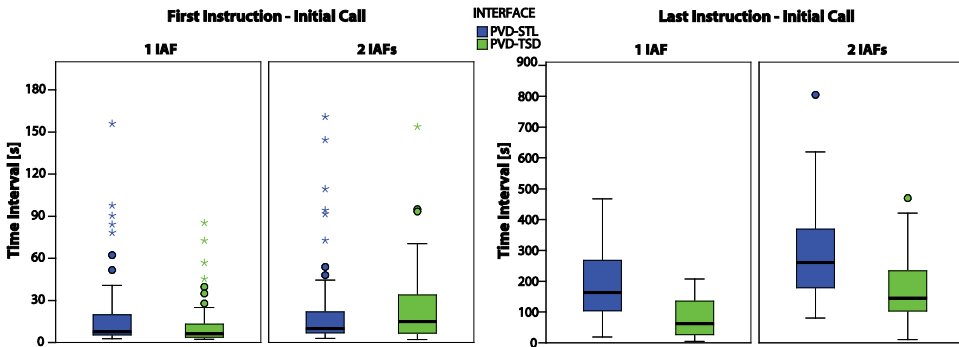
**Figure 5-11 Time intervals between the aircraft initial call and
the first and last instructions issued.**

The model explained 39% of the variance, (r_s = 0.62, p <0.001). In the model the interval between the initial call and last instruction increased by 87 s when increasing the number of IAFs. Another significant main effect was the INTERFACE. When controlling traffic using the PVD-TSD interface, the interval reduced by 182 s. However, the effect of the interface was smaller when controlling traffic for one IAF. Another significant interaction was the ENTRY POINT LAMSO when controlling traffic using the PVD-STL interface, the interval was 116 s shorter.

Table 5-4 Test of model effects for time interval between initial call and last instruction.

Source	Type III Wald χ2	df	Sig.
IAF	17.7	1	< 0.001
ENTRY POINT	21.5	3	< 0.001
INTERFACE	15.4	1	< 0.001
IAF * INTERFACE	9.1	1	< 0.01
IAF * ENTRY POINT	0.6	1	.44
INTERFACE * ENTRY POINT	297.2	3	< 0.001
IAF * INTERFACE * ENTRY	0.0	1	.87

CDO Clearance

The analysis of the timing of the instructions prompted a further analysis on the timing of the CDO clearance and the effects on the CDO performance. Figure 5-12 shows the box plot for the DTG and aircraft altitude when cleared for the CDO. A linear scale response model was used to investigate the effects of INTERFACE and IAF. The response

variable of the model was the DTG when cleared for CDO. The tests of the model effects are summarized in Table 5-5. The main effects INTERFACE, IAF, and ENTRY POINT were significant. Also the interactions INTERFACE * IAF and INTERFACE * ENTRY POINT were significant. The model explained 67% of the variance, ($r_s = 0.82$, $p < 0.001$).

From the model parameters and hypothesis test it was concluded that the main effect INTERFACE had a significant effect. The predicted DTG after the CDO clearance increased with 18 NM when using the PVD-TSD interface instead of the PVD-STL interface. Adding a second IAF also had a negative effect on the DTG. The predicted DTG decreased by 8.9 NM. From the interactions it was concluded that the effect of the IAF is not significant when controlling traffic using the PVD-TSD interface but only when controlling traffic using the PVD-STL interface, specifically for traffic arriving from LAMSO (-12 NM). For the other ENTRY points the effects were not significant.
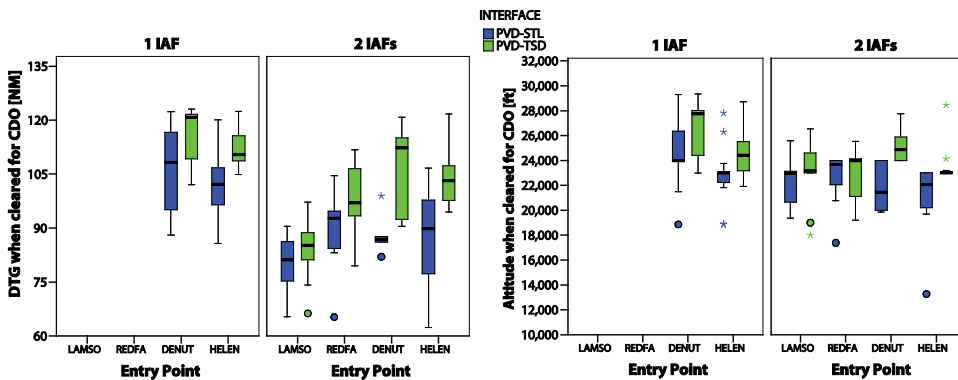
Figure 5-12 DTG and aircraft altitude when cleared for the CDO.

The altitude when cleared for the CDO was correlated with the DTG, ($r_s = 0.74$, $p < 0.001$). This indicates that aircraft were cleared for the CDO at a higher altitude.

Table 5-5 Test of model effects for DTG after CDO clearance.

Source	Type III Wald $\chi2$	df	Sig.
INTERFACE	20.6	1	< 0.001
IAF	15.6	1	< 0.001
ENTRY POINT	69.1	3	< 0.001
INTERFACE * IAF	7.2	1	< 0.01
INTERFACE * ENTRYPOINT	128.1	3	< 0.001
IAF * ENTRY POINT	1.5	1	.222
INTERFACE * IAF * ENTRY POINT	0.1	1	.809

5.7.5 Interface Usage

Figure 5-13 shows the usage of the DMIs. DMIs were mostly used for speed control and route clearances. The use of the DMI for speed control increased significantly with the number of IAFs, ($t(5)$, $p < 0.05$, $r = 0.77$). Use of the other DMIs was not significantly affected by the number of IAFs. The DMI for speed control was always controlled using the mouse wheel; subjects did not use the possibility to drag the label in the TSD to set the speed.
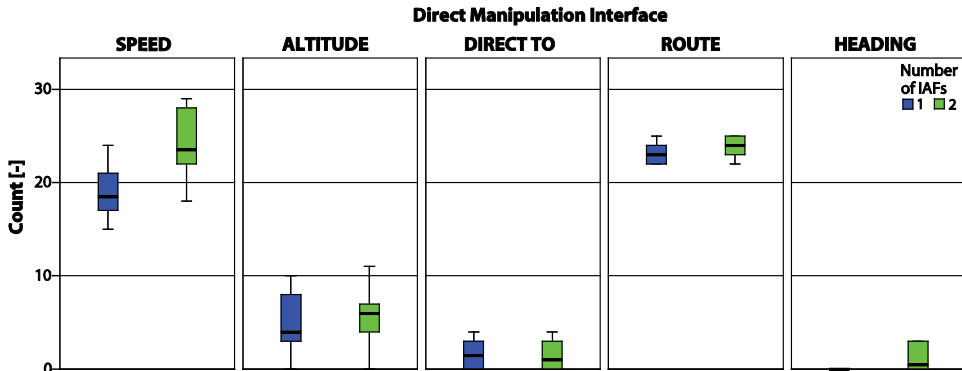
Figure 5-13 Use of DMIs per simulation run and experiment condition (14 aircraft).

Selection of objects in the TSD

Five out of six subjects used the TSD to select aircraft. Per run between 1% and 35% of the aircraft selections were made through the TSD, $\mu = 15\%$, $\sigma = 12\%$. The possibility to select conflicts and separation areas were not used by the subjects, expect for one subject who selected a separation area once.

5.7.6 Aircraft Trajectories

Track Miles

Figure 5-16 suggests a possible effect of the INTERFACE and IAF on the miles flown. Figure 5-15 shows the box plot for the miles flown after the initial call of the aircraft. A scale response model was used to further investigate the effects. The response of the model was the track mileage. Model predictors were the INTERFACE, IAF, and the ENTRY POINT. From the results given in Table 5-6, it was concluded that significant model parameters were the ENTRY POINT and INTERFACE * ENTRY POINT interaction. The model explained 71% of the variance, ($r_s = 0.85$, $p < 0.01$). The parameter estimates and the box plot showed that the effect of the PVD-TSD interface on the track miles can be both positive and negative. For entry points HELEN and REDFA, the model predicts an increase of the track millage when controlling track using the PVD-TSD interface. With

the PVD-STL interface traffic received directs to the IAF. With the PVD-TSD interface fewer direct-to instructions were given. For the points LAMSO and DENUT, the model predicts a decrease of the track millage for the PVD-TSD interface. In the baseline simulation runs, traffic at these entry points was vectored more than with the PVD-TSD interface. The only significant effect is a 1 NM decrease of the track millage for traffic at entering at DENUT.

Table 5-6. Test of model effects for track miles flown.

Source	Type III Wald χ2	df	Sig.
INTERFACE	.2	1	.65
IAF	2.1	1	.14
ENTRY POINT	2389.6	3	< 0.01
INTERFACE * ENTRY POINT	16.6	3	< 0.01
IAF * ENTRY POINT	.0	1	.95

Altitude Profile

Figure 5-14 shows the density plots of the altitude profiles together with the location of the CDO clearances for each experiment condition. From the plots it was concluded that with the PVD-TSD interface aircraft stay higher for a longer period of time. The effect of the INTERFACE on the altitude where the aircraft were cleared for the CDO is clearly reflected. Also visible is the maximum FL180 at the IAF at approximately 65 NM from the runway. After passing the IAF there were no significant differences between the altitude profiles.

5.7.7 Separation Violations

One loss of separation when controlling the aircraft using the PVD-STL interface for two IAFs was observed. The two aircraft involved were both cleared for a CDO. The subject commented that one of the aircraft descended slower than expected and was already monitoring the situation. However, the experiment design did not allow any interventions after the CDO clearance.
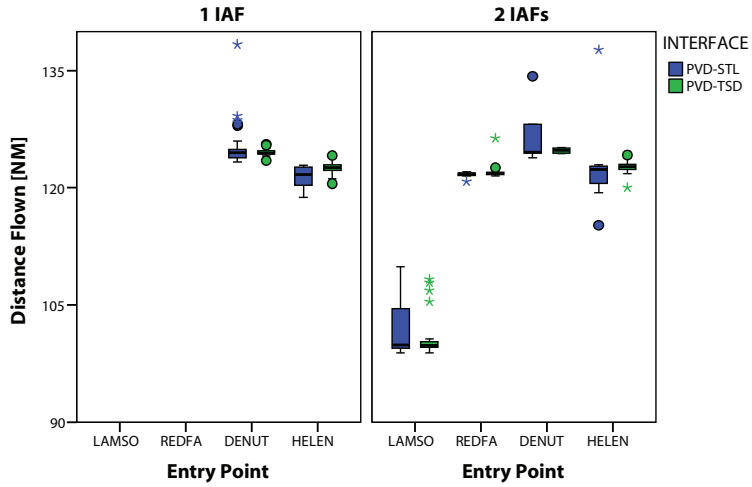
Figure 5-14 Track mileage after initial aircraft call.
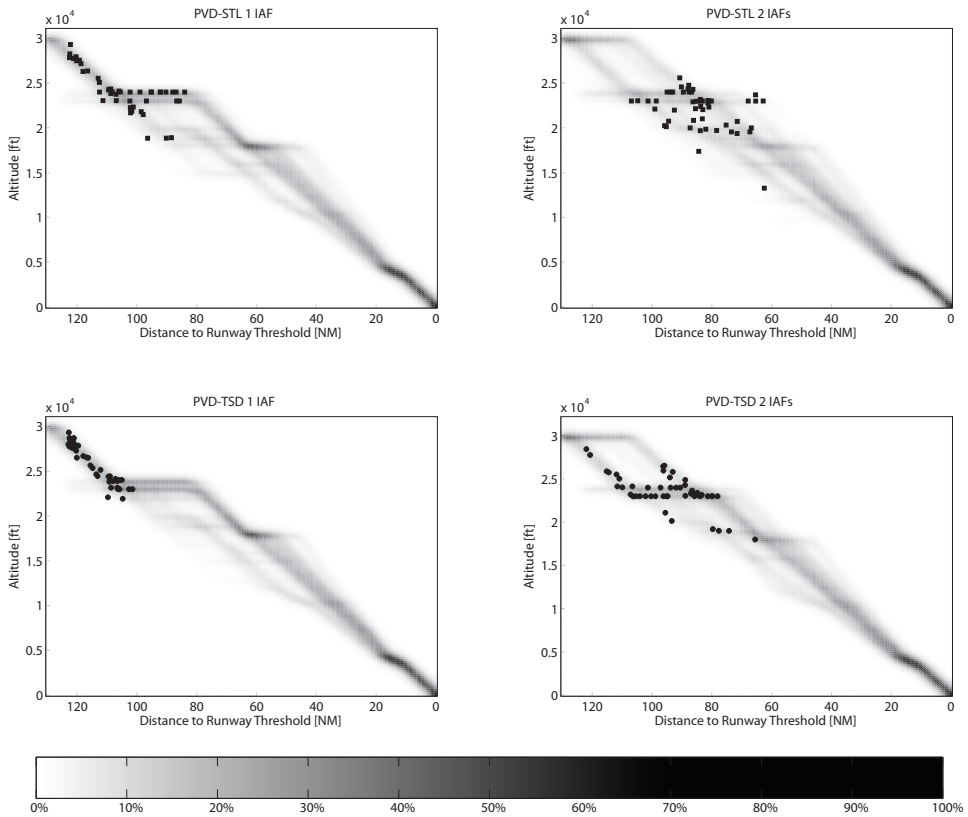
Figure 5-15 Altitude profiles and location aircraft were cleared for the CDO for all subjects.
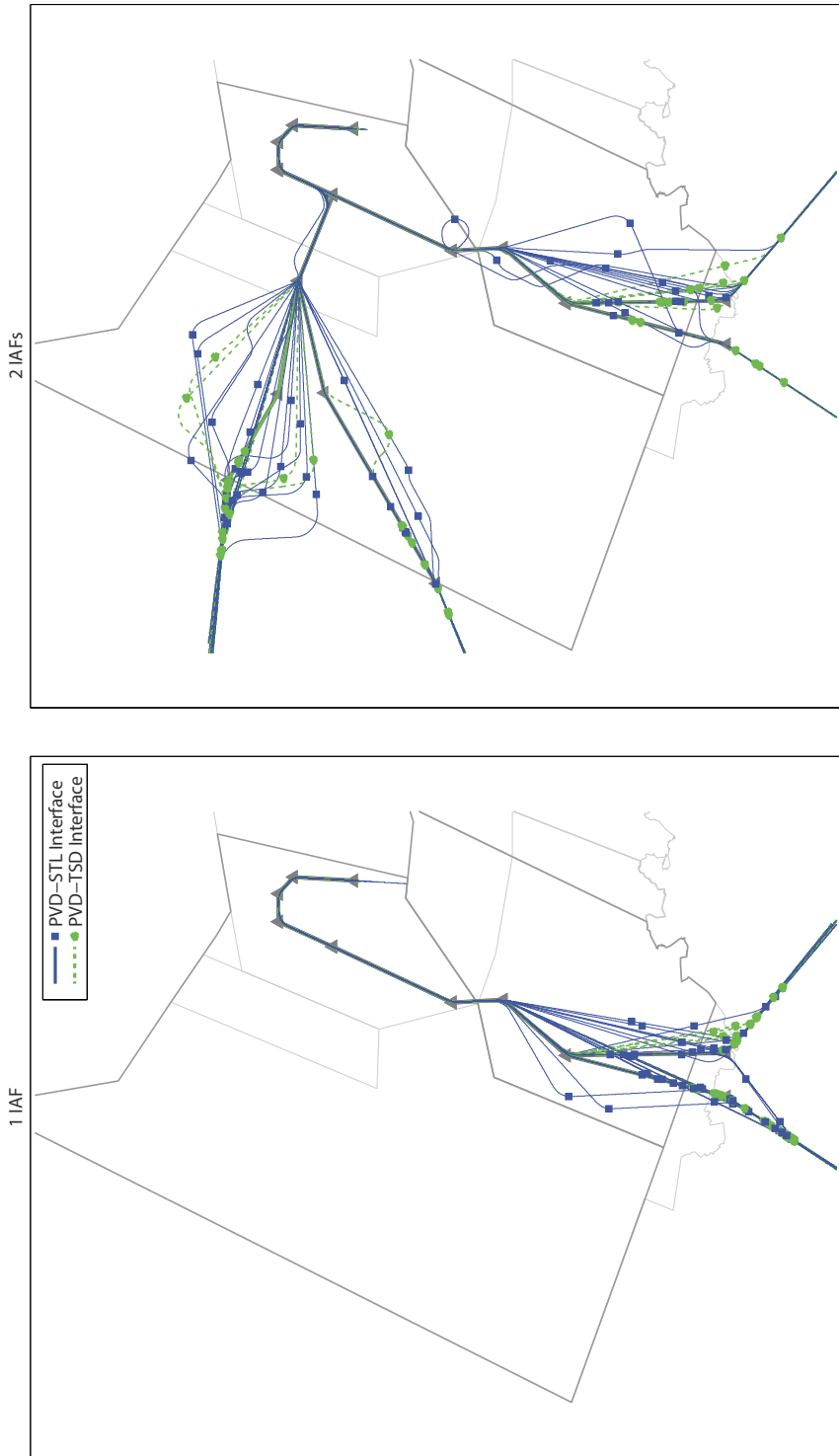
Figure 5-16 Aircraft trajectories and position when cleared for CDO.

5.7.8 Final Spacing

A histogram of the difference between the final spacing at the runway threshold and the wake separation minimum is plotted in Figure 5-17. A Friedman׳s ANOVA did not indicate any significant effect of the experiment conditions on the final spacing between aircraft, *(χ2(3) = 2.09, p = 0.55)*. The median of the difference between the final spacing and separation was 0.26 NM for both interfaces. In 20% of the cases the difference was negative, indicating a loss of separation. However, during the experiment only one loss of separation was observed. Further analysis revealed that the round off of numbers in the PVD-STL interface, conflicts being masked by the trajectory lines on the PVD-TSD interface caused minor losses. The wake vortex separation was not exceeded by more than 0.45 NM with a median of -0.09 NM and -0.14 NM for the PVD-STL and PVD-TSD interface, respectively.
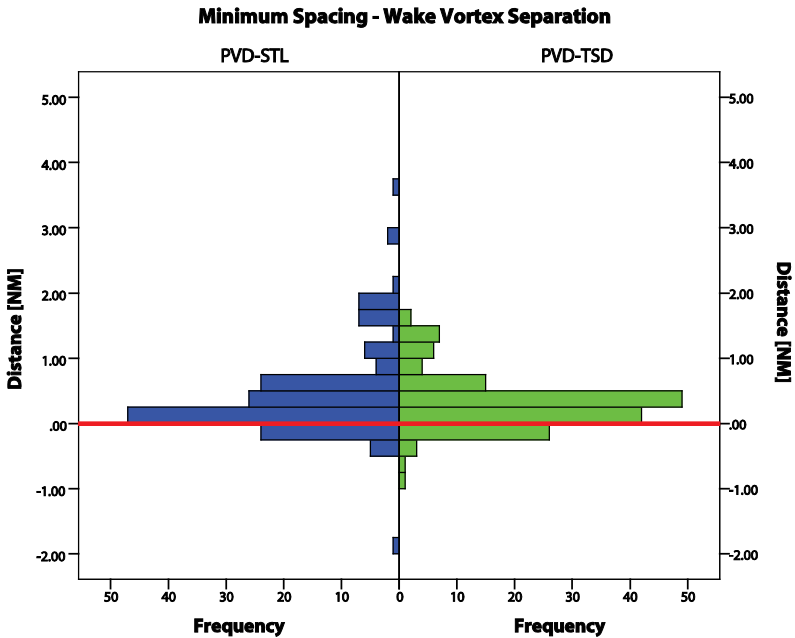
Figure 5-17 Difference between the minimum spacing and wake vortex separation inside the TMA.

5.7.9   Runway Throughput

The throughput was approximately 35 aircraft per hour in all scenarios. A Shapiro-Wilk test indicated the data of the hourly throughput for the four experiment conditions were not significantly different from a normal distribution ($p > 0.05$). A repeated measure ANOVA did not show any significant main effect of the INTERFACE, IAF on throughput measured at the runway threshold.

5.7.10   Final Questionnaire

Summarized in Figure 5-18 are the responses to statements about the completeness of the information displayed on the PVD-TSD, the use of the TSD for planning and implementation of actions, and integration of information. Most subjects agreed with the statement that all necessary information for spacing the aircraft was available in the PVD-STL and PVD-TSD interfaces. When available the subjects used the TSD for planning and implementing actions. Most subjects agreed with the statement that integrating information on the PVD and TSD was easy, indicating that visual momentum was high.
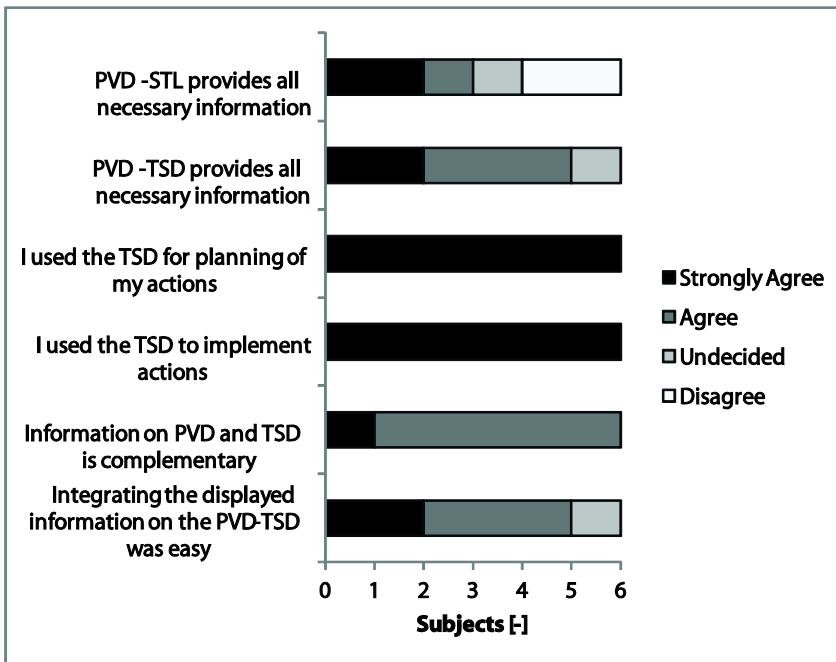
Figure 5-18 Response to questionnaire.

Direct Manipulation Interfaces

Figure 5-19 summarizes the response to the statement "The following DMI worked intuitively:" None of the DMIs was rate below 'undecided' and these ratings were

therefore removed from the figure. A Wilcoxon signed-rank test indicated that the DMIs for speed and altitude were rated significantly higher than the waypoint and heading DMIs, (p < 0.05).

Task Difficulty

A Wilcoxon signed-rank test was used to analyze the effect of the INTERFACE on the levels of the difficulty to identify conflicts, solutions to conflicts, gaps in the sequence, knock-on effects, and control of aircraft. The modes of the responses are given in Table 5-7. Conflict identification was rated significantly less difficult for the PVD-TSD interface than the PVD-STL interface, ($z = -2.27$, $p < 0.05$). Also the difficulty of identifying gaps, ($z = -2.06$, $p < 0.05$), knock on effects, ($z = -2.27$, $p < 0.05$), and control of the aircraft ($z = -2.00$, $p < 0.05$) were rated lower. The effect on identifying a solution to a conflict was not significant, $(z = -1.52, p = 0.13)$.
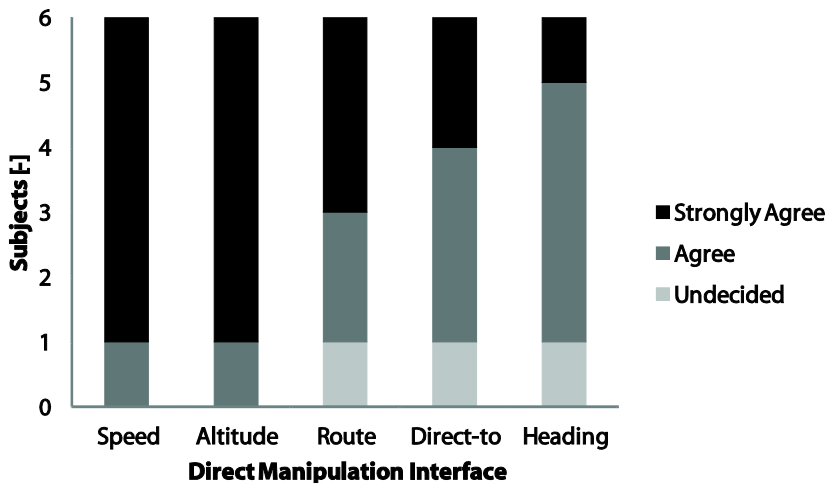
Figure 5-19 Response to the statement "the following DMI worked intuitively".

Table 5-7 Mode of the level of difficulty of tasks.

Task	PVD-STL	PVD-TSD
Identify conflicts	*Easy*	*Very easy*
Identify a solution to a conflict	*Easy*	*Very easy*
Identify knock-on effects	*Undecided*	*Very easy*
Identify gaps in the sequence	*Undecided*	*Very easy*
Control the aircraft	*Easy*	*Very easy*

Control Strategy

All subjects followed a strategy to first try to resolve a conflict using speed control. Four of the six subjects commented they also used altitude to resolve conflicts, but only for 'fine tuning'. Eventually, heading instructions were used if needed. The strategies did

were the same for both interfaces. Subjects did not comment on their strategy to close gaps in the arrival sequence.

5.8   Discussion

The impact of the TSD on the controller interface is significant. Therefore, as an alternative to the TSD, a support tool in the form of a stack list was developed that would require minimum changes of the interface. The experiment results showed no significant effects of the interface on the capacity and final inter-aircraft spacing. This result was hypothesized, as both interfaces provide the controller with the information to accurately space the aircraft (*H1*). However, significant effects on workload, situation awareness, controller instructions, aircraft trajectories, and CDO performance were found.

According to the ISA and NASA-TLX, workload was lower when using the PVD-TSD interface. The number of IAFs had a significant effect on the ISA score only. Adding a second IAF to the scenario led to an increase of the ISA score (higher workload). The NASA-TLX also gave insights in the factors contributing to the experienced workload. The PVD-TSD decreased the required effort and mental workload. Absolute judgments of the workload ratings are generally not very meaningful.[28] From observations and comments made by the subjects it was concluded that workload when using the PVD-TSD interface was very low. Subjects had considerable time to plan the traffic well ahead and were often waiting on the next aircraft to make its initial call.

The SASHA test allowed for a comparison of the level of situation awareness.[30] The level of situation awareness increased with the PVD-TSD interface and decreased when adding a second IAF independent of the interface. The impact of adding a second IAF was smaller for the PVD-TSD interface, but not on a significant level (*H3*). The main effect of the interface on the workload and situation awareness confirmed hypothesis *H2*.

Further analysis focused on the number of instructions per aircraft and the time interval in which the aircraft received instructions. With the PVD-TSD interface the total number of instructions decreased by 35% resulting in lower ATCO workload and freeing up capacity of the voice communication system. For the PVD-STL interface the number of instructions increased with the number of IAFs, but for the PVD-TSD interface there was no significant effect. This supported the hypothesis *H3* that the effect of the number of IAFs is smaller when using the PVD-TSD interface. The DMIs that were introduced enabled the subjects to accurately set the speed to resolve conflicts or close gaps in the sequence. As a result the number of speed instructions decreased by 50%. There was an even bigger effect on the number of instructions that change the aircraft lateral path. The number of heading instructions and directs decreased by 75%. This was not clearly

reflected in the miles flown and the sector time. When using the PVD-TSD interface more use was made of the available STARs was made. However, the STARs did not provide the most direct route between the entry points and IAFs, as can be seen in Figure 5-7. Aircraft that received instructions to fly a lateral path different from the arrival route possibly flew less track miles to the IAF than aircraft on the STAR, for example for the entry point HELEN as can be seen in Figure 5-15. Because fewer instructions were given, it was also expected that the instructions were given in a shorter time frame. The analysis showed that the first instruction and last instruction were received earlier when the PVD-TSD interface was used. The last instruction to the aircraft was the clearance for the CDO. This enabled the aircraft to start the CDO from larger distance to the runway and a higher altitude, to the benefit of the economical and environmental performance, as hypothesized in *H4*.

In previous research ATCOs reported difficulties integrating the information displayed on the PVD and TSD and started to focus on the TSD.[11,12] To resolve these issues the concept of visual momentum was applied. The effect of the visual momentum techniques applied could not be quantitatively determined because of the display configurations used in the experiment. Therefore, subjects were explicitly asked about any issues with the integration of information. The subjects responded the integration was easy and no problems were raised during the experiment. Also the SASHA questionnaire did not indicate any difficulties in building a mental picture of the traffic situation. To analyze whether subjects started to focus on the TSD the selection of aircraft and use of the DMIs was analyzed. Both indicated that subjects primarily used the PVD to make inputs to the system. These findings were supported by the display used for ISA; 3% of the total number of ratings was given through the TSD with a maximum of five of 13 ratings in one run. One subject commented that he had the feeling of being less aware of the greater picture and was focusing primarily on the TSD. This was partly reflected in the SASHA scores for this subject. This subject's SASHA score for the PVD-TSD interface was higher than for the PVD-STL interface when controlling traffic for one IAF. For all other subjects the SASHA scores for the PVD-TSD interface were always higher than the scores for the PVD-STL interface. Additionally, the same subject also had the second highest number of inputs on the TSD, but still made most inputs on the PVD. To unambiguously determine focus on either display, data from e.g., an eye-tracker would be needed.

At the end of the final questionnaire, subjects were asked if they had any suggestions or comments on the two interfaces. The suggestions that were given varied strongly and did not indicate clear areas for improvement or a lack of functionality. Various minor changes to the interface were proposed. For the simulator that was used two subjects commented on the text-to-speech technique that was used as part of the experiment

setup. The same voice was use for all flights; this did not allow the subjects to identify a flight by the voice.

The work presented on the TSD focused on the design of the interface. Development and testing of enabling system has been omitted. Enablers for the TSD include trajectory prediction and possibly new aircraft-ground data link capabilities. A trajectory predictor with good internal models of the aircraft performance and flight management system logic shall be available to ensure a good match between the actual and predicted trajectory. The prediction accuracy is the main determining factor for the accuracy of the tool. Low prediction accuracy can be detrimental for the trust a controller has in the support provided by the TSD.

In a real ATM system, arriving traffic will be under control of multiple ATCOs and the TSD would be used across multiple controllers. In the design and testing of the interface thus far the TSD was used by one ATCO controlling multiple IAFs. It is expected the TSD can be used in the required coordination between ATCOs. The TSD provides all controllers with the same picture of the arriving traffic. It is likely a planner will (still) be needed to determine the arrival sequence in order to avoid conflicting decisions and actions.

The information and tools provided by the TSD are not specific to spacing aircraft for CDO. Once the traffic is cleared for CDO, the traffic shall still be monitored. Also during monitoring the TSD can be used to show the controller if there are any conflicts and support in deconflicting the traffic. Other operational improvements that require accurate arrival time control could benefit from the TSD. However, the TSD representation of traffic imposes limits on operational concepts that can be visualized effectively. One example is that all aircraft must have at least one common trajectory point (e.g., the runway threshold).

5.9 Recommendations

The following three recommendations are made for further development and testing of the PVD-TSD interface. From the experiment the effects of the visual momentum techniques and direct manipulation interfaces could not be derived quantitatively. It is recommended to conduct a similar experiment as described in this paper that enables to quantitatively determine these effects. In a realistic ATM system the TSD will be used across multiple controllers. The simultaneous use of the TSD by multiple ATCOs shall be studied. Focus should be on shared use of the TSD and the role the TSD can play in the coordination between ATCOs. Trajectory prediction accuracy is the determining factor for the TSD accuracy and may have detrimental effects on the ATCO's trust in the tool. The effect of trajectory prediction uncertainty and the possibilities for displaying the uncertainty should be studied.

5.10 Conclusions

The Time-Space Diagram controller support tool (TSD) enables the air traffic controller to accurately space, sequence, and merge traffic for Continuous Decent Operation (CDO) for traffic coming from different directions. The TSD is presented on a second display next to the plan view display. Compared to a stack list providing the required spacing and time to lose or gain for CDO on the plan view display, controller workload is significantly lower at a higher level of situation awareness. Adding a second sector with traffic arriving from a different direction to the scenario has a less significant effect on the traffic handling. The TSD interface frees time to plan traffic ahead using direct manipulation interfaces, which according to all subjects work intuitively. Early accurate speed control was applied. The number of instructions per aircraft was decreased by 35% and instructions were given earlier. The number of heading instructions was reduced by 75%. More use was made of the fixed arrival routes. However, the track miles were not reduced significantly because the fixed arrival routes did not always provide the most direct routing. Because instructions were given earlier, aircraft commenced their CDO at a higher altitude and greater distance from the runway.

5.11 Acknowledgments

5.12 References

1. EUROCONTROL, "SESAR Master Plan D5: SESAR Definition Phase - Milestone Deliverable 5", DLM-0710-001-02-00, SESAR Consortium for the SESAR Definition Phase Project co-funded by the European Commission and EUROCONTROL, April 2008.

2. Joint Planning and Development Office (JPDO), "NextGen Integrated Work Plan: A Functional Outline," Tech. rep., Joint Planning and Development Office, 2008.

3. ICAO, "Environmental Report 2010, Aviation and Climate Change", 2010.

4. Ren, L., and Clarke, J.-P.B., "A Separation Analysis Methodology for Designing Area Navigation Arrival Procedures," *Journal of Guidance, Control, and Dynamics*, Vol. 30, No. 5, 2007, pp. 1319-1330. DOI: 10.2514/1.27067

5. Ren, L., and Clarke, J.-P.B., "Flight-Test Evaluation of the Tool for Analysis of Separation and Throughput," *Journal of Aircraft*, Vol. 45, No. 1, 2008, pp. 323-332. DOI: 10.2514/1.30198

6. Reynolds, H. J. D., Reynolds, T. G., and Hansman, R. J., "Human Factors Implications of Continuous Descent Approach Procedures for Noise Abatement in Air Traffic Control," *6rd USA/Europe Air Traffic Management R&D Seminar*, Baltimore, Washington, June, 2005, pp 1-10.

7. Erkelens, L.J.J., "Research into new noise abatement procedures for the 21st century," *Proceedings of the AIAA Guidance, Navigation and Control Conference and Exhibit*, Denver, Colorado, Aug. 14-17, 2000, No. AIAA 2000-4474, 2000, pp. 1-10.

8. Clarke, J.-P.B., "Systems Analysis of Noise Abatement Procedures Enabled by Advanced Flight Guidance Technology," *Journal of Aircraft*, Vol. 37, No. 2, 2000, pp. 266-273. DOI: 10.2514/2.2590

9. Tielrooij, M., In 't Veld, A.C., Mulder, M., and van Paassen, M.M., "Assisting ATC in Metering, Sequencing and Merging Arrival Streams in Three-Degree Decelerating Approaches," *Proceedings of the 27th European Annual Conference on Human Decision Making and Manual Control*, Delft, The Netherlands, June 12-13, 2008, pp. 1-8.

10. Tielrooij, M., In 't Veld, A.C., Mulder, M., and van Paassen, M.M., "Development of a Time-Space Diagram to Assist Air Traffic Controllers in Monitoring Continuous Descent Approaches," *Air Traffic Control*, edited by M. Mulder, Sciyo, Rijeka, Croatia, August 2010, pp. 135-147.

11. van der Eijk, A., Borst, C., Mulder, M., van Paassen, M.M., and in't Veld, A.C. "Assisting Air Traffic Control in Planning and Monitoring Continuous Descent Approach Procedures," *Journal of Aircraft*, Vol. 5, No. 5, 2012, pp. 1376-1390, DOI: 10.2514/1.C031686.

12. van Dijk, E., Mulder, M., Van Paassen, M.M., and Roerdink, M.I., "An Interface for Inbound Traffic Management by Air Traffic Control," *Proceedings of the AIAA Guidance, Navigation and Control Conference*, Chicago (IL), USA, August 10-13, No. AIAA 2009-6164, 2009.

13. ICAO, "Continuous Descent Operation (CDO) Manual," Doc. 9931 AN/479, advanced edition, 2010.

14. SESAR, "SESAR Master Plan D5," Deliverable 5, EUROCONTROL, April 2008.

15. Garber, N.J., and Hoel, L.A., *Traffic & Highway Engineering*, University of Virginia, Cengage Learning Engineering, 2010.

16. United States Department of Transport, *Traffic Signal Timing Manual*, Kittelson & Associates. Inc., Cengage Learning Engineering, June 2008.

17. Young, S. B., and Wells, A.T, "*Airport Planning & Management*," McGraw-Hill Companies, Inc., 6th ed., 2011, pp. 436.

18. Vicente, K.J., and Rasmussen, J., "Ecological Interface Design: Theoretical Foundations," *IEEE Transactions on Systems, Man, and Cybernetics,* Vol. 22, No. 4, 1992, pp. 589-606.

19. Peters, M., and Konyak, M.A., "The Engineering Analysis and Design of the Aircraft Dynamics Model for the FAA Target Generation Facility," Seagull Technology, Inc., Los Gatos, CA, November 2003

20. Ren, L., Tan Ho, N., and Clarke, J.-P.B., "Workstation Based Fast-Time Aircraft Simulator for Noise Abatement Approach Procedure Study," AIAA Paper 2004-6503, September 2004.

21. Anon., "Standard Aircraft Modeling Interface," Users guide (draft) rev. 4.2, EUROCONTROL Headquarters, Brussels, Belgium, April 2009.

22. Anon., "G.A.M.E. Aircraft Performance Model," Report ver. 2.0, EUROCONTROL Headquarters, Brussels, Belgium, September 2002.

23. Anon., "User Manual for the Base of Aircraft Data (BADA), Revision 3.6," EUROCONTROL Experimental Center, Brussels, Belgium, September 2004.

24. Woods, D.D., "Visual Momentum: A concept to improve the cognitive coupling of person and computer," *International Journal of Man-Machine Studies*, Vol. 21, No. 3, September 1984, pp. 229-244.

25. Kaber, D.B., Riley, J.M., Tan, K., and Endsley, M.R., "On the design of adaptive automation for complex systems," *International Journal of Cognitive Ergonomics*, Vol. 5, 2001, pp. 37-57.

26. Hutchins, E.L., Hollan, J.D., and Norman, D. A., "Direct Manipulation Interfaces," *Human-Computer Interaction*, Vol. 1, 1985, pp. 311-338.

27. Kirwan, B., Evans, A., Donohoe, L., Kilner, A., Lamoureux, T., Atkinson, T., and MacKendrick, "Human Factors in ATM System Design Life Cycle," *FAA/Europe ATM R&D Seminar*, Paris, France, 2007.

28. Hart, S. G. and Staveland, L. E., "Development of NASA-TLX (Task Load Index): Results of empirical and theoretical research," *Human Mental Workload*, edited by P. A. Hancock and N. Meshkati, Elsevier Science Publishers, Amsterdam, The Netherlands, 1988, pp. 139-183.

29. Field, A.P., *Discovering Statistics Using SPSS*, SAGE Publications Ltd., London (UK), 3rd ed., 2009.

30. Straeter, O., Woldring, V.S.M., Barbarino, M., Skoniezki, A., and Philipp, W., "The Development of Situation Awareness Measures in ATM Systems," Tech. Rep. HRS/HSP-005-REP-01; 1.0, EUROCONTROL Headquarters, Brussels, Belgium, June 2003.

31. Liao, T.F., *Interpreting Probability Models: Logit, Probit, and Other Generalized Linear Models*, SAGE Publications, 1994, Chapter 5, pp. 41-43.

6 Discussion, Conclusions and Recommendations

6.1 Discussion

This thesis focuses on the development of an Air Traffic Management (ATM) system that enables closed-path Continuous Descent Operation (CDO) in high-density traffic. In such a system the dependency on the ATCO's trajectory projection capabilities must be reduced. Two possible features of such an ATM system are:

- Delegation of the spacing task during the CDO (self-spacing);
- Controller support for accurate arrival time control.

Two key enabling technologies for these features are meteorological data acquisition and trajectory prediction. These enabling technologies were also included in the scope of this thesis. Figure 6-1 gives a schematic representation of the thesis scope and objectives. The next sections give an overview of the results and present the conclusions and recommendations.
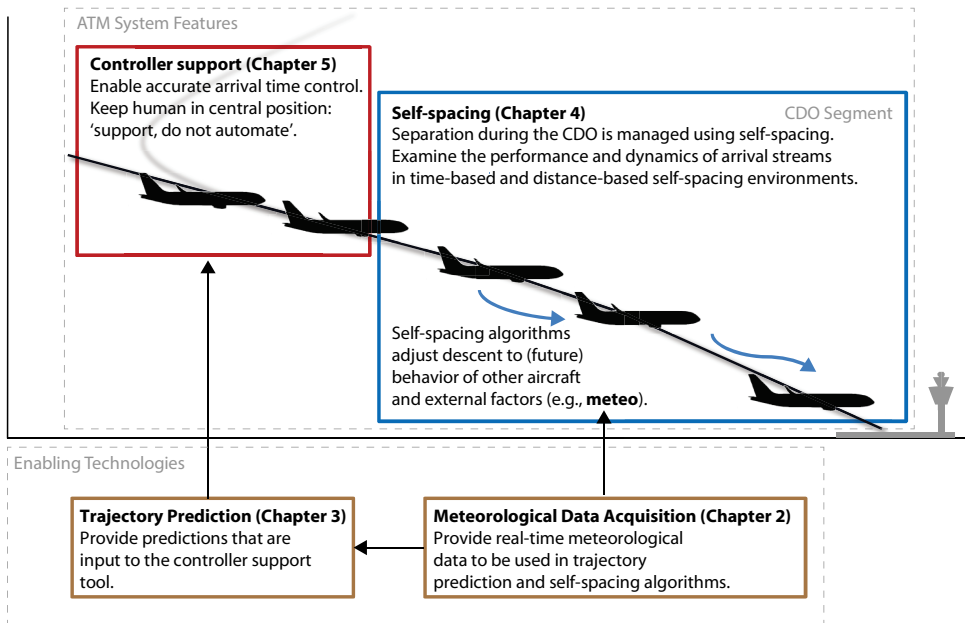
Figure 6-1 Schematic representation of scope and objectives.

6.1.1 Meteorological Data Acquisition

In Chapter 2, methods to estimate wind, air pressure, and temperature profiles in near real-time from Automatic Dependent Surveillance-Broadcast (ADS-B) data were described. The ADS-B system was selected to enable estimation of meteorological conditions using existing systems and communication protocols. The cost of ADS-B ground equipment is relatively low, and the estimation methods may also be applied onboard 'ADS-B In' equipped aircraft without requiring additional communication protocols. The latter can be considered an advantage over methods that rely on radar position data and Mode-S enhanced surveillance described in Refs [1, 2]. Radar and Mode-S surveillance data is only available on the ground.

Two methods to estimate wind from ADS-B data were developed. The main difference between the two methods was the number of aircraft used. Using only one aircraft resulted in constraints on the flight path as well as a dependency on the number of turning aircraft, which led to a low number of estimates. Also, a large track angle change was needed to limit the estimation error. This method is therefore not suited to provide wind estimates at fixed time and altitude intervals. When using multiple aircraft, wind estimates for a larger area could be produced at fixed time and altitude intervals. The wind estimation methods developed can be applied to other surveillance systems providing aircraft ground vector information. Application of the pressure and temperature estimation methods is expected to be specific to ADS-B, because of the availability of the difference between the Global Navigation Satellite System height and barometric altitude. From this altitude difference, the pressure could be readily computed. The resulting pressure profile, hydro-static equilibrium, and gas law were used to get a temperature profile estimate.

To test the methods, estimates were made for 100 days of ADS-B data and compared to forecasts at nine points of a three-by-three grid over the Netherlands. Amsterdam Airport Schiphol was located near the center grid point. The presence of the airport near the center grid point ensured that there was sufficient data available to make estimates between 1,000 ft and 40,000 ft. The comparison of the estimates with the Global Forecast System (GFS) forecasts provided an order of magnitude of the error that can be expected under actual traffic and meteorological conditions. The mean absolute differences between the forecast and estimate for wind speed and direction were 9.2 kts and 29.0 deg, respectively. The mean absolute differences for the pressure and temperature estimates were 1.5 hPa and 2.4 K, respectively.

An accurate independent measure of true wind, pressure, and temperature is needed to determine the accuracy of the proposed methods. Possible sources are better meteorological models and aircraft observations. Also it should be noted that the results

were based on the first iteration of the methods and it is expected they can be improved using more advanced filtering of the ADS-B data and a better understanding of the factors impacting the accuracy.

6.1.2 Trajectory Prediction

Following the work on meteorological data acquisition, an alternative approach to Trajectory Prediction (TP) was explored in Chapter 3. Trajectory prediction was formulated as a supervised machine learning regression problem. In this approach historical trajectory and meteorological data is used to train predictive models. The input variables used were limited to aircraft state parameters that are readily available through the radar and or ADS-B surveillance systems and wind data that can be obtained using the methods described in Chapter 2.

The TP performance was evaluated using ADS-B data of a 45 NM closed path CDO procedure with an average flying time of 727 s. The model explained 63% of the variance in the time over the runway threshold. The mean absolute error was 18 s with a root mean squared error of 24 s. Subsequently, the TP was used in a spacing analysis to assess the effect of the TP performance on the runway throughput for CDO. The required spacing between aircraft at the start of the CDO to remain separated during the CDO phase was computed using the TP. The simulation results showed a decrease of the number of conflicts between aircraft requiring tactical interventions compared to the use of fixed spacing interval at the same runway throughput. These results suggest that on a short term, runway throughput for CDO can be increased if the required initial spacing is tailored to each aircraft pair using the TP. The runway throughput that can be achieved depends on the number of conflicts that is acceptable. A similar approach was proposed by Ren and Clarke in their work on Tool for the Analysis of Separation and Throughput [5, 6]. The TP performance is expected to be insufficient for CDO in high-density traffic. This would require better TP performance or the use of self-spacing concepts as investigated in Chapter 4. For improvement of the TP performance, additional input parameters with explanatory power over the aircraft trajectory are needed. Likely candidates are the aircraft weight and aircraft intent information. Because of limitations of the current surveillance and data-link systems, and the commercial sensitivity of some parameters (e.g., weight and cost index), it is unlikely that these will be become available on a short term.

6.1.3 Self-Spacing

In this thesis a typical operational concept to enable CDO in high density traffic was used. Before the start of the CDO the Air Traffic Controller (ATCO) accurately spaces the traffic for CDO using a support tool. During the CDO phase the spacing task is delegated to the flight crew (self-spacing).

The use of self-spacing to keep traffic separated during the CDO was investigated in Chapter 4. Monte-Carlo simulations were carried out to examine the performance and dynamics of relative distance-based and absolute time-based self-spacing algorithms in arrival streams. The main result of the simulations was the runway capacity estimate. The runway capacity using relative distance-based spacing was at least 90% of the capacity when using conventional approach procedures. For absolute time-based spacing this percentage was 81%. The difference in runway capacity is due to buffer space that was needed in the absolute time-based scenario to account for aircraft that failed to meet their required time of arrival. In the relative distance-based concept, aircraft actively reacted to any path deviations of the preceding aircraft. Because relative distance-based self-spacing was the most promising concept in terms of runway capacity, additional simulations were carried out for this concept to assess the effect of disturbances and initial conditions. The sensitivity analysis underlined the importance of accurate initial spacing to enable aircraft to fly an optimized CDO. The limited flexibility of aircraft during the CDO imposes constraints on the initial spacing. Hence, the TP that was used in determining the initial spacing should be sufficiently accurate to position the aircraft within the feasible spacing interval. In the Monte-Carlo simulations this interval was several tens of seconds for a procedure that started at 11 NM from the airport. Although a different procedure was used for the work on the TP (Chapter 3), the root mean square error of 24 s suggests the TP performance is sufficient to initially space the aircraft for CDO in high-density traffic if self-spacing is used during the CDO.

6.1.4 Controller Support
Chapter 5 focused on the development of the Time-Space Diagram (TSD) controller support tool for spacing, sequencing and merging traffic for CDO. This tool was developed earlier following the principles of ecological interface design to provide the controller with the tools and information to be an active problem solver [3, 4]. Work in this thesis focused on the integration of the information displayed on the Plan View Display (PVD) and TSD interface using the concept of visual momentum. Also the solution guidance provided by the interface was redesigned. Static what-if tools showing the effect of computer selected actions were replaced by direct manipulation interfaces.

A human-in-the-loop experiment was performed to determine the effect of the PVD-TSD on controller workload, situation awareness, and traffic handling. A landing rate of approximately 35 AC/H was required to handle the traffic without delay. The PVD-TSD was tested against a more conventional support solution in the form of a stack list. Using either interface the participants could space the traffic accurately for CDO. The observed landing rate was approximately 35 AC/H. However, when using the PVD-TSD interface the ATCO workload was significantly lower at a higher level of situation awareness.

Using the PVD-TSD interface 35% fewer instructions were given and instructions were given earlier. In most cases accurate early speed control was sufficient to space the aircraft for CDO. As a result the CDOs started at higher altitude and a larger distance from the runway threshold, benefitting the environmental performance.

6.2   Recommendations

An ATM system that facilitates CDO in high-density traffic encompasses more procedures, processes, systems, and other traffic than were addressed in this thesis. Research and development in other areas, beyond the scope of this thesis, is also needed to eventually enable CDO in high-density traffic. Examples of areas that were not covered are pilot support, controller support during self-spacing operations, CDO procedure design, and communication systems. The ATM master plan developed for the future European ATM system outlines the enablers, systems, operational improvements (steps), and ultimately the lines of change for such a system.

The work done in this thesis has led to the following recommendations:

Controller support during the CDO phase

During the CDO phase the spacing between the aircraft shall be monitored and actions to resolve conflicts, despite accurate initial spacing, could be necessary. In this thesis self-spacing during the CDO phase was investigated. Self-spacing is considered a long-term solution requiring new aircraft systems and also legislative changes. Before self-spacing is available, it will be the task of the ATCO to space traffic during the CDO phase. Also during the CDO phase a form of controller support might be needed that provides information about which aircraft pairs will remain separated, conflicts that might occur. This should avoid unnecessary tactical interventions and allow for timely conflict resolution. Also when self-spacing is available, a support tool might still be needed to keep the ATCO aware of the traffic situation. Controller support during the CDO phase should be investigated both in case the ATCO is managing the spacing and when the spacing task is delegated. The support interface should visualize the operational and environmental constraints and provide the tools that allow the ATCO to be an active problem solver during the CDO phase. A first step could be to investigate the use of the TSD for these purposes.

Including trajectory prediction uncertainty

Trajectory prediction uncertainty has been omitted in the work on the PVD-TSD interface. Trajectory prediction uncertainty should be included in the decision making and planning processes. This could benefit CDO operations on the short term (e.g., increased capacity) without requiring more accurate trajectory prediction. The

presentation of, and procedures to deal with, trajectory prediction uncertainty should be investigated.

Trade-off between capacity and environmental performance
It has been shown that the capacity for CDO can be increased if tactical interventions are applied during the CDO. More tactical interventions yield a higher capacity at the cost of the environmental benefits. Another possibility is to impose more speed and altitude constraints along the route yielding in better predictability. Also in this case, the environmental performance of the CDO is likely to degrade. The impact on the environmental performance of imposing constraints and tactical interventions on the CDO should be investigated to make a trade-off between capacity and environmental performance.

Data Mining, Big Data Analytics, and Machine Learning
Work in this thesis has resulted in methods to derive meteorological data from ADS-B and a machine learning approach to trajectory prediction. These methods could be characterized as Data Mining, Big Data analytics, or Machine Learning techniques. The use of these techniques in ATM should be explored to exploit the vast volumes of surveillance and flight plan data that are currently available both in real-time and of many years of operation. These techniques may be used to infer aircraft state information (e.g., aircraft weight) from surveillance data. An accurate aircraft weight estimate could benefit trajectory prediction, noise and emission assessments etc. Another example is the use of machine learning to predict the aircraft taxi times and runway occupancy times that can be used in airport Collaborative Decision Making processes.

6.3   Conclusions

The main conclusions that can be drawn from the work presented in this thesis are:

Automatic Dependent Surveillance-Broadcast can be used for real-time meteorological data acquisition in ground and airborne systems. The methods developed to derive wind, pressure, and temperature profiles fully rely on existing systems and communication protocols, therefore enabling short-term implementation.

Trajectory Prediction (TP) can be formulated as a supervised machine learning regression problem. This approach does not require explicit modeling of aircraft performance, procedure, or airspace. In the approach, model inputs are selected based on their statistical significance in explaining the aircraft trajectory. The TP performance was analyzed using actual meteorological and trajectory data. Using the TP to tailor the

aircraft spacing to each aircraft pair yielded a higher landing rate up to 20% compared to the use of a fixed spacing interval.

Both relative distance-based and absolute time-based self-spacing are promising concepts to manage spacing during the CDO phase in high-density traffic. The runway throughput achieved in the simulations was comparable to the throughput realized using conventional procedures. The highest throughput was achieved using the relative distance-based self-spacing concept. In the absolute time-spacing concept, buffer space at the cost of capacity was required to account for aircraft that failed to meet their required time of arrival. Key factor for the CDO success rate is initial spacing between aircraft. Accurate spacing is required, because the maneuverability of an aircraft during the CDO is limited.

The Time-Space Diagram (TSD) interface enables the air traffic controller to accurately sequence, merge, and space traffic for CDO. Concepts applied in the design of the interface are ecological interface design, visual momentum, and direct manipulation. The TSD interface was tested against a conventional support solution. The TSD interface freed time to plan traffic ahead using direct manipulation interfaces, which according to all subjects worked intuitively. The number of instructions per aircraft was decreased by one third and instructions were given earlier. As a result CDOs started earlier at a higher altitude and greater distance from the runway. Air traffic controller workload was significantly reduced and situation awareness increased.

6.4   References

1. de Haan, S., and Stoffelen, A., "High resolution temperature and wind observations from commercial aircraft," , edited by Apituley, A., Russchenberg, H. W. J. , Monna, W. A. A. , Organizing Committee of the 8th International Symposium on Tropospheric Profiling, Delft, The Netherlands, 2009.

2. Delahaye, D., and Puechmorel, S., "TAS and wind estimation from radar data," *Digital Avionics Systems Conference 2009,* IEEE, Orlando, FL, 2009, pp. 2.B.5-1 - 2.B.5-16, DOI: 10.1109/DASC.2009.5347547.

3. Tielrooij, M., in 't Veld, A.C., Mulder, M., and van Paassen, M.M., "Development of a Time-Space Diagram to Assist Air Traffic Controllers in Monitoring Continuous Descent Approaches," *Air Traffic Control*, edited by Mulder, M., Sciyo, Rijeka, Croatia, August 2010, pp. 135- 147.

4. van der Eijk, A., Borst, C., Mulder, M., van Paassen M.M., and in't Veld, A.C. "Assisting Air Traffic Control in Planning and Monitoring Continuous Descent Approach Procedures," *Journal of Aircraft*, Vol. 5, No. 5, 2012, pp. 1376-1390. DOI: 10.2514/1.C031686

5. Ren, L., and Clarke, J.-P.B., "A Separation Analysis Methodology for Designing Area Navigation Arrival Procedures," *Journal of Guidance, Control, and Dynamics*, Vol. 30, No. 5, 2007, pp. 1319- 1330. DOI: 10.2514/1.27067

6. Ren, L., and Clarke, J.-P.B., "Flight-Test Evaluation of the Tool for Analysis of Separation and Throughput," *Journal of Aircraft*, Vol. 45, No. 1, 2008, pp. 323-332. DOI: 10.2514/1.30198

Nomenclature

Latin Symbols

D	drag	N
g	gravitational acceleration	m/s^2
h	altitude	m, ft
h$_{VAPP}$	altitude approach speed reached	ft
K	kalman gain	
k	time step	
L	lift	N
L$_{Amax}$	maximum instanteouous noise level	dB(A)
m	mass	kg
P	error covariance matrix	
P	pressure	hPa
Q	noise covariance matrix	
R	correlation coefficient	
R	noise covaraince matrix	
R	universal gas constant	J/K mol
T	temperature	˚C, K
T	thrust	N
$\overline{V}_a$	airspeed vector	kts
$\overline{V}_{app}$	approach speed	kts
$\overline{V}_g$	ground speed vector	kts
$\overline{V}_w$	wind speed vector	kts
$\overline{w}$	solution vector	
$\overline{x}$	state vector	

Greek Symbols

α	angle of attack	deg
γ	flight path angle	deg
γ_a	aerodynamic flight path angle	deg
γ_k	kinetmatic flight path angle	deg
λ	temperature lapse rate	°/m
μ	mean	
ρ	air density	kg/m^3
σ	standard deviation	
χ_k	aircraft track angle	deg
χ_w	wind direction	deg

Acronyms

AAS	Amsterdam Airport Schiphol
AC	Aircraft
ADS-B	Automatic Dependent Surveillance Broadcast
AMAN	Arrival Management
AMDAR	Aircraft Meteorological Data Relay
AMSL	Above Mean Sea Level
ANOVA	Analysis of Variance
ATC	Air Traffic Control
ATCO	Air Traffic Controller
ATM	Air Traffic Management
BADA	Base of Aircraft Data
CAS	Calibrated Airspeed
CDA	Continuous Descent Approach
CDO	Continuous Descent Operation
DAP	Downlink Airborne Parameters
DME	Distance Measuring Equipment
DMI	Direct Manipulation Interface
dof	degree-of-freedom

DOP	Dilution of Precision
DTG	Distance To Go
EID	Ecological Interface Design
ETA	Estimated Time of Arrival
FL	Flight Level
FMS	Flight Management System
GFS	Global Forecast System
GLM	Generalized Linear Model
GNSS	Global Navigation Satellite System
HAE	Height Above Ellipsoid
IAF	Initial Approach Fix
IAS	Indicated Airspeed
ICAO	International Civil Aviation Organisation
ILS	Instrument Landing System
LPLD	Low Power Low Drag
MAE	Mean Absolute Error
ME	Mean Error
MEKF	Modified Extended Kalman Filter
METAR	Meteorological Aerodrome Report
MLW	Maximum Landing Weight
MOS	Modeling Output Statistics
MSL	Mean Sea Level
NASA	National Aeronautics and Space Administration
NASA-TLX	NASA Task Load IndeX
NextGen	Next Generation Air Transportation System
NM	Nautical Mile
NUC	Navigation Uncertainty Category
NWO	Netherlands Organisation for Scientific Research
OEW	Operating Empty Weight
PF	Packing Factor
PVD	Plan View Display
RMSE	Root Mean Square Error
RTA	Required Time of Arrival
SA	Situation Awareness
SASHA	Solutions for Human Automation Partnerships in European ATM
SESAR	Single European Sky ATM Research

SSR	Secondary Surveillance Radar
STAR	Standard Arrival Route
STL	Stack list
TAS	True Airspeed
TCB	Thrust Cutback
TDDA	Three-Degree Decelerating Approach
THR	Runway Threshold
TP	Trajectory Predictor
TSD	Time-Space Diagram
WGS	World Geodetic System

Samenvatting

Dag en Nacht Stiller Landen

A.M.P. de Leege

De luchtvaartsector streeft naar een afname van de milieu-impact per vlucht. Het volgen van geluidsarme naderingsprocedures is een van de operationele maatregelen om de emissie van geluid en stoffen te beperken. In tegenstelling tot bij conventionele naderingsprocedures met horizontale segmenten daalt het vliegtuig tijdens een geluidsarme nadering continu. Het glijpad en snelheidsprofiel zijn beide geoptimaliseerd om met minimaal motorvermogen de luchthaven te naderen. Het lage motorvermogen en een toename van de afstand zorgen voor een lager geluidsniveau op de grond in vergelijking tot conventionele naderingsprocedures.

Instructies van de luchtverkeersleiding tijdens de geluidsarme naderingsprocedure beperken de mogelijkheden om langs het, in termen van geluid en emissies, optimale glijpad de luchthaven te naderen. Daarom dienen instructies tijdens het uitvoeren van geluidsarme naderingen zoveel mogelijk te worden vermeden. Of instructies tijdens de nadering nodig zijn, hangt af van de onderlinge afstand tussen vliegtuigen bij het oplijnen van het verkeer. Indien de onderlinge afstand tussen twee vliegtuigen aan het begin van de nadering te kort is, lopen vliegtuigen te veel op elkaar in en zijn instructies van de luchtverkeersleiding nodig voor het behouden van separatie. Indien de onderlinge afstand tussen twee vliegtuigen te groot is, daalt de landingscapaciteit tot onder het niveau dat met conventionele procedures behaald wordt.

Op dit moment hanteren luchtverkeersleiders bij het oplijnen van het verkeer voor geluidsarme naderingen arbitraire marges ten koste van de landingscapaciteit om instructies tijdens de nadering te vermijden. De luchtverkeersleider schat de benodigde onderlinge afstand tussen vliegtuigen aan de start van de geluidsarme nadering. Deze schatting is onvoldoende nauwkeurig om geluidsarme naderingen bij een groot verkeersaanbod mogelijk te maken. Een luchtverkeersleidingssysteem dat geluidsarme naderingen mogelijk maakt in hoge verkeersdichtheid, zal minder afhankelijk moeten zijn van deze inschatting. Mogelijke oplossingsrichtingen zijn:

- Ondersteunen van de luchtverkeersleider bij het oplijnen van verkeer.
- Delegeren van de separatietaak tijdens de geluidsarme nadering aan vliegers of aan een automatiseringssysteem.
- Ontwikkelen van geluidsarme naderingen waarvoor eenvoudiger een inschatting kan worden gemaakt van de benodigde onderlinge afstand.

Doel van dit proefschrift is de ontwikkeling van een luchtverkeersleidingssysteem dat geluidsarme naderingen bij een groot verkeersaanbod mogelijk maakt. Dit proefschrift richt zich op twee aspecten van een dergelijk systeem:

- Ondersteuning van de luchtverkeersleider bij het oplijnen van verkeer voor geluidsarme naderingen.
- Delegeren van de separatietaak gedurende de geluidsarme nadering van de luchtverkeersleider aan de vlieger (self-spacing).

In dit luchtverkeersleidingssysteem volgt het vliegtuig tijdens de geluidsarme nadering een vaste naderingsroute. Het glijpad en snelheidsprofiel zijn vrij voor optimalisatie aan boord van het vliegtuig t.b.v. minimale milieu-impact.

Bij beide eerder genoemde aspecten wordt gebruik gemaakt van trajectvoorspellingen. De nauwkeurigheid en betrouwbaarheid van deze voorspellingen zijn daarmee bepalend voor de algehele prestaties van het luchtverkeersleidingssysteem.

Meteorologische omstandigheden bepalen in significant mate het traject van het vliegtuig. De beschikbaarheid van nauwkeurige meteorologische informatie is daarom een voorwaarde voor een accurate trajectvoorspelling en daarmee uiteindelijk voor het kunnen uitvoeren van geluidsarme naderingen bij een groot verkeersaanbod. Dit proefschrift beschrijft methoden om meteorologische informatie af te leiden van Automatic Dependent Surveillance Broadcast (ADS-B) data. ADS-B is een surveillance systeem dat positie- en snelheidsgegevens levert. ADS-B gegevens zijn naar verwachting in de nabije toekomst beschikbaar op zowel de grond als aan boord van vliegtuigen. Met de in dit onderzoek ontwikkelde methoden kunnen wind-, druk- en temperatuurprofielen worden afgeleid, zowel aan boord van het vliegtuig als op de grond, gebruikmakend van bestaande systemen. Om de effectiviteit van de ontwikkelde methoden te testen, zijn van ADS-B afgeleide meteorologische data vergeleken met meteorologische voorspellingen.

Naast meteorologische informatie is informatie over de toestand van het vliegtuig, vliegtuigprestaties en intenties nodig om een trajectvoorspelling te maken. Deze informatie is vaak onvolledig. In dit onderzoek is een methode ontwikkeld waarmee trajectvoorspellingen kunnen worden gemaakt op basis van historische trajectgegevens en meteorologische gegevens. Anders dan bij gangbare trajectvoorspellers wordt geen gebruik gemaakt van expliciete modellen van de vliegtuigprestaties, procedures en luchtruim. Trajectvoorspelling is hier gedefinieerd als een machinaal leren probleem. Op basis van historische traject- en meteorologische gegevens is een model getraind om een trajectvoorspelling te maken. Hierbij is alleen gebruik gemaakt van gegevens die

beschikbaar zijn in huidige surveillance en meteorologische systemen. Tijdens het trainen worden de modelparameters gekalibreerd om de fout in de voorspellingen te minimaliseren. De effectiviteit van de ontwikkelde methode is getest door voorspellingen te doen van de aankomsttijden van vluchten die een geluidsarme nadering uitvoerden. Deze resultaten bevestigden de werking van de trajectvoorspeller. Vervolgens is de trajectvoorspeller gebruikt om de benodigde onderlinge afstand van vliegtuigen bij het oplijnen voor geluidsarme naderingen te bepalen. Wanneer gebruik wordt gemaakt van de hier ontwikkelde trajectvoorspeller, is een groter aantal geluidsarme naderingsprocedures mogelijk bij een gelijk verkeersaanbod.

Self-spacing is het delegeren van de separatietaak van de luchtverkeersleider naar de vlieger. In een self-spacing omgeving plannen de vliegers, ondersteund door boordsystemen, een geluidsarme nadering waarbij het vliegtuig gesepareerd blijft van ander verkeer. De aanpassingen die aan een geluidsarme nadering kunnen worden gemaakt zijn beperkt en worden in grote mate bepaald door de vliegtuigprestaties. De actuele vliegtuigprestaties zijn bekend aan boord van het vliegtuig, wat delegatie van de separatietaak aan de vliegers logisch maakt. Twee eerder ontwikkelde self-spacing concepten zijn *'relative distance-based self-spacing'* en *'absolute time-based self-spacing'*. Belangrijk verschil tussen deze concepten is de interactie tussen vliegtuigen. In het relative distance based self-spacing concept reageert het vliegtuig actief op het gedrag van zijn voorganger. In het absolute time-based self-spacing concept is er geen interactie. In plaats daarvan krijgt ieder toestel een *required time of arrival* toegewezen om de separatie te waarborgen. In dit proefschrift zijn Monte-Carlo simulaties uitgevoerd om inzicht te krijgen in de capaciteit die self-spacing procedures bieden en in de operationele aspecten die een rol spelen bij de capaciteit en stabiliteit van de operatie. De hoogste doorvoer werd behaald met het relative distance-based self-spacing concept. In het absolute time-based self-spacing concept moesten buffers ten koste van capaciteit worden toegepast, omdat niet alle vliegtuigen de required time of arrival haalden. De simulaties lieten tevens zien dat het nauwkeurig oplijnen van het verkeer noodzakelijk is, omdat de mogelijkheden voor het maken van aanpassingen beperkt zijn.

Als laatste stap in het onderzoek is het *Time-Space Diagram* (TSD), een ondersteuningssysteem voor de luchtverkeersleider bij het oplijnen van verkeer voor geluidsarme naderingen, verder ontwikkeld en gevalideerd. Het TSD geeft de luchtverkeerleider informatie en hulpmiddelen om vliegtuigen op te lijnen voor het uitvoeren van geluidsarme naderingen. Het TSD wordt weergegeven naast het conventionele radarscherm. Bij de ontwikkelingen van het TSD is een drietal interface ontwerpprincipes toegepast: ecological interface design, visual momentum en direct manipulation. In dit proefschrift ligt de nadruk op toepassing van de laatste twee

ontwerpprincipes. De integratie van informatie gepresenteerd op het TSD en radarscherm is verbeterd, gebruikmakend van visual momentum. Statische computergegenereerde oplossingen zijn vervangen door direct manipulation interfaces. Direct manipulation interfaces zijn ontwikkeld voor het geven van o.a. snelheids-, richting- en hoogte-instructies.

Na aanpassing van het interface ontwerp is een experiment opgezet. In het experiment werd deelnemers gevraagd verkeer op te lijnen voor geluidsarme naderingen in hoge verkeersdichtheid, ondersteund door ofwel het TSD ofwel een *stack list* met de vereiste onderlinge afstand tussen twee vliegtuigen. De resultaten laten, in vergelijking tot de stack list, duidelijk de positieve effecten van het TSD op de prestaties van de luchtverkeersleider en verkeersafhandeling zien. Wanneer gebruik werd gemaakt van het TSD plande de luchtverkeersleider het verkeer verder vooruit. De direct manipulation interfaces werkten daarbij volgens alle deelnemers intuïtief. Het aantal instructies per vlucht nam met eenderde af en instructies werden eerder gegeven. Als resultaat daarvan konden de geluidsarme naderingen op een grotere hoogte en afstand van de luchthaven beginnen. De werkbelasting van de luchtverkeersleider was significant lager, bij een hoger niveau van situatiebewustzijn.

Belangrijkste resultaten van dit proefschrift zijn nieuwe methoden om meteorologische informatie af te leiden en trajectvoorspellingen te doen, nieuwe inzicht in de effecten van het toepassen van *self-spacing* en de verdere ontwikkeling en validatie van het TSD. De Monte-Carlo simulaties hebben laten zien dat de landingscapaciteit bij self-spacing vergelijkbaar is met de capaciteit die met conventionele procedures behaald kan worden. De simulaties toonden tevens aan dat nauwkeurig oplijnen van het verkeer noodzakelijk is. Het TSD ondersteunt de luchtverkeersleider bij nauwkeurig oplijnen van verkeer voor het uitvoeren geluidsarme naderingen in hoge verkeersdichtheid bij een acceptabel werkbelastingniveau en hoog situatiebewustzijn. Ook geeft het TSD een voorbeeld van het toepassen van ecological interface design, visual momentum en direct manipulation interface ontwerpprincipes om de mogelijkheden en prestaties van een luchtverkeersleidingssysteem te verbeteren. In lijn met de ontwikkeling van toekomstige luchtverkeersleidingssystemen binnen SESAR en NextGen, blijft de mens een centrale rol spelen, ondersteund door automatisering. Een deel van de resultaten van dit promotieonderzoek is naar verwachting breder inzetbaar dan voor het beoogde doel van dit proefschrift. De ontwikkelde methoden voor het afleiden van meteorologische informatie en het doen van trajectvoorspellingen zijn bruikbaar in andere systemen en procedures van een nieuw luchtverkeersleidingssysteem. Deze methoden zijn mogelijk ook buiten de luchtvaart toepasbaar.

Een luchtverkeersleidingssysteem dat geluidsarme naderingen bij een groot verkeersaanbod mogelijk maakt omvat meer procedures, processen en systemen dan in dit proefschrift aan bod zijn gekomen. Voorbeelden van aspecten die niet aan bod zijn gekomen zijn ondersteuning van vliegers bij het uitvoeren van de separatietaak, het ontwerp van de geluidsarme naderingsprocedures en de benodigde communicatie-systemen. Aanbevolen wordt om naar deze aspecten nader onderzoek te doen.

Acknowledgments

This thesis is the result of four years of research within the Control and Simulation Division at Delft University of Technology. During these years, I had the opportunity to both pursue a Ph.D. degree and a commercial career at To70. The academic and commercial worlds are very different, yet both essential. I am grateful to many people who enabled me to excel in both worlds and would like to mention some people in particular.

First of all, I would like to thank prof. Max Mulder, my promotor, for giving me the opportunity to pursue a Ph.D. degree and introducing me to the idea of combining this with a position at To70. Also, I would like to thank Max for his guidance, support, and for providing me with the freedom to define and carry out my Ph.D. research project.

Next, I would like to thank my co-promotor dr. René van Paassen, who has contributed greatly to the academic quality of this thesis. Throughout my research, René provided valuable insights and challenged my work, which led to significant improvements of the algorithms, methods and designs described in this thesis. Valuable input from the pilot's perspective was given by Xander in 't Veld.

My thanks also go out to Harjan Boering and Aedo Hoekstra at To70, for offering me an aviation consultant position and for their support during my Ph.D. research. To my To70 colleagues Martijn Beekhuyzen, Nicoline Beunders, Arie van der Eijk, Ruud van den Heuvel, Nikki Limtanakool, Gustavo Mercado, Michael Portier, Maarten Repko, Catrien Schweigman, Jeromy Snel, Ella Soltani, Jonas van Straaten, Jeroen Timmers, Ruud Ummels, Theo van de Ven, Marc Verschoor, Kjeld Vinkx, and Wenjing Zhou: thanks for your collegiality, support, interest in my research, and flexibility. I am also thankful to Marc for proofreading my publications and thesis, and to Arie for extensively testing the air traffic control simulator.

I would also like to thank my fellow Ph.D. students at the Control and Simulation Division for all the discussions we had, the tips and tricks for a successful Ph.D., and the unforgettable conference trips. My roommates, Maarten Tielrooij and Mariam Abdul Rahman, thank you or terima kasih for your company and fun in the office. Maarten, thanks for proofreading my publications and thesis. My thanks also go out to all other staff members for their support and the facilities available.

I would also like to thank the M.Sc. graduate students I supervised: Sander Ardinois, Martijn Beekhuyzen, Floris Freeman, Ruud van Gils, Paul de Jong, Pierre Maere, Maarten Niemantsverdriet, Leon de Poorter, and Lennart Prins. It has been a great experience to be involved in your graduation projects.

Above all, I am very thankful to my parents, Piet and Magré, my brother Martijn, family, and friends. Without your unconditional love and support I would never have been able to achieve this.

Arjen de Leege   Berkel en Rodenrijs, June 2013

Curriculum Vitae

Arie Marinus Pieter (Arjen) de Leege was born on August 28, 1982 in Delft, The Netherlands. From 1994 to 2001 he attended the R.K. Sint-Laurenscollege in Rotterdam, the Netherlands.

In 2001 he enrolled as a student at the Faculty of Aerospace Engineering at Delft University of Technology. As part of his study he performed an internship at the Boeing Research and Technology Center Europe (BRTE) in Madrid, Spain. In October 2007 he obtained his M.Sc. degree in Aerospace Engineering at the Control and Simulation Division of the Faculty of Aerospace Engineering.

In October 2007 he joined To70 B.V. in The Hague, the Netherlands as a Junior Aviation Consultant. In September 2008, he returned to the Control and Simulation Division at the Faculty of Aerospace Engineering to pursue a Ph.D. degree, after being awarded a grant by the Netherlands Organisation for Scientific Research. He combined his Ph.D. research with his position of Aviation Consultant at To70.

Currently Arjen holds the position of Senior Aviation Consultant at To70. He is involved in projects in the area of air traffic management, airport operations, environmental impact assessment, and flight data analysis.

Publications

1. de Leege, A.M.P., in 't Veld, A.C., Mulder, M., and van Paassen, M.M., "Three-Degree Decelerating Approaches in Arrival Streams Continuous Descent Approaches at High Density Traffic Airports," *TRAIL Research School Delft October 2008*, 2008, pp. 1–18.
2. de Leege, A.M.P., in 't Veld, A.C., Mulder, M., and van Paassen, M.M., "Three-Degree Decelerating Approaches in High-Density Arrival Streams," *Journal of Aircraft*, Vol. 46, No. 5, Sep. 2009, pp. 1681–1691. DOI: 10.2514/1.42420
3. de Leege, A.M.P., in 't Veld, A.C., Mulder, M., and van Paassen, M.M., "A Time-Space Diagram as Controller Support Tool for Advanced Continuous Descent Operations," *Air Transport and Operations Symposium 2010*, 2010, pp. 1–9.
4. de Leege, A.M.P, in`t Veld, A.C., Mulder, M., and van Paassen, M.M., "A Time-Space Diagram as Controller Support Tool for Closed Path Continuous Descent Operations," *AIAA Guidance, Navigation, and Control Conference*, American Institute of Aeronautics and Astronautics, 2011.
5. de Leege, A.M.P., Tielrooij, M., van der Eijk, A., and Mulder, M., "A Time-Space Diagram based Controller Support Tool for Continuous Descent Operations," *HCI-Aero*, 2012.
6. de Leege, A.M.P., Mulder, M., and van Paassen, M.M., "Novel Method for Wind Estimation using Automatic Dependent Surveillance-Broadcast," *Journal of Guidance Control and Navigation and Control*, Vol. 35, No. 2, March 2012, pp. 648-653. DOI: 10.2514/1.55833
7. de Leege, A.M.P., van Paassen, M.M., and Mulder, M., "Using Automatic Dependent Surveillance-Broadcast for Meteorological Monitoring," *AIAA Guidance, Navigation, and Control Conference*, American Institute of Aeronautics and Astronautics, 2012.
8. de Leege, A.M.P., van Paassen, M.M., and Mulder, M., "Using Automatic Dependent Surveillance-Broadcast for Meteorological Monitoring," *Journal of Aircraft*, Vol. 50, No. 1, January 2013, pp. 249-261. DOI: 10.2514/1.C031901
9. de Leege, A.M.P., in`t Veld, A.C., Mulder, M., and van Paassen, M.M., "A Time-Space Diagram as Controller Support Tool for Closed Path Continuous Descent Operations," *Journal of Aircraft*, a*ccepted for publication.*
10. de Leege, A.M.P., van Paassen, M.M., and Mulder, M., "A Machine Learning Approach to Trajectory Prediction," *submitted to AIAA Guidance, Navigation, and Control Conference, American Institute of Aeronautics and Astronautics,* 2013.